

AN ANALYSIS OF REMOTE SENSING TECHNIQUES  
FOR GENERATING WILDFIRE MODELS OF  
WILDLAND URBAN INTERFACE SITES  
IN TEXAS

THESIS

Presented to the Graduate Council of  
Texas State University-San Marcos  
in Partial Fulfillment  
of the Requirements

for the Degree

Master of SCIENCE

by

Shelby Coder, B.S.

San Marcos, Texas  
December 2012

AN ANALYSIS OF REMOTE SENSING TECHNIQUES  
FOR GENERATING WILDFIRE MODELS OF  
WILDLAND URBAN INTERFACE SITES  
IN TEXAS

Committee Members Approved:

---

Susan Macey, Chair

---

T. Edwin Chow

---

Jennifer Jensen

Approved:

---

J. Michael Willoughby  
Dean of the Graduate College

**COPYRIGHT**

by

Shelby M. Coder

2012

## **FAIR USE AND AUTHOR'S PERMISSION STATEMENT**

### **Fair Use**

This work is protected by the Copyright Laws of the United States (Public Law 94-553, section 107). Consistent with fair use as defined in the Copyright Laws, brief quotations from this material are allowed with proper acknowledgment. Use of this material for financial gain without the author's express written permission is not allowed.

### **Duplication Permission**

As the copyright holder of this work I, Shelby M. Coder, authorize duplication of this work, in whole or in part, for educational or scholarly purposes only.

## **ACKNOWLEDGEMENTS**

This research was made possible by the influence and support of many individuals. First and foremost, a resounding thank you to Dr. Macey for your unwavering support and infinite patience. You were always available when I was in a rut and never failed to give your full attention. Thank you to my committee, Dr. Chow and Dr. Jensen, for your astute guidance and direction on a topic for which I had little expertise and you had a lot. Thank you to the Department of Geography at Texas State University-San Marcos including the hard-working staff that helped me along my way (particularly Allison Glass-Smith). Finally, thank you to my colleagues, friends and family for your flexibility, understanding and empathy while I tackled this new challenge. I look forward to the next one.

This manuscript was submitted on October 18<sup>th</sup>, 2012.

## TABLE OF CONTENTS

	<b>Page</b>
ACKNOWLEDGEMENTS .....	v
LIST OF TABLES .....	viii
LIST OF FIGURES .....	ix
CHAPTER	
I. INTRODUCTION .....	1
1.1 Objective .....	5
II. LITERATURE REVIEW .....	7
2.1 Wildland Fire .....	7
2.2 Wildfire Modeling .....	9
2.3 Fuel Estimation .....	12
2.3.1 <i>Passive Remote Sensing Methods</i> .....	13
2.3.2 <i>Active Remote Sensing Methods</i> .....	15
2.4 Fuel Classification Models .....	21
2.5 Role of Vegetation Moisture Content .....	23
2.5.1 <i>Vegetation Moisture Content in Wildfire Models</i> .....	23
2.5.2 <i>Remote Sensing of Vegetation Moisture Content</i> .....	25
2.5.3 <i>Vegetation Moisture Content in Drought Conditions</i> .....	27
III. METHODOLOGY .....	29
3.1 Area of Study .....	30
3.2 Data Collection .....	40
3.2.1 <i>Existing Data Resources</i> .....	40
3.2.2 <i>Data Preparation for FlamMap</i> .....	45
3.3 Wildfire Modeling .....	58

3.3.1 <i>Model Setup for Research Question I</i> .....	58
3.3.2 <i>Model Setup for Research Question II</i> .....	65
IV. RESULTS .....	77
4.1 Research Question I .....	77
4.1.1 <i>LANDFIRE Inputs</i> .....	77
4.1.2 <i>Lidar Inputs</i> .....	87
4.1.3 <i>FlamMap Output</i> .....	101
4.2 Research Question II.....	120
4.2.1 <i>Moisture Conditioning</i> .....	121
4.2.2 <i>Effect of Foliar Moisture Content on Fire Spread</i> .....	137
V. DISCUSSION .....	141
5.1 Research Question I.....	141
5.2 Research Question II.....	144
VI. CONCLUSION.....	146
REFERENCES .....	149

## LIST OF TABLES

<b>Table</b>	<b>Page</b>
Table 1. Eight Data Layers for FlamMap Listed by Source .....	44
Table 2. NFFL Fuel Model Data Dictionary .....	51
Table 3. Input Data Layers for Use in FlamMap .....	60
Table 4. Result of Kolmogorov-Smirnov Test for Normality .....	139

## LIST OF FIGURES

<b>Figure</b>	<b>Page</b>
1. Texas Drought Map .....	30
2. 2011 Wildfire Perimeters in Texas .....	31
3. Study Area in Kerr County .....	32
4. Land Cover and Wildland Urban Interface in Kerr Study Area .....	33
5. Kerr Study Area Landsat 5 TM .....	34
6. Possum Kingdom Wildfire Perimeter.....	36
7. Land Cover in Texas.....	37
8. Possum Kingdom Complex Wildfire Burn Perimeter .....	38
9. Landsat 5 TM Scene of Possum Kingdom Complex Burn Perimeter.....	39
10. Lidar Sample in Kerr County.....	43
11. Canopy Fuel Estimator Surface Model.....	47
12. Canopy Fuel Estimator Configuration .....	49
13. LANDFIRE NFFL Fuel Model .....	52
14. Kerr Study Area 1-meter DEM.....	55
15. Rasters Aligned to Points.....	57
16. Work Process Diagram for Research Question I .....	59
17. FlamMap Landscape File Parameters.....	61
18. FlamMap Fuel Moisture File Parameters .....	62
19. Work Process Diagram for First Component of Research Question II .....	66

20. FlamMap Weather File; FlamMap Wind File .....	67
21. NDII Formula for Landsat 5 TM .....	68
22. ERDAS Imagine NDII Model Layout .....	69
23. ERDAS Imagine NDII Model Parameters.....	70
24. Work Process Diagram for Second Component of Research Question II.....	71
25. Possum Kingdom Before Fire Image.....	72
26. Possum Kingdom NDVI Map.....	74
27. Possum Kingdom Unsupervised Classification Map.....	75
28. LANDFIRE 30-meter DEM in Kerr Study Area.....	79
29. LANDFIRE Slope in Kerr Study Area .....	80
30. LANDFIRE Aspect in Kerr Study Area .....	81
31. LANDFIRE Canopy Height in Kerr Study Area.....	82
32. LANDFIRE Canopy Base Height in Kerr Study Area .....	84
33. LANDFIRE Canopy Cover in Kerr Study Area.....	85
34. LANDFIRE Canopy Bulk Density in Kerr Study Area.....	86
35. Lidar 5-meter DEM in Kerr Study Area .....	88
36. Lidar Slope in Kerr Study Area .....	89
37. Lidar Aspect in Kerr Study Area .....	91
38. Lidar Canopy Height in Kerr Study Area.....	93
39. Lidar Canopy Base Height in Kerr Study Area .....	95
40. LANDFIRE Canopy Base Height Scaled to Lidar Data Range .....	96
41. Lidar Canopy Cover in Kerr Study Area .....	98
42. Lidar Canopy Bulk Density in Kerr Study Area.....	100

43. Flame Length Diagram .....	102
44. Lidar Flame Length Output .....	103
45. LANDFIRE Flame Length Output .....	104
46. Flame Length Change Detection .....	105
47. LANDFIRE Fireline Intensity Output .....	107
48. Lidar Fireline Intensity Output .....	109
49. Fireline Intensity Change Detection .....	110
50. LANDFIRE Crown Fire Activity Output .....	112
51. Lidar Crown Fire Activity Output .....	113
52. Crown Fire Activity Change Detection .....	114
53. Lidar Spread Rate Output .....	117
54. LANDFIRE Spread Rate Output .....	118
55. Spread Rate Change Detection .....	119
56. Fireline Intensity Output Comparison .....	123
57. Fireline Intensity Change Detection for Moisture Conditioning .....	124
58. Crown Fire Activity Output Comparison .....	127
59. Crown Fire Activity Change Detection for Moisture Conditioning .....	128
60. Flame Length Output Comparison.....	129
61. Flame Length Change Detection for Moisture Conditioning .....	130
62. Fireline Intensity Output Comparison .....	131
63. Fireline Intensity Change Detection for Moisture Conditioning .....	132
64. NDII of Kerr Study Area .....	135
65. NDII Map of Kerr Study Area; Natural Color Image of Kerr Study Area .....	136

66. NDII and Burn Scar in Possum Kingdom Study Area .....	138
67. Histogram of Burned NDII Values .....	139
68. Histogram of Remnant NDII Values .....	140

# CHAPTER I

## INTRODUCTION

Wildfire behavior modeling is located at the intersection of many diverse scientific disciplines (Arroyo, Pascual and Manzanera 2008) including but not limited to ecology, forestry, meteorology, urban planning, economics, agronomy, and geography. These models simulate real-world physical and atmospheric conditions to predict possible location and severity of wildfire for such applications as forest health, soils management and natural hazard assessment. Many models apply a spatial component to the process and function within a geographic information system (GIS). The wildland urban interface (WUI), the zone where expansive tracts of undeveloped and sometimes densely vegetated land abuts human development (Theobald and Romme 2007), is a key target for wildfire behavior modeling due to the high potential for hazard to human lives and property. WUI areas in the United States have increased over the past few decades (Shafran 2008), mostly due to booming low-density residential and recreational development outside of the urban core and adjacent to wildlands (Lein and Stump 2009; Theobald and Romme 2007).

Wildfire within these WUI areas creates a situation riddled with social and environmental complexities in which the need to protect people, structures, watershed health, timber resources, scenic beauty, recreation facilities, and atmospheric clarity (Lein and Stump 2009) are at odds with the natural progression of wildfire which has

historically maintained ecosystem balance (Garcia et al. 2011; Su et al. 2003). For this reason, it is imperative that effective environmental management, urban planning and hazard mitigation are employed to ensure harmony between the natural and human agendas. Crucial to this effort is wildfire behavior modeling.

The accuracy (and therefore usefulness) of information output from wildfire models is contingent upon the accuracy of the data inputs (Garcia et al. 2011). As Mutlu et al. (2008, 274) states, “Improving the accuracy of mapping fuel models is essential for fuel management decisions and explicit fire behavior prediction for real-time support of suppression tactics and logistics decisions.” Common inputs for GIS-based wildfire models include elevation, slope, aspect, weather, and vegetative fuel calculations such as canopy cover, crown bulk density, and crown base height (Mutlu et al. 2008; Popescu and Zhao 2008). These data inputs can be found or created from a variety of sources and at varying temporal and spatial scales (Arroyo, Pascual and Manzanera 2008). The appropriate combination of variables and parameters is often unique to the modeling application at hand and can depend on timeframe, funding, hardware or software resources, and geographic considerations. Perhaps the most critical inputs for wildfire behavior modeling are the fuel calculations, which are also very difficult to quantify and describe (Arroyo, Pascual and Manzanera 2008).

“Remote sensing can support many aspects of fire management and it can be used to decrease fire risk and to reduce fire damage” (Mutlu et al. 2008, 275). Since it came about in the 1960’s, passive remote sensing has provided a means for mapping fuel types and extent through aerial photo interpretation (Popescu and Zhao 2008). Multispectral satellite and aerial imagery is often readily available for any given location due to regular

satellite coverage and the occasional state, local or regional airborne orthoimagery acquisition (Riano et al. 2003). Due to its pervasiveness and usefulness for extracting relevant fuel characteristics such as tree height and biomass (Zheng et al. 2007), imagery has become one of the most common methods to map fuels for wildfire modeling (Arroyo, Pascual and Manzanera 2008; Avitabile et al. 2012; Popescu and Zhao 2008). However, there are disadvantages, such as spatial resolution being too coarse to distinguish vegetation type and inability to see below dense foliage or structures (Garcia et al. 2011; Riano et al. 2003).

One geospatial data product derived from satellite Landsat TM data is called LANDFIRE, or Landscape Fire and Resource Management Planning Tools. LANDFIRE is a joint project by the U.S. Department of Agriculture (USDA) and Department of the Interior that was initiated in 2004 to produce a comprehensive, consistent and scientifically credible suite of data layers spanning the entire U.S. for wildland fire management and land conservation (U.S. Department of Agriculture 2011b). LANDFIRE data products include more than fifty spatial data layers which are developed using peer-reviewed, consistent and repeatable scientific methods including satellite remote sensing, systems ecology, landscape modeling, relational databases, and vegetation and disturbance dynamics (U.S. Department of Agriculture 2011b). These datasets were created to be analyzed “at a landscape scale in support of strategic vegetation, fire, and fuels management planning to evaluate management alternatives across boundaries” (U.S. Department of Agriculture 2011b).

Another method for mapping fuel types is airborne light detection and ranging, or lidar (Andersen, McGaughey and Reutebuch 2005; Popescu and Zhao 2008). This

method is a key active remote sensing technology in which a sensor emits near-infrared light pulses from an airborne platform toward the ground and then records the signal return. The result is a three dimensional cloud of points which contains horizontal x and y-values along with the vertical z-value. Through computer algorithms, points can then be filtered into relevant classifications such as ground, buildings, and vegetation. This technique is a powerful tool for estimation of surface fuels since the laser pulses can penetrate gaps in vegetation canopy to access a wider range of fuel attributes including vegetation understory (Garcia et al. 2011; Mutlu et al. 2008; Popescu and Zhao 2008).

Within the past decade there has been a marked increase in demand for lidar from the geospatial community (Avitabile et al. 2012; Koch 2010; Maune 2007). Though expensive relative to imagery (Popescu et al. 2011), lidar acquisition and processing costs have decreased as the hardware and software to produce these data have become more affordable. Although lidar is still more costly than orthoimagery, public and private entities alike are becoming enlightened to the broad scope of benefits from lidar data. Some agencies, such as The Railroad Commission of Texas (RRC), have realized the cost benefit from acquiring highly accurate remotely sensed data in lieu of expensive field collections combined with human error-prone aerial interpretation (from personal communication with Jon Brandt of the Texas RRC Abandoned Mine & Land Reclamation Program).

Another critical input to GIS-based wildfire behavior models is vegetation fuel moisture (Mutlu et al. 2008; Scott and Burgan 2005), which affects the ignitability of fuels (Verbesselt et al. 2007). Traditionally, these models assume a constant value for moisture content of all dead vegetation litter (woody duff) throughout the project area,

but fail to include moisture content of live vegetation. This approach was developed by the U.S. Forest Service (Missoula Fire Sciences Laboratory 2011) for wildfire modeling applications in large forests under normal climate conditions, where moisture content is likely to be relatively homogeneous. However drought conditions in a WUI environment present a vastly different scenario in which vegetation moisture content can have a high spatial variability (Caccamo et al. 2011). Trees in landscaped areas or adjacent to rivers and lakes have access to considerably more water than trees in open areas, and this difference is magnified in a drought. It is possible to account for live vegetation moisture content within the wildfire model inputs (in a fuel class model), even if the wildfire model itself does not account for heterogeneous moisture content. However in this instance, the spatial resolution of vegetation moisture is limited to the area of extent for each fuel class in a given location and ignores moisture variability within the same fuel model.

### 1.1 Objective

The objective of this research is to evaluate selected techniques for wildfire behavior modeling in a wildland urban environment. One portion of the study will compare the use of state-of-the-art technology against an established methodology for producing data inputs from a wildfire model. The other portion of the study will incorporate live vegetation moisture into the same wildfire model, which could contribute to wildfire behavior in a drought. Specifically, this study will address the following research questions:

- I. How do wildfire behavior maps created from high resolution airborne lidar compare to those created from Landsat TM-derived LANDFIRE data in terms of both scale and method of data acquisition?
  
- II. How do wildfire behavior maps created with constant foliar moisture content (FMC) compare to maps with variable FMC measured from Landsat TM imagery, and is FMC related to wildfire spread in a drought environment?

These “methods and mapping products have the potential for driving changes in forest resource management practices related to mitigating fire hazard that threatens the public, human lives, and environmental health in Texas and nationwide” (Mutlu et al. 2008, 284). The results of this analysis could prove useful to environmental and land managers who must make improved fire behavior predictions by identifying areas in need of fuel mitigation efforts (Mutlu et al. 2008; Popescu and Zhao 2008). Informed decision-making is aided by an awareness of the best and most relevant sources of data capable of meeting the minimum project parameters and budget.

## CHAPTER II

### LITERATURE REVIEW

#### 2.1 Wildland Fire

The area where natural wildlands meet the fringe of urbanization is called the wildland urban interface (WUI). Intermix describes the portion of a WUI where sparse housing and development is mixed within dense vegetation, and interface exhibits development surrounded by sparse vegetation adjacent to the dense wildland vegetation (Zhang, He and Yang 2008). Approximately 89% of land in the WUI is privately owned (Theobald and Romme 2007), demonstrating its popularity as a lifestyle alternative to urban living. However, the scenery and closeness to nature's bounty comes at a price - the potential for fire hazard. Resource managers must contend with the social and technical complications of wildfire near the presence of humans, their homes, and development adjacent to the lands they manage (Lein and Stump 2009). The WUI environment also poses a unique challenge to firefighting mitigation and response efforts. Response teams must contend with fire behavior as it burns through not only vegetation but large fuel loads of highly flammable construction materials and possessions in urban structures (Bhandary 2007; Flaxman 2001). Decentralization in the U.S. is escalating the issue even further (Lein and Stump 2009); the current extent of land in the U.S. characterized as WUI is about 14% larger than the state of California (Theobald and Romme 2007).

Wildfire in WUI areas is most common in the eastern U.S. due to high population density, but fires there are typically low in intensity (Theobald and Romme 2007). By contrast, WUI fires in the western part of the country are less frequent but far more severe since this area is where stand-replacing fires dominate both historical and the most recent fire regimes (Theobald and Romme 2007). If the conditions are right, wildfire can happen anywhere, unlike geographically restricted hazards such as tsunamis, hurricanes and earthquakes. Elements that influence the propagation of wildfire include the presence and quality of fuels to burn, location of ignition, weather patterns, and topography (Bar Massada et al. 2009). Drought can further exacerbate the vulnerability of a region to wildfire by tapping the water content in vegetation fuels from lack of rainfall and high evapotranspiration, greatly increasing the odds of ignition and fire longevity (Caccamo et al. 2011). The hot and sometimes windy weather patterns that are often instigated or escalated by drought also reinforce a high probability of wildfire. These contributors to wildfire risk can be modeled using GIS technology (Arroyo, Pascual and Manzanera 2008).

Understanding fire behavior aids in improved land management and allows managers and planners to anticipate areas at risk (Arroyo, Pascual and Manzanera 2008; Garcia et al. 2011). According to Bar Massada et al. (2009, 1991)

Risk is influenced both by changing patterns of the landscape values at risk (i.e. homes) and the process generating the risk (ignitions and fire spread). The large and increasing number of lives and structures that are potentially exposed to wildfire hazard highlights the need to quantify wildfire risk in the WUI so that this risk can be minimized.

While wildfire risk and behavior modeling has been around for some time (Arroyo, Pascual and Manzanera 2008), updated technology and widespread data collection from an amalgam of sources can be used to conduct detailed analysis requiring less time and computational resources than ever before. These technological and data resources are crucial to promote awareness in high risk areas, for city planning and development, and for wildfire mitigation and response strategies.

## 2.2 Wildfire Modeling

Wildfire modeling spans a broad range of functionality including empirical models that describe the fundamentals of fire behavior, fire models that produce graphical and tabular outputs of perimeter spread distance, spatially-based fire behavior analysis programs, specialized systems that focus on specifics like wind fields and tree mortality rates, and finally, comprehensive decision support systems encompassing many aspects of study (Arroyo, Pascual and Manzanera 2008).

Many North American wildfire decision support systems are founded on Rothermel's (1972) surface fire spread model which was published as a result of a 1968 plan for a national fire danger rating system (Flaxman 2001; Missoula Fire Sciences Laboratory 2011). Van Wagner (1977) then introduced the crown fire initiation model, and Rothermel (1991) later proposed the crown fire spread model. In conjunction with Rothermel's 1972 model, the U.S. created the pioneering National Fire Danger Rating System (NFDRS), a broad scale seasonal weather system analyzed with nine pre-classified vegetation fuel types (later expanded to twenty) and moisture content of dead fuels (Arroyo, Pascual and Manzanera 2008; Garcia et al. 2011). This system is the

precursor to the modern public domain National Systems, a suite of wildfire behavior and fire danger software developed by the U.S. Forest Service and the U.S. Department of the Interior (including the National Park Service and Bureau of Land Management) for use by federal, state and local fire and land managers (Missoula Fire Sciences Laboratory 2011).

National Systems is really two distinct sets of software: three models comprising the National Fire Behavior Systems and two models known as the National Fire Danger Systems (Missoula Fire Sciences Laboratory 2011). The National Fire Behavior Systems models rely upon the same empirical fire behavior framework originally developed by Rothermel (1972) and other existing models for surface fire, crown fire, spotting post-frontal combustion and fire acceleration including those from Van Wagner (1977), Albin (1984) and Nelson (2000). The tools perform complementary functions to produce output information such as flame length, spread rate, perimeter and more.

One of the most commonly used models (Flaxman 2001) is FARSITE, a fire growth simulator developed by Finney and Andrews (2001) that utilizes spatial and tabular inputs to predict fire behavior over time. FARSITE can be used for conducting “what if” scenarios and comparing results to improve mitigation and response strategies (Missoula Fire Sciences Laboratory 2011). It also distinguishes between surface fires and crown fires, utilizing different underlying empirical models from Rothermel (1972) and Van Wagner (1977), respectively (Bar Massada et al. 2009).

FARSITE requires an input ‘Landscape’ file comprised of spatial data themes including elevation, slope, aspect, canopy cover, fuel model, canopy bulk density, canopy

base height, and canopy height (Missoula Fire Sciences Laboratory 2011). An 'Initial Fuel Moisture' file estimates the percentage of moisture present in dead woody debris after running simulated weather patterns based on user-defined parameters. Additional optional files include spatial and temporal weather conditions such as relative humidity, rainfall and wind. FARSITE produces outputs in maps, tables and graphs including information such as flame length, rate of spread, heat per unit area and fireline intensity (Missoula Fire Sciences Laboratory 2011).

These same inputs are also required for FlamMap (Finney 2006), a fire mapping and analysis system that focuses on the spatial dimension to model potential fire behavior across the landscape (Missoula Fire Sciences Laboratory 2011). Outputs are in a geographic format similar to raster maps produced in FARSITE, and include fireline intensity, crown fire activity, flame length, and spread rate. Unlike FARSITE, FlamMap does not include a temporal component; conditions are constant in time but vary spatially. Similar to its counterparts FARSITE and FlamMap, BehavePlus (Andrews 2007) is another fire behavior prediction model and fire environment system which produces tabular and graphical data describing conditions after a number of variables have been input (Missoula Fire Sciences Laboratory 2011). For instance, rate of spread can be compared relative to percent fuel moisture simultaneously for several different scenarios under varying weather or terrain conditions.

The other component of the National Systems, the National Fire Danger Rating System (NFDRS), produces fire indices to indicate the possibility for fire activity (Arroyo, Pascual and Manzanera 2008). FireFamilyPlus (Missoula Fire Sciences Laboratory 2011) is an integrated database of weather and fire occurrence. It can

calculate fire danger rating indices and perform analysis for climatological summaries used by fire management. These reports of historical weather conditions relative to number of fire outbreaks are critical for tracking seasonal progression of fire danger. Analysis of current weather information provides data to estimate continued fire growth which is integral for response planning (Missoula Fire Sciences Laboratory 2011). The Wildland Fire Assessment System is the primary component of the NFDRS and uses a multitude of indices including those grouped under: 'Fire Potential & Danger' (fire danger rating, lightning efficiency, the Haines Index for atmospheric stability, and the National Digital Forecast Database forecasts); 'Weather' (fire weather index); and 'Moisture & Drought' (dead fuel moisture index, Advanced Very High Resolution Radiometer (AVHRR) derived normalized difference vegetation index (NDVI), the Keetch-Byram Index for evapotranspiration and transportation, the Palmer Drought Index, and fuel moisture from the National Fuel Moisture Database)(U.S. Forest Service 2011).

### 2.3 Fuel Estimation

An essential constituent of a wildfire model is the calculation of surface fuel parameters, which are the fundamental component of fire risk (Arroyo, Pascual and Manzanera 2008; Garcia et al. 2011; Popescu and Zhao 2008; Riano et al. 2003). Accordingly, an accurate record of the characterization and distribution of these fuels is paramount, although it is particularly difficult to calculate given the complex and dynamic nature of vegetative and structural properties at different scales and locations (Garcia et al. 2011). Vegetation biomass is the weight of plant materials across a given area, and can be calculated by measuring canopy structure metrics such as percent canopy

cover, canopy base height, leaf area index (LAI), canopy bulk density (weight per volume), fuel loading (weight per area) and often, particle size (stem diameter) (Andersen, McGaughey and Reutebuch 2005; Arroyo, Pascual and Manzanera 2008; Chen et al. 2012; Jensen et al. 2006; Popescu and Zhao 2008; Riano et al. 2003). Other parameters such as crown bulk density are also important given that fire spreads more quickly and is more difficult to extinguish in tree crowns than on the ground (Riano et al. 2004).

In addition to wildfire modeling, biomass estimation is performed for many other areas of study, including sustainable forest management, deforestation monitoring, timber management, carbon sequestration (Avitabile et al. 2012; Chen et al. 2012; Popescu and Zhao 2008; Tian et al. 2012; Zhao, Popescu and Nelson 2009), ecosystem productivity estimation (Jensen et al. 2006), hydrology (Tian et al. 2012), recreation and wildlife habitat monitoring (Shan and Toth 2008). Measurement of vegetation characteristics for biomass estimation can be accomplished using both passive and active remote sensing methods (Tian et al. 2012), each with varying degrees of complexity, scale, accuracy and cost.

### *2.3.1 Passive Remote Sensing Methods*

Referring to satellite imagery, Avitabile et al. (2012, 366) states “remote sensing provides the key source of data for updated, consistent and spatially explicit assessment of biomass and its dynamics, especially in large countries with limited accessibility.” Regional to country-scale areas can utilize moderate resolution imagery from satellites like the Moderate Resolution Imaging Spectroradiometer (MODIS), while local-scale areas rely on medium resolution imagery from Landsat TM and ASTER (Avitabile et al.

2012; Garcia et al. 2011). Higher resolution sensors such as SPOT, IKONOS and QuickBird have allowed for finer scale mapping (Garcia et al. 2011). Regular coverage from these sources can provide years of historical image scenes, although generating cloud-free datasets can be challenging over large areas (Avitabile et al. 2012).

Optical remote sensing enables biomass estimation by quantifying canopy density. However, the result is not a direct measurement and can produce questionable data (Zheng et al. 2007). Inability to penetrate dense canopy cover is the primary limitation of passive remote sensing, and vegetation height does not change reflectance patterns, causing some disparate fuel types to exhibit minimal spectral differences in imagery (Garcia et al. 2011).

Due to the highly complex and variable nature of fuel characteristics across the landscape, particularly in a WUI environment, estimates of on-the-ground conditions must be considered based on project scale and application (Zheng et al. 2007). Many existing studies for wildfire hazard assessment and modeling rely upon satellite imagery or high-resolution orthoimagery for extraction of vegetation and/or structures (Baldwin 2003; Bhandary 2007; Halligan 2007; Hawbaker 2009; Hunter 2005; Lampin-Maillet et al. 2010; Lein and Stump 2009; Luo 2004; Xu 2006; Zheng et al. 2007). The imagery used in these studies vary in resolution from 1 km AVHRR and MODIS (Hawbaker 2009; Hunter 2005), to 30 meter Landsat (Lein and Stump 2009; Xu 2006; Zheng et al. 2007), 1-4 meter IKONOS (Bhandary 2007), 2.5 meter SPOT (Lampin-Maillet et al. 2010), and 1 meter orthoimagery (Baldwin 2003). Coarse data inputs work well for large extent mapping pursuits (Hawbaker 2009), but are not sufficient for estimating vegetation

or structures as wildfire fuel from a large scale or neighborhood perspective (Halligan 2007; Hunter 2005; Luo 2004).

### *2.3.2 Active Remote Sensing Methods*

Active remote sensing in the form of light detection and ranging, or lidar, provides a state-of-the-art technique for highly accurate biomass estimation (Andersen, McGaughey and Reutebuch 2005; Chen et al. 2012; Garcia et al. 2011; Mutlu et al. 2008; Popescu et al. 2011; Zhao, Popescu and Nelson 2009). According to Lefsky et al. (2005, 555-556), “Predicting aboveground biomass from lidar-measured canopy height has now been shown to be (a) straightforward exercise in a variety of forested biomes, and physiognomic types.” The technology measures the time it takes a laser pulse from an airborne sensor to reach an object on or above the ground and return to the sensor. Since light travels at a known speed, it is possible to distinguish the distance covered by the duration of time it took the pulse to return. In addition to the lidar sensor, an onboard Global Positioning System (GPS) receiver records the sensor’s precise location so that distance can be accurately measured. The GPS is assisted by an internal measurement unit (IMU) with an accelerometer to precisely record the aircraft positional information such as speed, heading, pitch, yaw and roll (Jensen 2000; Maune 2007). The resulting data collected is a three-dimensional point cloud comprised of millions (or billions) of point locations with recorded attributes for positional x, y, and z, 8-bit integer of return pulse intensity, GPS timestamps and more. Additional information about light detection and ranging principles can be found in the DEM Users Manual (Maune 2007).

Although different from current systems, lasers have been used to measure vegetative characteristics like stem volume, biomass and tree height for over 30 years

(Maune 2007; Maclean 1986; Shan and Toth 2008, 336). Small-footprint lidar came into use in forestry in the late 1990's (Naesset 1997; Shan and Toth 2008, 336) and within the past two decades lidar has steadily gained popularity for a variety of applications (Avitabile et al. 2012; Koch 2010; Maune 2007; Zhao, Popescu and Nelson 2009) - particularly for deriving elevation data but also for vegetation mapping, both of which are necessary for wildfire modeling.

Unlike optical remote sensing, in which biomass characteristics such as height and volume are estimated using photogrammetric techniques (and often confirmed with field work), the same parameters can be derived with a high level of accuracy directly from the geographically oriented three dimensional point cloud generated from a lidar sensor (Arroyo, Pascual and Manzanera 2008; Avitabile et al. 2012; Lefsky et al. 1999; Maune 2007; Popescu et al. 2011; Popescu and Zhao 2008; Riano et al. 2003). A single laser pulse from the airborne sensor can make a direct hit on a tree top and produce one return, or can be more complex and hit several branches and even the ground before returning, producing multiple returns (Shan and Toth 2008).

Modern lidar sensors are capable of recording multiple discrete returns, anywhere from the neighborhood of two or three all the way up to fifteen or more (Maune 2007; Shan and Toth 2008). Full-waveform lidar digitizes the entire return signal and therefore allows for many multiple returns with short separation, providing a more complete view of the object sensed. While this is highly useful for vegetation studies, it creates an immense amount of data. Intensive processing and large data storage make this type of lidar not only more expensive, but often too cumbersome for projects beyond a very large scale.

The number of discrete returns detected from a single laser pulse depends on the complexity of the vegetation (or other object), the capabilities of the lidar sensor, flying altitude and the sensor settings (Shan and Toth 2008). Flying lower to the ground with lower scan angles and a high pulse rate over vegetation with a dense understory will produce a higher number of returns (Shan and Toth 2008). Because of this ability, lidar is also capable of producing canopy surface information and vegetation parameters such as stem density and crown dimensions (Mutlu et al. 2008).

According to Flaxman (2001, 82), traditional passive optical remote sensing gives no access to vegetation understory: “These surface fuel loads are the most important single factor in predicting fire spread and intensity, yet they are not easily correlated with the above-canopy view from aircraft and satellites.” A more complete and accurate approach to calculating vegetation and structure fuels is to use a dense, high-resolution three-dimensional lidar point cloud (Arroyo, Pascual and Manzanera 2008; Avitabile et al. 2012; Popsecu et al. 2011; Popsecu and Zhao 2008) in lieu of two-dimensional coarse pixel extractions based on image classification (Flaxman 2001).

Lidar is also successfully utilized to quantify leaf area index and biomass (Lefsky et al. 2005). One study by Jensen et al. (2011) compared a 1-kilometer LAI raster provided from MODIS against a 30-meter LAI grid derived from lidar during the same timeframe for an evergreen forest in northern Idaho. They analyzed differences in certain variables such as sun/sensor geometry and sub-pixel heterogeneity (for vegetation and terrain) to determine the suitability of lidar as a replacement for passive remote sensing techniques which do not provide adequate estimates for areas of high LAI. Jensen et al. (2011, 3637) concluded that “lidar data provide better estimates over the entire range of

field-measured LAI values since the data respond more directly to the structural characteristics of forest canopies and aren't subject to the same saturation issues commonly observed with passive optical sensors".

A different study by Jensen et al. (2008) compares three methodologies for LAI estimates: lidar only, spectral vegetation indices (SVIs) derived from passive optical remote sensing using 10-meter SPOT5 imagery, and lidar data supplemented with the SPOT5 SVIs. The authors found that lidar accounted for significant variation in LAI relative to the SPOT5 SVIs, even for two ecologically diverse study areas. The passive optical remote sensing method offered little improvement when combined with the lidar-derived LAI. These results compare to the previous study (Jensen et al. 2011) in that LAI values calculated from lidar were still found to be superior to LAI from passive optical remote sensing, even considering a difference in spatial resolution of the two sensors.

Large-footprint, full waveform satellite lidar data that is sensitive to vegetation structure can be obtained from the Geoscience Laser Altimeter System (GLAS) located on the Ice Cloud and Land Elevation Satellite (ICESat) (Avitabile et al. 2012; Popescu et al. 2011; Riano et al. 2003). Avitabile et al. (2012) and Popescu et al. (2007) found that under favorable topographic conditions GLAS data could produce accurate terrain elevation as well as estimate height metrics over large areas. The researchers were also in concordance that GLAS data pairs well with airborne lidar data captured for the same area. The GLAS metric Height of Median Energy (HOME) is highly correlated with above ground biomass and the large-area footprint supports the use of this satellite-derived lidar data for biomass estimation at global and country-scale study.

As Mutlu et al. (2008, 275) states, “There is a limited number of studies in the literature that used airborne scanning laser (lidar) systems to estimate forest fuel parameters”, and more recently Garcia et al. (2011, 1370) reiterates, “although lidar has been proved suitable to estimate fuel properties, fewer studies have tested the usefulness of these data to map fuel types”. However, a few do exist. Riano et al. (2003) generated automatic extraction methods to calculate spatial forest fuel parameters from airborne lidar including tree height, crown base height, tree cover, surface canopy height, understory cover, crown bulk density, crown volume and foliage biomass. The authors concluded that lidar “should help accomplish a precise characterization of fuels” (Riano et al. 2003, 185) and argue that fusion of lidar with optical remote sensing is an optimal solution for identification of tree species and surface canopy types. Following the 2003 study, Riano et al. (2004) successfully used lidar to estimate crown bulk density (foliage biomass divided by crown volume) for *Pinus sylvestris* in Spain.

Andersen, McGaughey and Reutebuch (2005) calculated forest canopy fuel parameters (canopy bulk density, canopy height, canopy fuel weight and canopy base height) using lidar data at a point density of 3.5 points per square meter. These fuel parameters were then measured in the field and added to residual plots for a multiple regression analysis. Each fuel parameter exhibited a strong relationship between predicted lidar metrics and field-based estimates, leading the authors to conclude that lidar data provides a very reliable model of forest canopy fuel parameters.

One of the earlier studies was conducted by the Norwegian scientist Naesset (1997), who measured the mean tree height of forest stands using airborne laser scanning data (lidar). Naesset found that the mean heights estimated from the lidar seriously

underestimated the ground truth mean height of the forest by 4.1 – 5.5 meters, however concluded that this method still obtained forest stand heights with an accuracy greater than or equal to current aerial interpretation methods.

In addition to Naesset (1997), other studies (Riano et al. 2003; Zhao, Popescu and Nelson 2009) suggest that stand heights are underestimated due to a large probability of missing treetops, even with a high sampling density. It would be folly to attempt a universal correction factor, since such an algorithm would be dependent on highly variable project parameters such as flight altitude, forest type, sensor system and coverage. As such, a higher pulse density still provides the best odds of sampling treetops (Shan and Toth 2008) thus increasing accuracy of vegetation height and biomass calculation.

Due to its large file size as well as project-specific standards for positional and classification accuracy, airborne lidar can be expensive to acquire and process (Popescu et al. 2011; Jensen et al. 2006). The cost has dropped over the past few years (Maune 2007) resulting in the technology becoming more accessible, but due to lidar's higher price tag relative to satellite or aerial imagery, geographic coverage of airborne lidar across the U.S. is relatively sparse. Most medium-sized acquisitions (spanning a handful of counties to an entire state) are for the purpose of floodplain mapping or hydraulic studies and in many instances only the bare earth ground points are extracted. When only ground points are classified, point returns representing vegetation are grouped with all other unidentified point returns, which means additional processing is necessary for fuels estimation. In addition to cost as a factor, multiple lidar collections of the same area are somewhat rare since the bare earth surface derived for many projects can remain static for

several years. Despite the current deficit, the U.S. Geological Survey (USGS) is coordinating with all levels of government to expand the national database of lidar coverage in an effort to increase the quality of GIScience and engineering nationwide (Claire DeVaughan, USGS State Liaison for Texas, March 16, 2011, email message to author).

#### 2.4 Fuel Classification Models

In wildfire modeling, biomass metrics are often combined with fuel classifications, or vegetation types, to marry the physical and structural measurements with qualitative properties relevant to fire behavior and flammability (Arroyo, Pascual and Manzanera 2008; Chen et al. 2012; Garcia et al. 2011; Riano et al. 2003). Fuel classification is convenient for categorizing vegetation into groups and subgroups of common characteristics which are based on similar potential fire behavior (Mutlu et al. 2008). The NFDRS created their own set of twenty classifications while FARSITE, FlamMap and BehavePlus employ the thirteen Northern Forest Fire Laboratory (NFFL) fuel models (Arroyo, Pascual and Manzanera 2008; Mutlu et al. 2008; Riano et al. 2003). The NFFL fuel classes vary in terms of amount, size and arrangement (Mutlu et al. 2008); some examples include Grasses (including sawgrass and pine-grass savannah) and Forest (including Western pines and Hardwoods)(Arroyo, Pascual and Manzanera 2008). FARSITE, FlamMap and BehavePlus also allow for inclusion of custom categories which could be derived by classifying remotely sensed satellite imagery or by taking *in situ* records. According to the U.S. Forest Service (2011b), fuel models are used within wildfire models to “compute shading, wind reduction factors, spotting distances, crown

fuel volume, spread characteristics of crown fires and to incorporate the effects of ladder fuels for transitions from a surface (fire) to a crown fire.”

Modeling fuels based on classification renders the modeling process simple and cost effective (for pre-determined classes), but assumes spatial homogeneity which does not often accurately reflect real-world conditions at a large scale (Arroyo, Pascual and Manzanera 2008). Similarity between alternate sets of classifications can make selection for a particular application confusing. Also, vegetation classes can be broad in scope to accommodate more regions, but at the expense of excluding diversity. The alternative situation finds classifications that meet the needs of one study but are not applicable anywhere else (Arroyo, Pascual and Manzanera 2008).

Scott and Burgan (2005) created a new fuel model designed specifically for wildfire modeling that classifies vegetation based on fire-carrying fuel type instead of vegetation type. Within the seven fuel types (for example Grass, Timber Litter, Timber-Understory), fuel models are given a number which reflects an increasing heat per unit area based on live fuel moisture content. Scott and Burgan (2005) designed the new system such that a user familiar with the NFFL set of thirteen classes can easily port their existing model into the new configuration. Like the NFFL fuel classes, this fuel model set was created for wildfire modeling programs that use Rothermel’s (1972) surface fire spread model, such as FARSITE, FlamMap and BehavePlus. Also similar to the NFFL model, spatial homogeneity and continuity are assumed. Due to differences in the way fuel types are calculated to respond to fire, Scott and Burgan’s fuel model is not appropriate for the NFDRS, even though the NFDRS also uses Rothermel’s fundamental principles. According to Scott and Burgan (2005, 2), the purpose of their fuel model was

to provide an alternative to the NFFL classes that performs better in situations of “prescribed fire, wildland fire use, simulating the effects of fuel treatments on potential fire behavior and simulating transition to crown fire using crown fire initiation models.” Scott and Burgan’s system is unique in that fuel models are considered dynamic, meaning that live herbaceous fuel types can shift between live and dead, depending on a specified live herbaceous moisture content.

## 2.5 Role of Vegetation Moisture Content

### *2.5.1 Vegetation Moisture Content in Wildfire Models*

Verbesselt et al. (2007, 357) states, “The moisture content of fuels is one of the most important variables in fire ignition and behavior modeling and is included in most fire risk models worldwide.” Indeed, Rothermel (1972) acknowledges the major influence of fuel moisture on fire behavior: the drier the fuel, the hotter it will burn, while wetter fuels are less likely to burn. Dead wood with little moisture will retain about 10% water content while photosynthetically productive green vegetation can contain close to 300%. A saturation point or “moisture of extinction” hovers around 20-30% at which point vegetation will not burn (Flaxman 2001, 78). Dead fuel moisture is entirely contingent upon surrounding conditions whereas live vegetation is influenced by roots and shoots as well as soil moisture (Verbesselt et al. 2007). These environmental effects are accounted for within wildfire models by separate weather tables that include information such as air temperature, relative humidity, solar radiation (cloud cover), rainfall amount and duration, as well as by topographic factors like elevation, slope, aspect and canopy cover (Missoula Fire Sciences Laboratory 2011).

The NFDRS, FARSITE and FlamMap incorporate vegetation moisture content as percent moisture absorbed by dead forest litter from rain and humidity as compared to their dry weight (Flaxman 2001). FARSITE and FlamMap both use Nelson's (2000) model to determine dead fuel moisture, which calculates the amount of water absorbed or transpired from the surface of woody aboveground debris (assuming round wooden sticks)(Missoula Fire Sciences Laboratory 2011). Fuel moisture changes at a pace relative to fuel particle size; small twigs can absorb or transpire moisture within hours while large felled tree trunks can take hundreds or thousands of hours to reach equilibrium with the surrounding conditions.

For this reason, these models categorize the moisture state of fuel particles into fine fuels and 1, 10, 100 and 1000-hour fuels, which is the amount of time necessary to absorb or transpire 63.2% of its moisture content (Flaxman 2001; Missoula Fire Sciences Laboratory 2011). These fuel classifications correspond to round sticks ranging in sizes of 0-0.25 inches, 0.25-1 inch, 1-3 inches, and 3-8 inches respectively (Missoula Fire Sciences Laboratory 2011). Live vegetation with fuel moistures which have dropped below 30% are then categorized as dead fuels (Verbesselt et al. 2007), but it is important to remember that these live "dead" fuels will not exhibit the same behavior under modeled weather conditions as truly dead vegetation.

One drawback to these models is that moisture content of live vegetation, while accounted for, is assumed to remain spatially consistent (Verbesselt et al. 2007). Beginning a model run, downed woody debris also has homogeneous moisture content. Then after a "conditioning" period, weather patterns from the weather input files begin to influence the amount of water held by the dead woody matter until there is a more

realistic distribution of moisture content, if only for the dead vegetation. However, the programs ignore the spatio-temporal variability of moisture content across the live vegetation. Moisture content is not directly related to fire ignition, however it “is critical in fire propagation modeling because the amount of water in live vegetation is directly related to the rate of fire spread” (Verbesselt et al. 2007, 358). A recurrent climate scenario such as a drought can dramatically reduce the moisture content of the live vegetation as well as the dead woody debris (Gao, Gao and Chang 2011) through excessive evapotranspiration. However, crops and trees which may be irrigated or adjacent to streams will have much higher foliar moisture content and will be less likely to burn. The result is a dynamic range of moisture content across a wide variety of vegetation types.

Although the wildfire models themselves do not address live vegetation moisture, it is possible to include this information in the fuel model, such as in the Scott and Burgan (2005) fuel model. Vegetation moisture content is accounted for by assigning a level of curing in terms of percent to the fuel model based on the percentage of live herbaceous moisture content present. But before these values can be assigned, they must first be measured.

### *2.5.2 Remote Sensing of Vegetation Moisture Content*

Vegetation moisture content, also known as vegetation water content (VWC) is the total amount of water in stems and leaves, measured in kilograms per square meter (Yilmaz et al. 2008). A fractional component of VWC that represents leaves and canopies only is equivalent water thickness (EWT), which measures foliar water volume (cubic meters) per leaf area (square meters) (Yilmaz et al. 2008). EWT can be remotely

sensed due to high reflectivity in the near-infrared (NIR) and shortwave infrared (SWIR) portions of the electromagnetic spectrum (Ceccato, Flasse and Gregoire 2002; Cheng et al. 2006; Clevers, Kooistra and Schaepman 2010; Danson and Bowyer 2004; Davidson, Wang and Wilmshurst 2006; Gao 1996; Yilmaz et al. 2008). The Normalized Difference Infrared Index (NDII) approximates levels of EWT by taking advantage of the inverse relationship between SWIR and water content, and contrasting it with NIR (Ceccato, Flasse and Gregoire 2001; Yilmaz et al. 2008):

$$NDII = \frac{\rho_{0.85} - \rho_{1.65}}{\rho_{0.85} + \rho_{1.65}}$$

Where:

$\rho_{0.85}$  = reflectance at 0.85  $\mu\text{m}$

$\rho_{1.65}$  = reflectance at 1.65  $\mu\text{m}$

These estimates have been validated against *in situ* canopy water content measurement and were found to be reliable (Cheng et al. 2006; Rhee, Im and Carbone 2010). The VWC can then be derived from an allometric relationship with EWT (Sims and Gamon 2003), which has a linear relationship to NDII (Yilmaz et al. 2008). NDII was originally proposed by Hunt, Rock and Nobel (1987), and then redefined as the Normalized Difference Water Index (NDWI) by Gao (1996) who appreciated its similarity to the popular and simple Normalized Difference Vegetation Index (NDVI) (Rouse et al. 1974).

One challenge to estimating EWT using NDII is the need to calculate leaf area index (LAI) in the field (Verbesselt et al. 2007). Instead, foliar moisture content (FMC, also known as ‘fuel moisture content’ in terms of wildfire modeling), which also has a linear relationship to NDII, can be used to calculate water mass per mass of dry matter

(Danson and Bowyer 2004; Verbesselt et al. 2007). FMC as a variable is far more important for estimating fire risk than EWT or VWC because it affects fire ignition and propagation (Danson and Bowyer 2004; Verbesselt et al. 2007). Historically, FMC measurements were collected in the field or based on meteorological fire risk indices, but now can be estimated from satellite imagery which has been atmospherically, geometrically and radiometrically corrected (Danson and Bowyer 2004; Verbesselt et al. 2007). Verbesselt et al. (2006; 2007) utilized the French SPOT VEGETATION sensor to calculate NDII, and Davidson, Wang and Wilmshurst utilized the Landsat TM sensor. Both used the 1.58 – 1.75  $\mu\text{m}$  SWIR band (along with Landsat ETM+). Gao (1996) and Zarco-Tejada, Rueda and Ustin (2003) used the 1.24  $\mu\text{m}$  SWIR band found on MODIS while Cheng et al. (2006) conducted studies using both MODIS and AVIRIS. Landsat TM sensors produce imagery of a higher spatial resolution (30-meter) than MODIS (250/500/1000-meter) but the infrequent 16-day temporal coverage can be a limiting factor for some. Comparatively, MODIS is carried on two satellites, Aqua and Terra, allowing for twice-daily coverage for most locales.

### *2.5.3 Vegetation Moisture Content in Drought Conditions*

Drought is a normally occurring, complex climatological event (Gao, Gao and Chang 2011) that causes characteristic change in vegetation from unusually low precipitation and sometimes excessive heat (McVicar and Jupp 1998). It is recognized as an environmental disaster since drought leads to reduced water supply, deteriorated water quality, crop failure, altered riparian ecosystems, reduced rangeland, diminished power generation, and other detrimental social and economic repercussions (Mishra and Singh 2010). Droughts have the ability to affect more people than any other natural hazard, but

onset and conclusion occur gradually (Mishra and Singh 2010). In high biomass environments drought can increase wildland fire potential by creating highly combustible fuels. Lack of rainfall reduces the moisture content of both live and dead fuels, “thereby contributing to an increase in the overall availability and spatial connectivity of fuel that is sufficiently dry to burn” (Caccamo et al. 2011, 2626). Drought has historically been correlated with large fires in global forested/woodland regions, particularly in areas such as Africa (Mishra and Singh 2011) and Australia (Caccamo et al. 2011; McVicar and Jupp 1998). “Mapping the dynamic patterns of drought in high biomass ecosystems at medium spatial resolution (i.e. 500 m) provide the basis for: (i) monitoring the state, extent and connectivity of flammable fuels; and (ii) prediction of the potential for propagation of fires” (Caccamo et al. 2011, 2626).

The NFDRS’s Wildland Fire Assessment System relies on meteorological indices from weather data to address wildfire risk relative to drought conditions (U.S. Forest Service 2011). However, weather station networks are often sparse, particularly in the densely forested areas commonly under wildfire threat, and continuity is sometimes lacking. Remote sensing is a key method for providing near real-time monitoring of drought-related changes to vegetation with continuous coverage worldwide. The Advanced Very High Resolution Radiometer (AVHRR) sensor is the most frequently used for drought monitoring (Caccamo et al. 2011; McVicar and Jupp 1998) but Caccamo et al. (2011) argues that MODIS is superior due to a finer radiometric resolution in the SWIR bands.

## **CHAPTER III**

### **METHODOLOGY**

This study explores two key methodological aspects of wildfire behavior modeling in the wildland urban interface. The first section of the methodology chapter describes two distinct areas of study. The second section identifies all existing data sources as well as the measures taken to prepare the remaining required data. The third section defines the required steps and parameters to generate wildfire behavior maps produced from both satellite imagery-derived inputs and lidar-derived inputs. Additionally, steps are given for the spatial analysis of the resulting model raster outputs from both methods.

The third section also outlines how the same wildfire model was used again but this time under drought conditions, so vegetation moisture content is considered as an input. Wildfire behavior maps generated to address the first research question (created with the default setting of homogeneous vegetation fuel moisture) were compared against maps of the same area showing variable vegetation fuel moisture as measured from satellite imagery. Finally, the process is described for comparing pre-fire vegetation moisture patterns relative to burned and unburned areas within the burn scar perimeter of a particular wildfire to see if moisture content was significantly higher in the unburned areas.

### 3.1 Area of Study

In 2011, the Texas State Climatologist, John Nielsen-Gammon, declared the worst one-year drought on record for Texas with over 85% of the state listed in the Exceptional Drought category of the U.S. Drought Monitor (National Drought Mitigation Center 2011), as of the end of September 2011 (Figure 1).

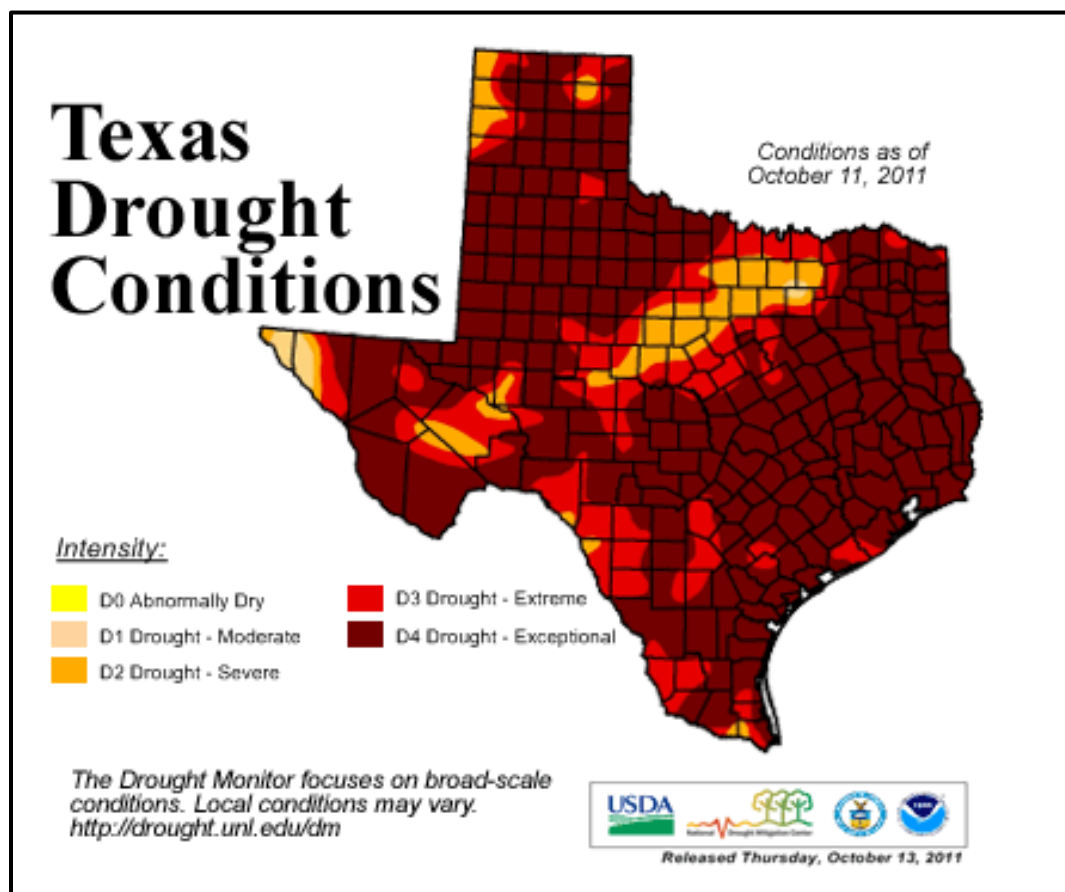


**Figure 1.** Texas Drought Map (The National Drought Mitigation Center 2011).

The state also experienced the hottest summer on record with an average temperature of 86.8°F (NOAA 2011). Dry vegetation coupled with exceptionally hot and windy weather patterns created an environment in Texas ripe for wildfire. During an

eleven month period from November 2010 to September 2011, the Texas Forest Service responded to 23,519 fires (Figure 2) that burned 3.8 million acres and destroyed 2,742 homes, although 34,756 homes were fortunately saved (Texas Forest Service 2011). Increasing population in Texas (Texas State Data Center 2011) has spurred development within the wildland urban interface, thus increasing risk of ignition and putting life and property in the direct path of wildfires. According to the Texas Forest Service (2011), in the two years preceding their report, 85% of the wildfires in Texas occurred within two miles of a community.

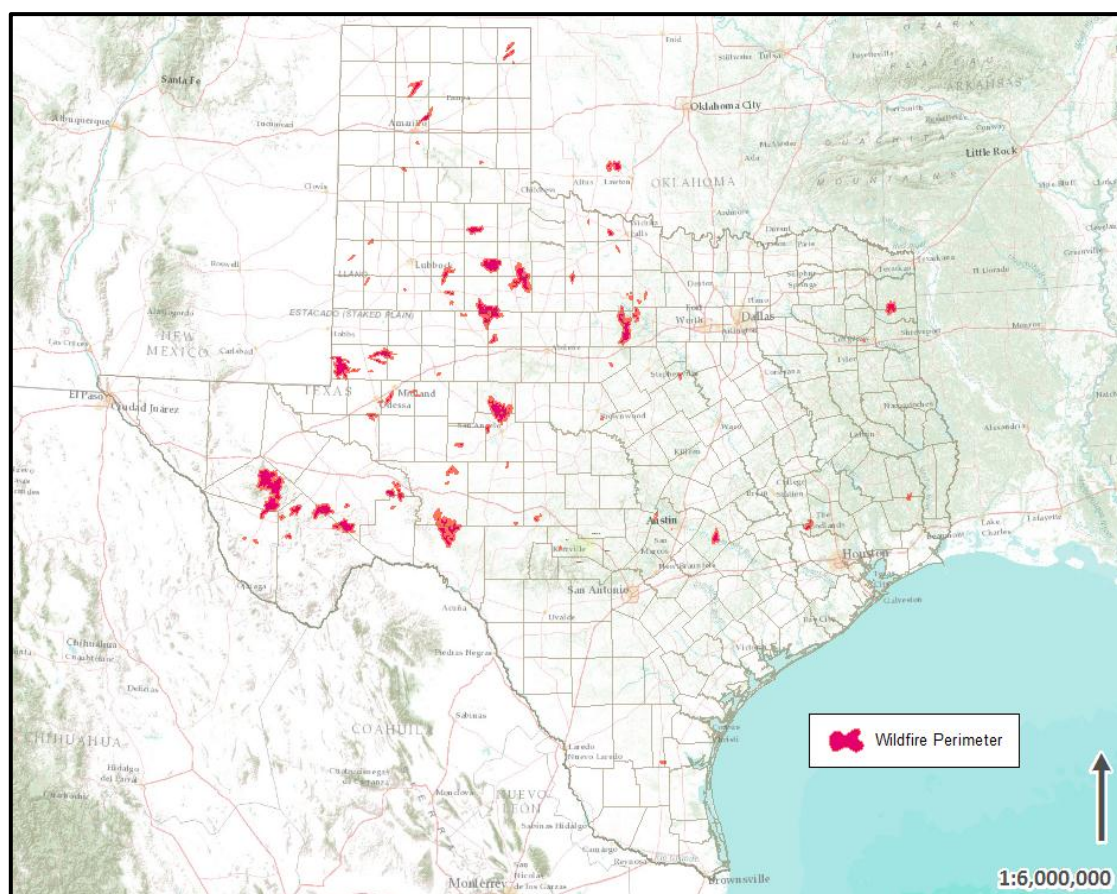


**Figure 2.** 2011 Wildfire Perimeters in Texas. Fire perimeter data obtained from the Texas Natural Resources Information System (2011).

Kerr County, Texas is an ideal area of study (Figure 3) to compare wildfire behavior maps from different source data due to a combination of factors: it exhibits the interface and intermix WUI pattern of development mixed with large, uninterrupted tracts of brush and forest; it is located in the Texas hill country where steeper topography can encourage fire spread (Lein and Stump 2009); the many parks and recreation facilities create opportunity for human sources of ignition; and finally, the area of study is covered by a 2011 lidar acquisition.

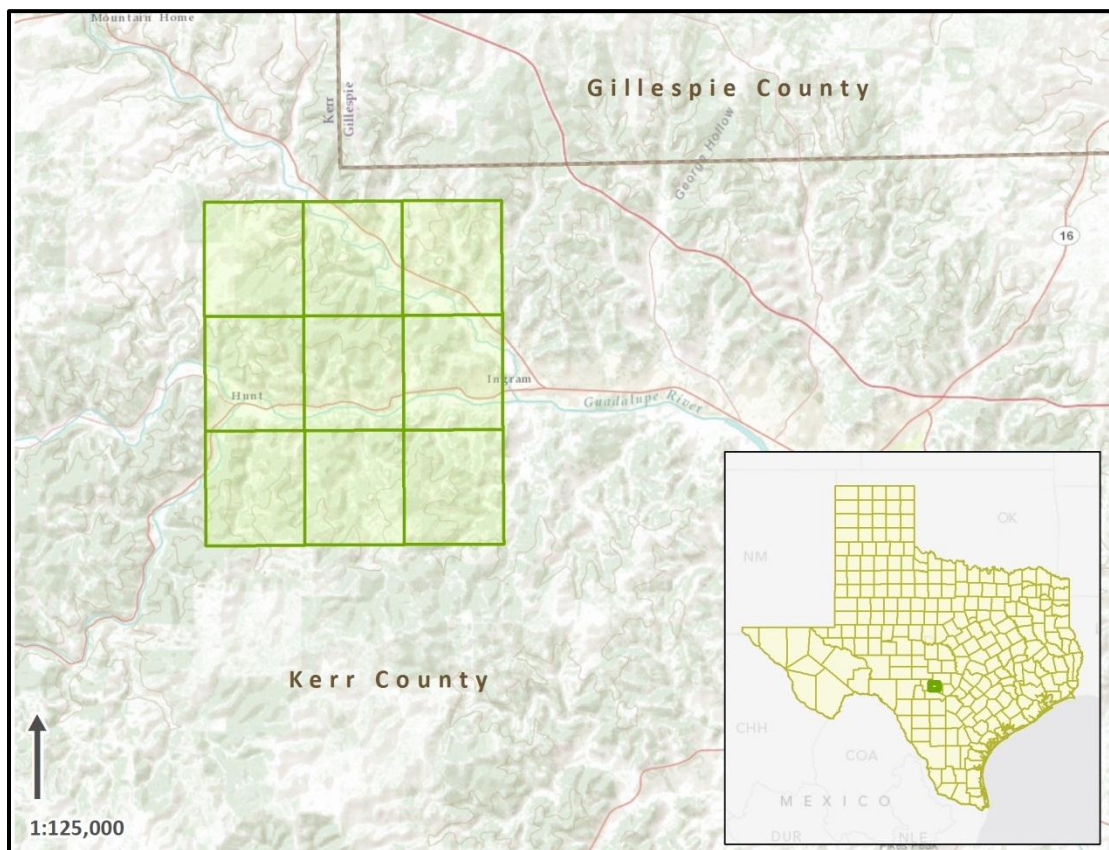


**Figure 3.** Study Area in Kerr County. Nine green tiles represent blocks of lidar data; each tile is approximately one square mile.

The study boundary was designed based on the tiling scheme of the source lidar, where each tile represents 1/16<sup>th</sup> of a USGS 7.5 minute map quadrangle. The study area does not extend to the whole county but includes 9 tiles adjacent to the City of Kerrville, covering the surrounding WUI (Figure 4) as defined by the University of Wisconsin SILVIS Lab (Radeloff et al. 2005). The Kerr study area spans approximately 30 square miles of Texas Hill country and includes the small towns of Hunt and Ingram settled along the Guadalupe River (Figure 5). Johnson Creek cuts across the northern bounds of the study area to join the Guadalupe River on the eastern side and evergreen-covered hills fill the space in between. More vegetated hilltops can be found in the study area south of the river, though tracts of forest here are fragmented by grassland and deciduous patches.

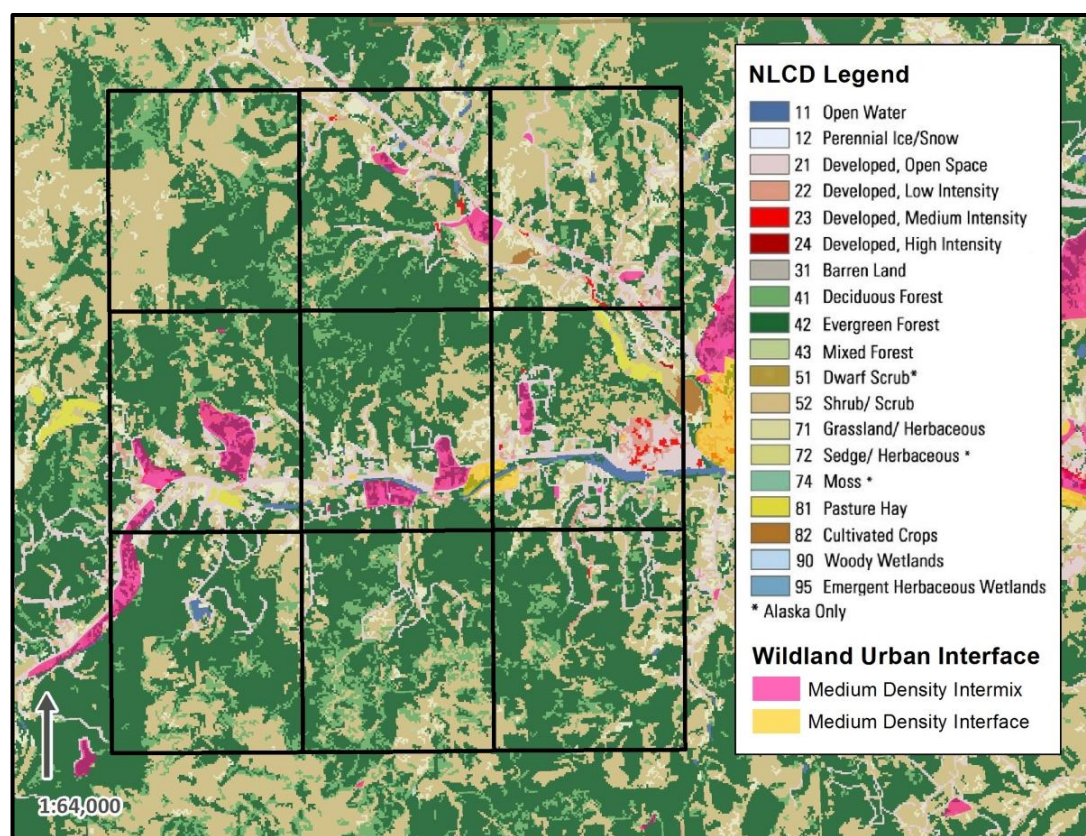


**Figure 4.** Land Cover and Wildland Urban Interface in Kerr Study Area. Land cover data from USGS National Land Cover Database (U.S. Geological Survey 2012) and WUI from the University of Wisconsin SILVIS Lab (Radeloff et al. 2005).

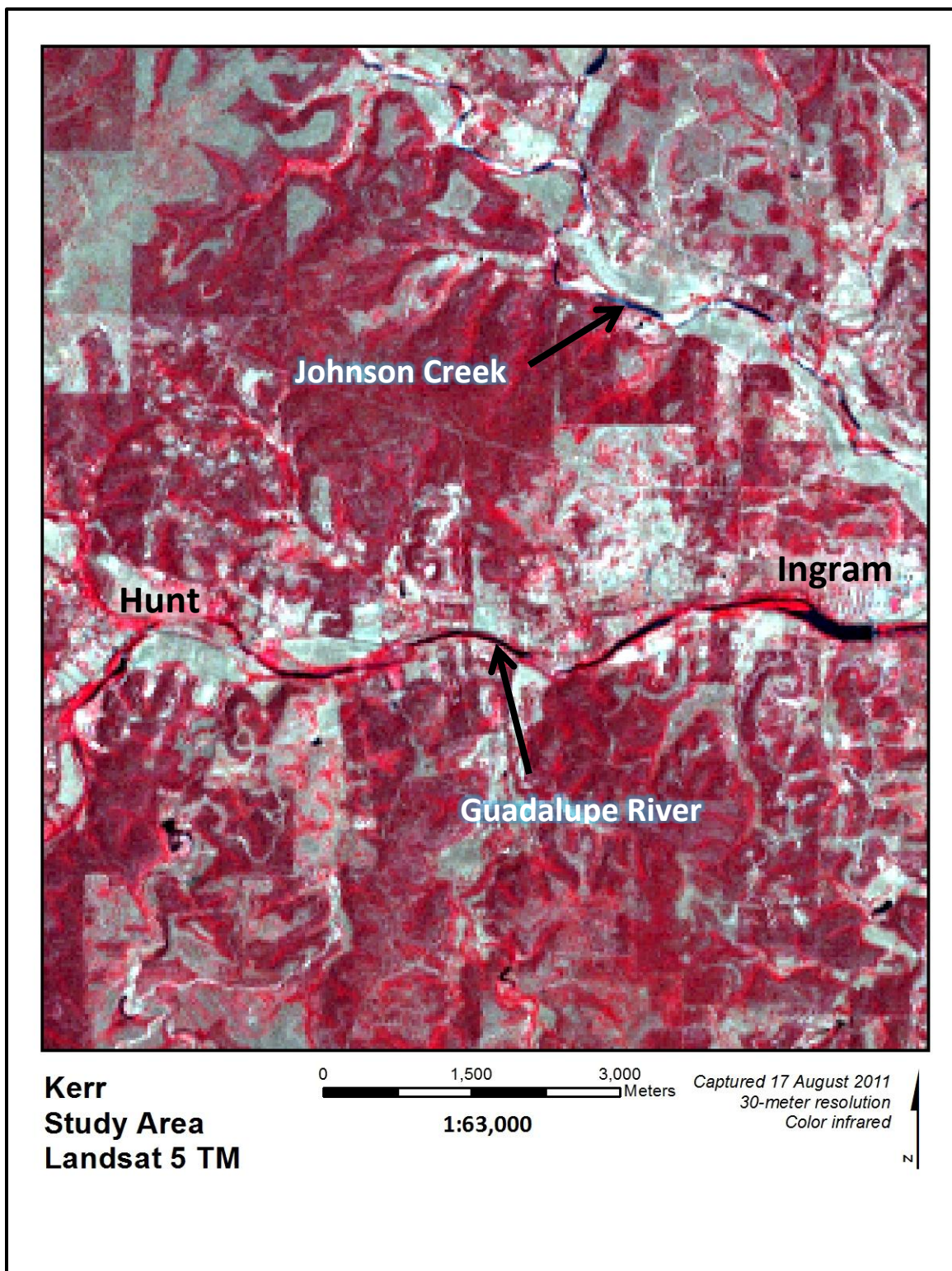


**Figure 5.** Kerr Study Area Landsat 5 TM. Enhanced image shown in color infrared (band combination 4,3,2). Image obtained from U.S. Geological Survey (2011).

This portion of central Texas lies on the elevated boundary of the Balcones Escarpment and according to the USGS National Land Cover Database (NLCD) is vegetated by an evergreen/deciduous forest mix (primarily evergreen) and shrubland (Fry et al. 2011). The evergreen mix is composed primarily of hardy Texas live oak (*Quercus fusiformis*) (Natural Resources Conservation Service 2012) and the scrubby Ashe juniper (*Juniperus ashei*), also known as Mountain Cedar (U.S. Forest Service 2012).

The second research question requires a WUI area in Texas that experienced a significant wildfire during the 2011 drought to compare pre-fire vegetation moisture patterns with post-fire burned areas. For the purposes of this study, a significant fire is defined as creating a burn scar area extending to at least 10,000 acres (4047 hectares), which is a sufficiently large extent to compare burned and remnant areas with 30-meter resolution Landsat imagery. Ideally this study site would be the same as that used for both research questions, however the wildfires in Kerr County (and those in surrounding areas with lidar coverage) were either not large enough to meet the project requirement, or were not in close proximity to a WUI.

Instead, a site near Possum Kingdom Lake (Figure 6) with similar land cover (Figure 7) to the Kerr AOI was selected for its large burn scar encompassing an interface WUI (Figure 8).

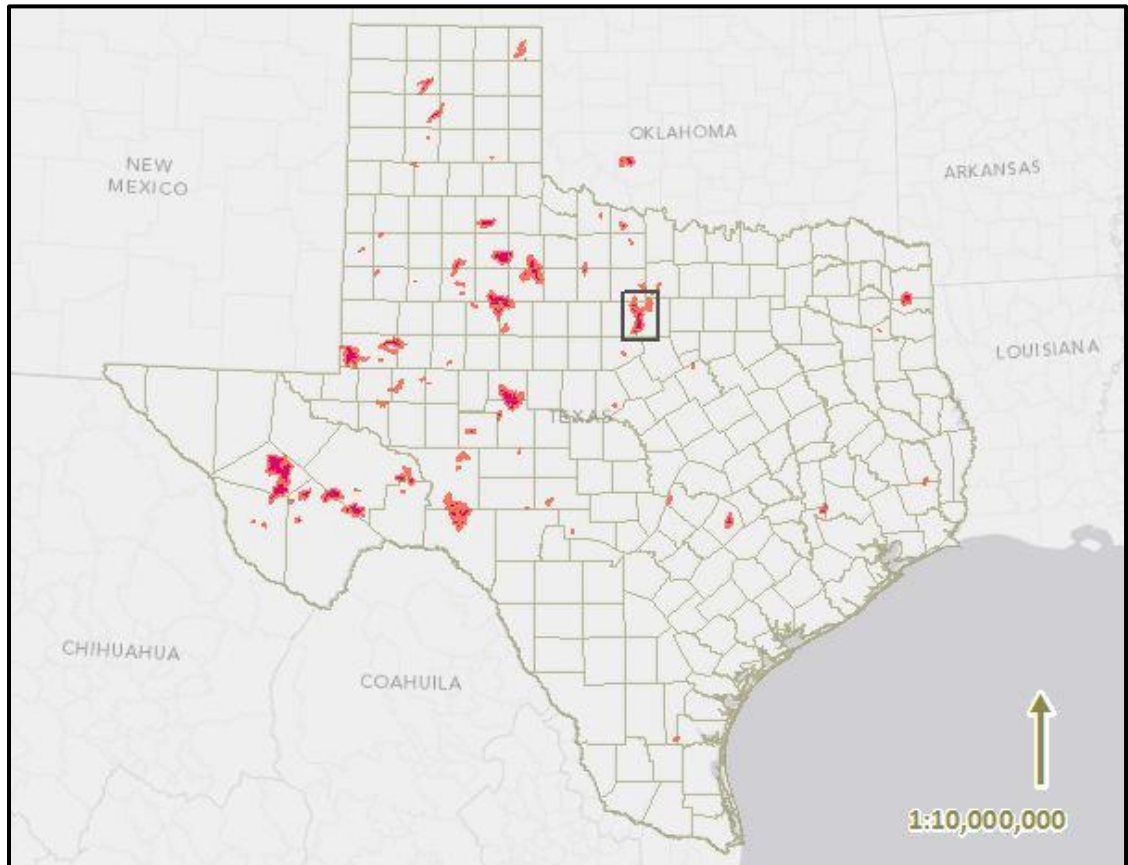


**Figure 6.** Possum Kingdom Wildfire Perimeter. Fire perimeter data obtained from the Texas Natural Resources Information System (2011).

Four fires began near the lake on April 13, 2011 and rapidly merged into one massive fire due to high winds and dry vegetation (Texas Forest Service 2011). The large fire was officially named the PK Complex Fire by the U.S. Forest Service and proceeded to destroy dozens of homes and force the evacuation of many more. The fire was 100%

contained by April 29, 2011, after burning through almost 150,000 acres (Figure 9) (Texas Forest Service 2011).

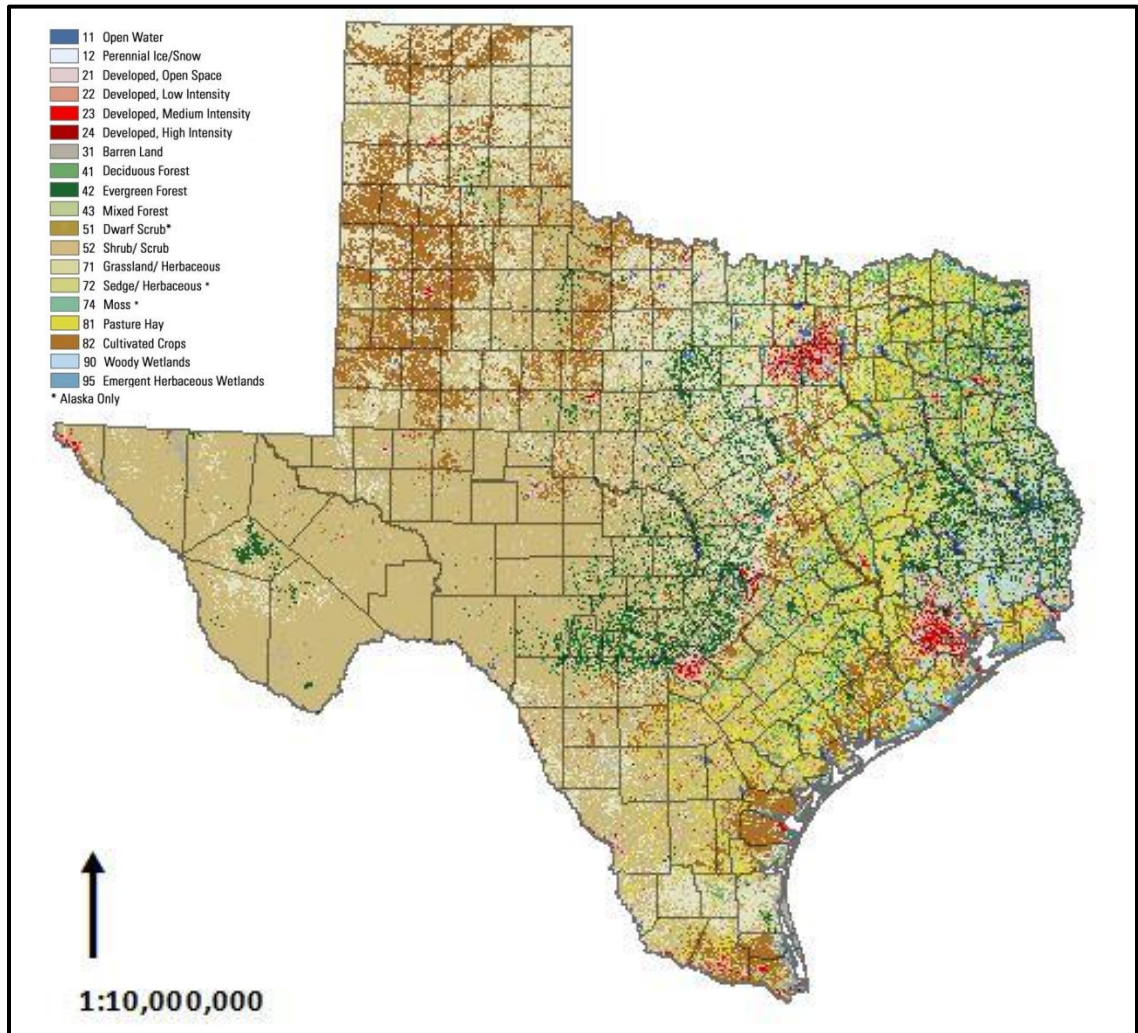


**Figure 7.** Land Cover in Texas. Data from USGS National Land Cover Database (U.S. Geological Survey 2012).

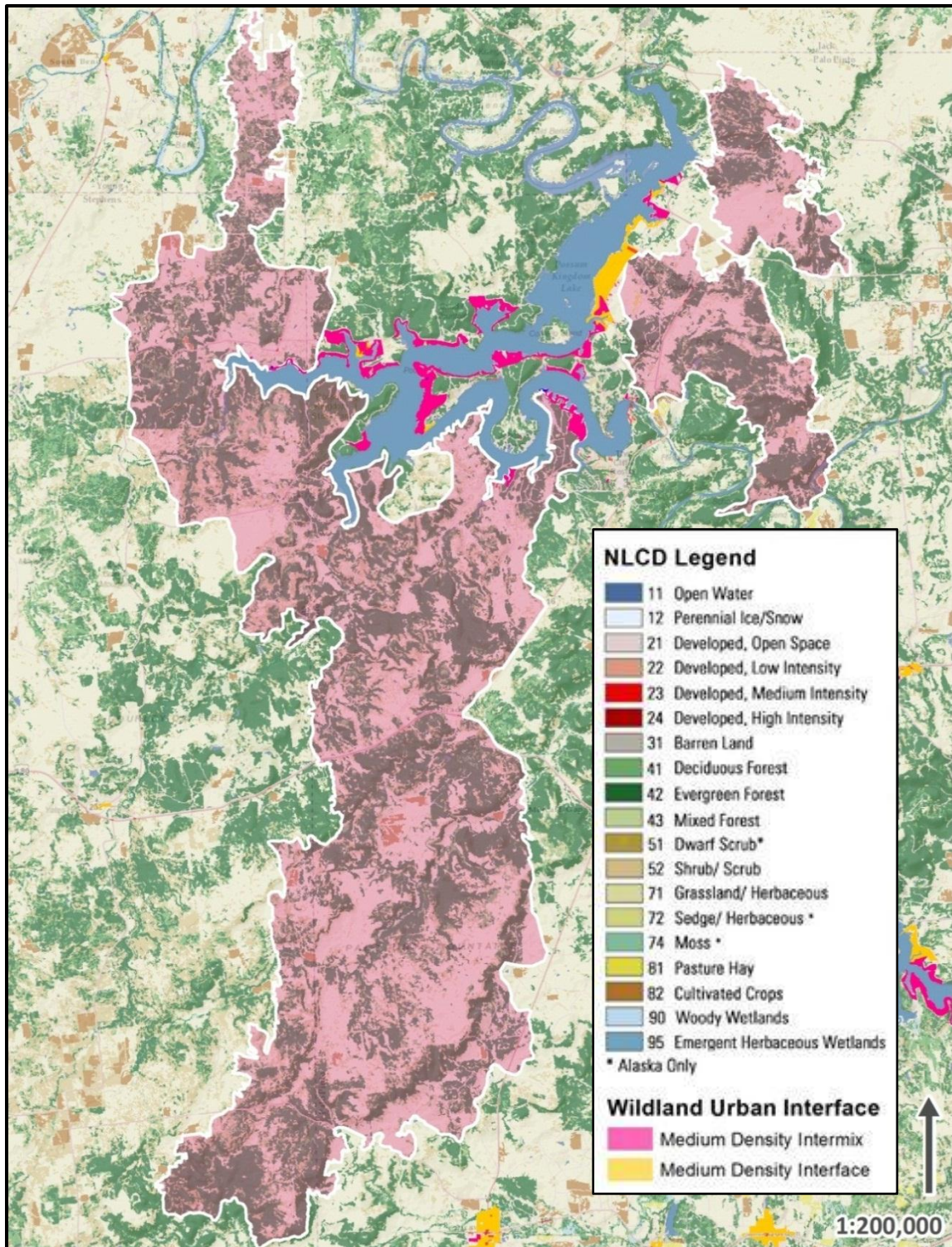


**Figure 8.** Possum Kingdom Complex Wildfire Burn Perimeter. Land cover data from USGS National Land Cover Database (U.S. Geological Survey 2012) and WUI from the University of Wisconsin SILVIS Lab (Radeloff et al. 2005). Fire perimeter data obtained from the Texas Natural Resources Information System (2011).

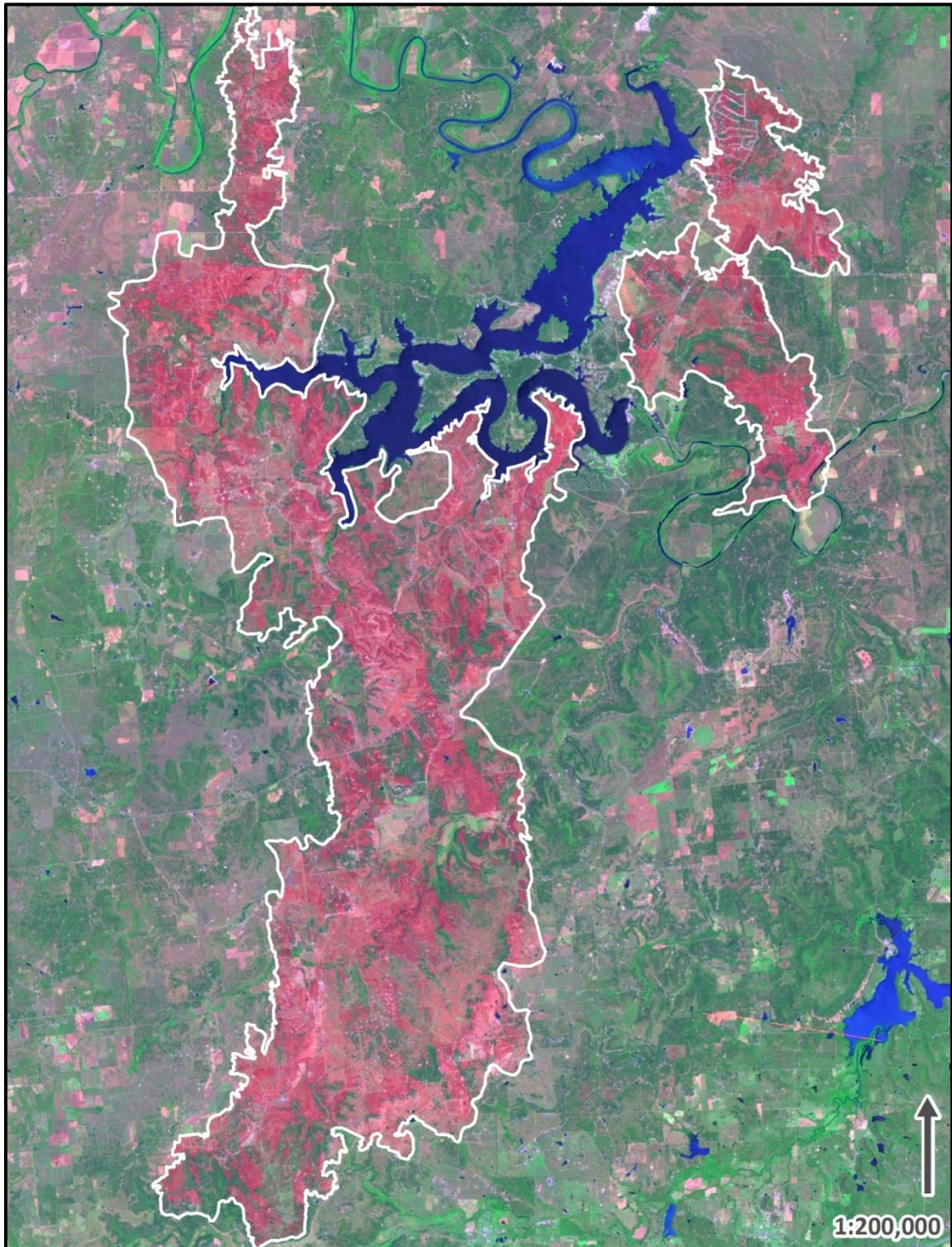


**Figure 9.** Landsat 5 TM Scene of Possum Kingdom Complex Burn Perimeter. Image captured May 2011 and acquired from U.S. Geological Survey (2011). Enhanced image shown in 7, 4, 2 band combination in which burned areas appear red and vegetation green. White outline with no fill delineates the burn scar and was obtained from the Texas Natural Resources Information System (2011).

### 3.2 Data Collection

All maps and data for this project were projected into Universal Transverse Mercator (UTM) Zone 14N using the horizontal North American Datum of 1983 (NAD83) with the vertical North American Vertical Datum of 1988 (NAVD88) referencing Geoid09. The primary reason for choosing UTM was to utilize a common projection for both study areas in north and central Texas but that would also minimize distortion for each and maintain units in metric (meters). Additionally, the lidar data were delivered in this projection.

#### *3.2.1 Existing Data Resources*

Much of the data used for this study were generated by external sources and were therefore already in existence. The data listed below are all freely available in the public domain via download from their respective websites or data order through TNRIS (Texas Natural Resources Information System 2011). The following datasets were necessary to gather for both study areas: WUI types and areas, land cover data, and Landsat TM satellite imagery. Data for the Kerr County area only includes: lidar point cloud, lidar-derived digital elevation model (DEM) and LANDFIRE raster data sets. Burn scar delineation for the PK Complex Fire was needed for the Possum Kingdom study area only and was created by the Texas Forest Service and provided by TNRIS (Texas Natural Resources Information System 2011).

The wildland urban interface areas in the U.S. are available online for download in an Esri (Esri 2012) polygon shapefile format from the University of Wisconsin SILVAS Lab (Radeloff et al. 2005). WUI areas were delineated by the SILVIS Lab into

four areas: High Density Intermix, Medium Density Intermix, High Density Interface and Medium Density Interface. The 2006 U.S. Geological Survey (USGS) National Land Cover Dataset (NLCD) covering the conterminous U.S. is available online for download from the Multi-Resolution Land Characteristics Consortium (Fry et al. 2011). There are 16 land cover classes which were generated from an unsupervised classification of Landsat Enhanced Thematic Mapper + (ETM+) satellite imagery from 2006 (Fry et al. 2011). The data are in a raster format at a 30-meter spatial resolution. Both the WUI areas and the NLCD were used to help define appropriate areas of study for this research.

Landsat 5 Thematic Mapper (TM) satellite imagery is available for free download via the USGS Global Visualization Viewer (GLOVIS) website from the Earth Resources Observation and Science Center (U.S. Geological Survey 2012). Landsat 5 TM scenes may be obtained as a Level 1T (terrain corrected) product including disaggregated TIF images for each of the seven bands recorded by the TM sensor. These Level 1T products were needed for the Possum Kingdom study area of the last cloud-free scene before the April 2011 PK Complex fire (hereafter called Before Fire), and the first cloud-free scene after the fire (hereafter called After Fire) was extinguished. The Before Fire image was captured two days before the fire on 11 April 2011 and the After Fire image was captured on 13 May 2011, approximately two weeks after the fire was contained. No rain was recorded for the area during this time period.

Another cloud-free set of Landsat 5 TM Level 1T products was required to cover the Kerr County study area for a late summer or early fall date coincident with the 2011 Texas drought. The image chosen to meet these requirements was captured on 17 August

2011 and was also obtained from the USGS GLOVIS website (U.S. Geological Survey 2012).

Small footprint high resolution discrete return airborne lidar in LAS 1.2 format was obtained from the Texas Natural Resources Information System (TNRIS), where the author is employed as the lidar project manager. The data were collected and post-processed by the engineering and geospatial firm Merrick & Company and third-party quality assurance and quality control (QA/QC) was conducted by URS Corporation to ensure the data met project specifications. The lidar was acquired between January and March 2011 during the leaf-off season and covers portions of Blanco, Caldwell, DeWitt, Gonzales, Kendall and Kerr Counties in central Texas, although only the data in the study area shown in Figure 2 will be studied. Merrick & Company deployed a Leica ALS-50II lidar sensor on a fixed wing aircraft and achieved an average point density of approximately six points per square meter, which equates to a ground sampling distance (GSD) of 0.4 meters.

Vertical accuracy was tested by URS Corporation according to standards from the National Standard for Spatial Data Accuracy and the RMSEz (vertical Root Mean Square Error) was reported at 0.06 meters. The data were classified into the following American Society for Photogrammetry and Remote Sensing (ASPRS) class schema: Class 1 Unclassified; Class 2 Ground; Class 4 Vegetation; Class 6 Buildings; Class 7 Low Point (noise); Class 9 Water; and Class 13 Bridges and Culverts (Figure 10) (American Society for Photogrammetry and Remote Sensing 2012). Data units are in meters and reference orthometric height above sea level.

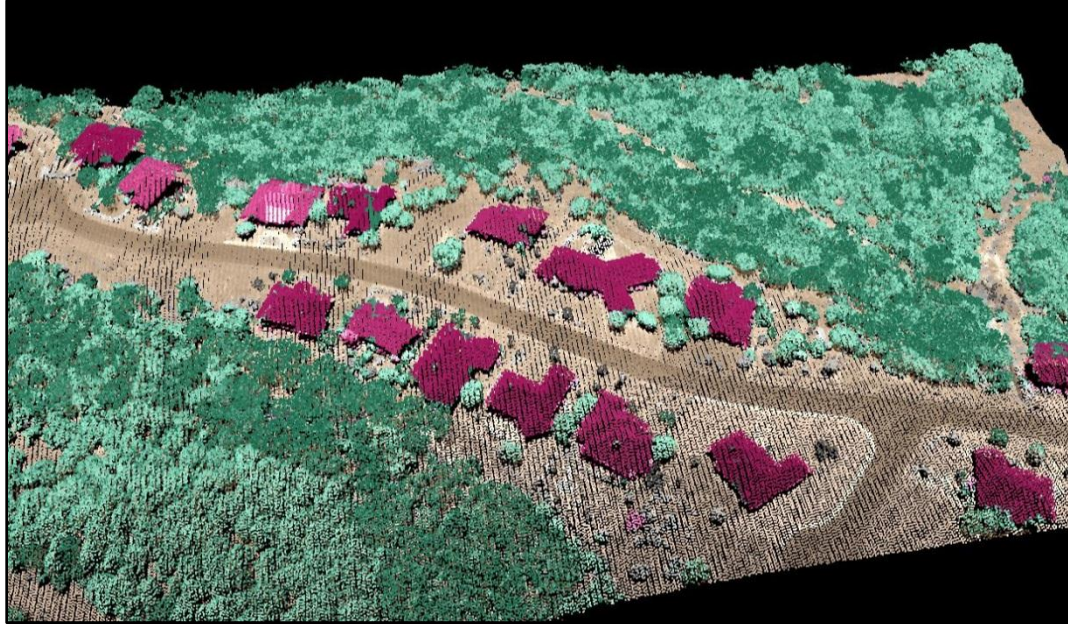


**Figure 10.** Lidar Sample in Kerr County. Point classifications shown with Ground in brown, Vegetation in green and Buildings in red. Data obtained from the Texas Natural Resources Information System (2011).

The 2011 lidar data are ideal for this application since the data are recent, were collected in leaf-off conditions allowing for greater canopy penetration and understory representation (Mutlu et al. 2008), are relatively dense for discrete-return lidar giving better estimation of canopy height (Shan and Toth 2008), include a vegetation class (ASPRS Class 4) for deriving vegetation metrics, and include a high resolution DEM for use in measuring topography.

The DEM for the first research question is an ancillary data product derived from the lidar and was included in the quality assurance and quality control (QA/QC) process. It was generated by Merrick & Company from a triangular irregular network (TIN) of the bare-earth lidar and then hydrologically-enforced for accurate hydraulic modeling. The DEM raster has a 1-meter pixel resolution with 32-bit floating point elevation values and is in ERDAS Imagine IMG format.

To generate a Landscape .LCP File, FlamMap requires a fuel model, canopy/crown base height (CBH), canopy/stand height (CH), canopy/crown bulk density (CBD), canopy/crown cover (CC), elevation, slope and aspect (Table 1).

**Table 1.** Eight Data Layers for FlamMap Listed by Source.

<b>Passive Remote Sensing</b>	<b>Lidar</b>		<b>Model</b>	<b>Abbreviation</b>
<i>LANDFIRE</i>	<i>CFE Tool</i>	<i>ArcGIS</i>	<i>FlamMap (.LCP)</i>	<i>All</i>
forest canopy cover		canopy cover	canopy cover	CC
forest canopy height		canopy height	stand height	CH
forest canopy bulk density	crown bulk density		crown bulk density	CBD
forest canopy base height	canopy base height		crown base height	CBH
NFFL fuel model		resampled NFFL	NFFL fuel model	NFFL
slope		slope	slope	N/A
elevation		elevation	elevation	DEM
aspect		aspect	aspect	N/A

The LANDFIRE raster data sets were obtained from the U.S. Department of Agriculture (2011b) and they were developed using satellite imagery from the Landsat 5 TM sensor. These LANDFIRE input rasters include: fuel model (NFFL fuel model inventory), forest canopy cover (CC), forest canopy height (CH), forest canopy bulk density (CBD), forest canopy base height (CBH), slope, elevation (DEM) and aspect. Temporal resolution falls along a spectrum between 2001 and 2011 and is dependent upon the selected area and data type. Like Landsat scenes, these data are delivered at a 30-meter spatial resolution.

LANDFIRE canopy cover was calculated from the Existing Vegetation Cover (EVC) dataset with the LANDFIRE Total Fuel Change toolbar created for ArcMap. Forested vegetation derived from EVC values was translated into canopy cover values using increments of 10 percent from 15-95 (U.S. Department of Agriculture 2011b). Canopy height was also calculated with the LANDFIRE Total Fuel Change toolbar.

The U.S. Department of Agriculture (2011b) estimated CBD values from 45,000 field plots spread throughout the U.S. They were able to model the surrounding CBD using the plot-level values within canopy fuel estimation software. Non-vegetated areas were coded as zero and certain hardwood stands resistant to crown fire were given extremely low values. Finally, canopy base height was computed using datasets for Existing Vegetation Height, Existing Vegetation Type, and Existing Vegetation Cover to determine the most logical CBH value for a given area.

Additional detail for all LANDFIRE data creation methods can be found in U.S. Department of Agriculture (2011b) LANDFIRE metadata. It should be noted that LANDFIRE layers will not include canopy characteristics in fuel types where the tree canopy is considered a part of the surface fuel and the surface fire behavior fuel model is chosen to reflect these conditions. This is because LANDFIRE assumes that the potential burnable biomass in the shorter tree canopies has been accounted for in the surface fuel model parameters. For example, “maps of areas dominated by young or short conifer stands where the trees are represented by a shrub type fuel model will not include canopy characteristics” (U.S. Department of Agriculture 2011b).

### *3.2.2 Data Preparation for FlamMap*

Whereas the data listed in section 3.2.1 were already in existence and obtained from external sources, other datasets had to be generated from the raw data using various techniques and software packages. The vegetation metrics outlined in this section were all generated from the lidar data (LAS format) or data products (DEM raster) and then converted to rasters (ASC format) to run in FlamMap. Since the point density of the lidar was able to support a 1-meter DEM, it would have been possible to generate the

vegetation rasters at the same resolution. However, a 5-meter resolution was chosen instead to provide a cell size large enough to aggregate the information of one tree. It is possible that a smaller 1-meter window would produce a noisy output with many intermittent null or erroneous values between cells with actual measured values.

The 1-meter DEM was re-sampled to 5-meters in ERDAS Imagine using the nearest neighbor technique to match the 5-meter spatial resolution of the other lidar-based model inputs. Nearest neighbor was chosen to preserve the actual elevation values derived from the lidar as opposed to the smoothing effect of a higher order interpolation method.

The U.S. Department of Agriculture (2011a) developed publicly available software called Canopy Fuel Estimator (CFE) to calculate vegetation canopy characteristics from a three dimensional lidar point cloud. The tool separates the ground points from all other points to generate a surface model (Figure 11) and then computes metrics on the lidar point cloud. These vegetation metrics are based on the methodology proposed by Naesset (1997) and they include point count, point density ( $D$ ), point density above 2.0 meters, minimum height, maximum height, mean height, standard deviation of height, coefficient of variation ( $h_{cv}$ ) and finally, height at the 5<sup>th</sup>, 10<sup>th</sup>, 25<sup>th</sup>, 50<sup>th</sup>, 75<sup>th</sup>, 90<sup>th</sup>, and 95<sup>th</sup> percentile of maximum height ( $h_5$ ,  $h_{10}$ ,  $h_{25}$ ,  $h_{50}$ ,  $h_{75}$ ,  $h_{90}$ , and  $h_{95}$ ).

These metrics can then be plugged into a set of predetermined model equations in the CFE software which references the Andersen, McGaughey and Reutebuch (2005) predictive models for calculating canopy bulk density and canopy base height. The models were intended for forests in western and eastern Washington which are

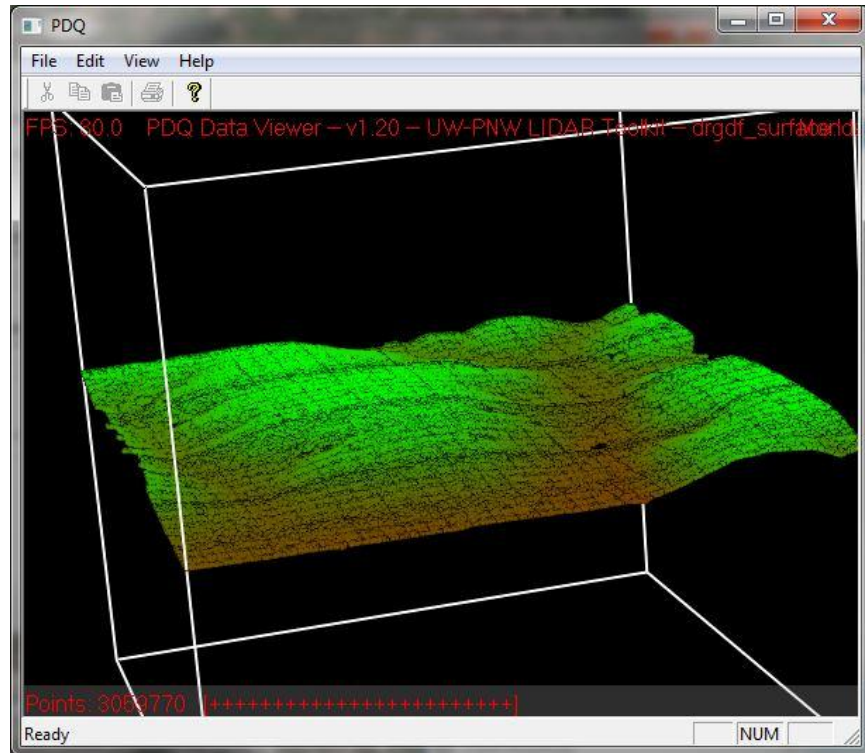


**Figure 11.** Canopy Fuel Estimator Surface Model (U.S. Department of Agriculture 2011a).

characteristically very different than the live oak and Ashe juniper land cover in central Texas. However, due to a dearth of options for deriving these metrics from lidar, this study relies upon the same models for an alternate land cover.

The Andersen, McGaughey and Reutebuch (2005) model for canopy bulk density is:

$$\ln(\text{canopy bulk density}) = -4.3 + (3.2)h_{cv} + (0.02)h_{10} + (0.13)h_{25} + (-0.12)h_{90} + (2.4)D$$

Where:

$h_{cv}$  = coefficient of variation

$h_{10}$  = height at the 10<sup>th</sup> percentile

$h_{25}$  = height at the 25<sup>th</sup> percentile

$h_{90}$  = height at the 90<sup>th</sup> percentile

$D$  = point density

and the model for canopy base height is:

$$\text{canopy base height} = 3.2 + (19.3)h_{cv} + (0.7)h_{25} + (2.0)h_{50} + (-1.8)h_{75} + (-8.8)D$$

Where:

$h_{cv}$  = coefficient of variation

$h_{25}$  = height at the 25<sup>th</sup> percentile

$h_{50}$  = height at the 50<sup>th</sup> percentile

$h_{75}$  = height at the 75<sup>th</sup> percentile

$D$  = point density

The authors collected field measurements to test the predictive lidar models and found that the CBD model had a coefficient of determination of 0.84 and the CBH model had a coefficient of determination of 0.77.

The spatial resolution of the outputs is user-defined and can be set in the CFE tool before running the models (Figure 12). When a model is run, the output is a comma delineated text file in .csv format which includes the metric calculated, row number, column number, X-coordinate and Y-coordinate in UTM meters (set by user).

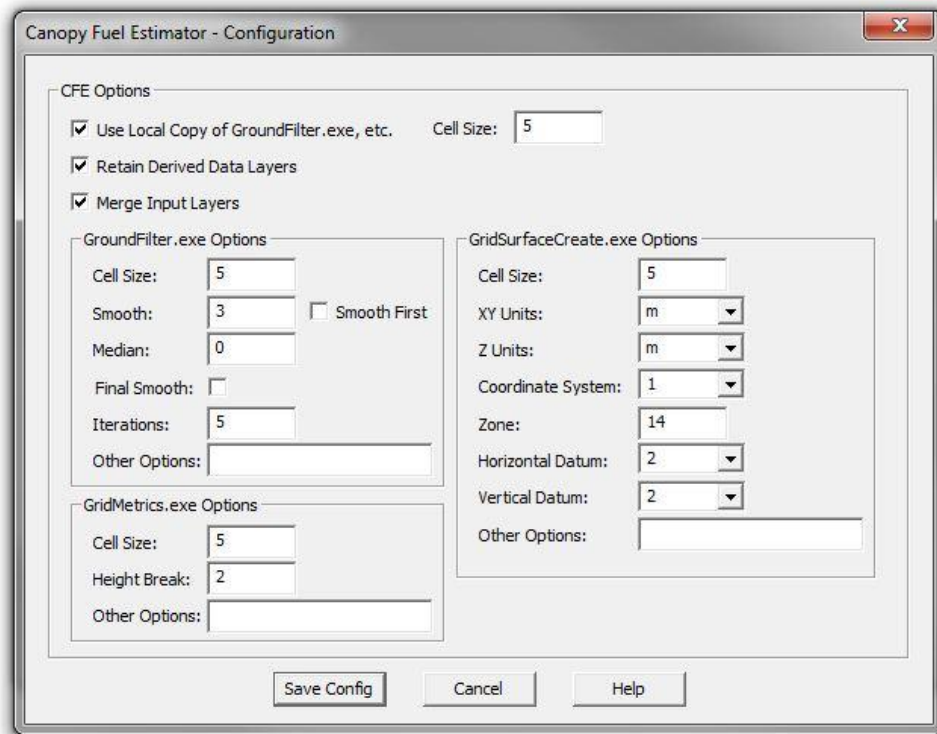


**Figure 12.** Canopy Fuel Estimator Configuration (U.S. Department of Agriculture 2011a).

Although the CFE tool is capable of calculating CBH, CH, CBD and canopy fuel weight, FlamMap does not require canopy fuel weight and so it was not calculated for this project. The NFFL fuel model used for Flam Map (Table 2) is only available at a 30-meter resolution and so the NFFL file downloaded with the LANDFIRE data (Figure 13) was also used for the lidar portion but resampled to 5-meter using ERDAS Imagine. Additionally, CH was not calculated from CFE, but was created via another means to be discussed below and canopy cover (CC) is not available from CFE and so was also created separately. The remaining two input variables, CBH and CBD, were calculated from the lidar using the CFE tool for input into FlamMap.

The first step was to strip the lidar covering the Kerr study area of all classes except for Class 2 Ground and Class 4 Vegetation in an effort to eliminate potential sources of error during calculation of the vegetation metrics. The CFE does not distinguish between the ASPRS lidar classifications and would have treated such things as buildings, light poles and noise points as vegetation, leading to many erroneous raster cell values during processing. This data manipulation process to reduce the classes was conducted using the Export tool in Merrick's MARS lidar software.

To prevent the CFE tool from maxing out computer RAM during calculations (it can access only one processing core at once), the lidar data was tiled and split into 108 smaller files so as not to exceed a file size of approximately 500 megabytes (MB). This is the approximate threshold before the CFE tool is overwhelmed and crashes.

For the CFE parameters, the spatial reference information was set to UTM with units in meters and an output spatial resolution of five meters was selected to compromise between long processing time for a higher resolution and loss of detail for a lower resolution. Each of these 108 LAS files were run through the CFE individually to create 108 output .csv text files which include fields for both CBH and CBD values. The 108 text files were aggregated to 11 Microsoft Excel files (.xlsx) in Microsoft Access for ease of manipulation but also to avoid surpassing the total number of records per spreadsheet allowed in Microsoft Excel (~1 million).

**Table 2.** NFFL Fuel Model Data Dictionary (U.S. Department of Agriculture 2011b)

FBFM1	Surface fires that burn fine herbaceous fuels, cured and curing fuels, little shrub or timber present, primarily grasslands and savanna
FBFM2	Burns fine, herbaceous fuels, stand is curing or dead, may produce fire brands on oak or pine stands
FBFM3	Most intense fire of grass group, spreads quickly with wind, one third of stand dead or cured, stands average 3 ft tall
FBFM4	Fast spreading fire, continuous overstory, flammable foliage and dead woody material, deep litter layer can inhibit suppression
FBFM5	Low intensity fires, young, green shrubs with little dead material, fuels consist of litter from understory
FBFM6	Broad range of shrubs, fire requires moderate winds to maintain flame at shrub height, or will drop to the ground with low winds
FBFM7	Foliage highly flammable, allowing fire to reach shrub strata levels, shrubs generally 2 to 6 feet high
FBFM8	Slow, ground burning fires, closed canopy stands with short needle conifers or hardwoods, litter consist mainly of needles and leaves, with little undergrowth, occasional flares with concentrated fuels
FBFM9	Longer flames, quicker surface fires, closed canopy stands of long-needles or hardwoods, rolling leaves in fall can cause spotting, dead-down material can cause occasional crowning
FBFM10	Surface and ground fire more intense, dead-down fuels more abundant, frequent crowning and spotting causing fire control to be more difficult
FBFM11	Fairly active fire, fuels consist of slash and herbaceous materials, slash originates from light partial cuts or thinning projects, fire is limited by spacing of fuel load and shade from overstory
FBFM12	Rapid spreading and high intensity fires, dominated by slash resulting from heavy thinning projects and clearcuts, slash is mostly 3 inches or less
FBFM13	Fire spreads quickly through smaller material and intensity builds slowly as large material ignites, continuous layer of slash larger than 3 inches in diameter predominates, resulting from clearcuts and heavy partial cuts, active flames sustained for long periods of time, fire is susceptible to spotting and weather conditions
Urban	Urban
Snow/Ice	Snow/Ice
Agriculture	Agriculture
Water	Water
Barren	Barren

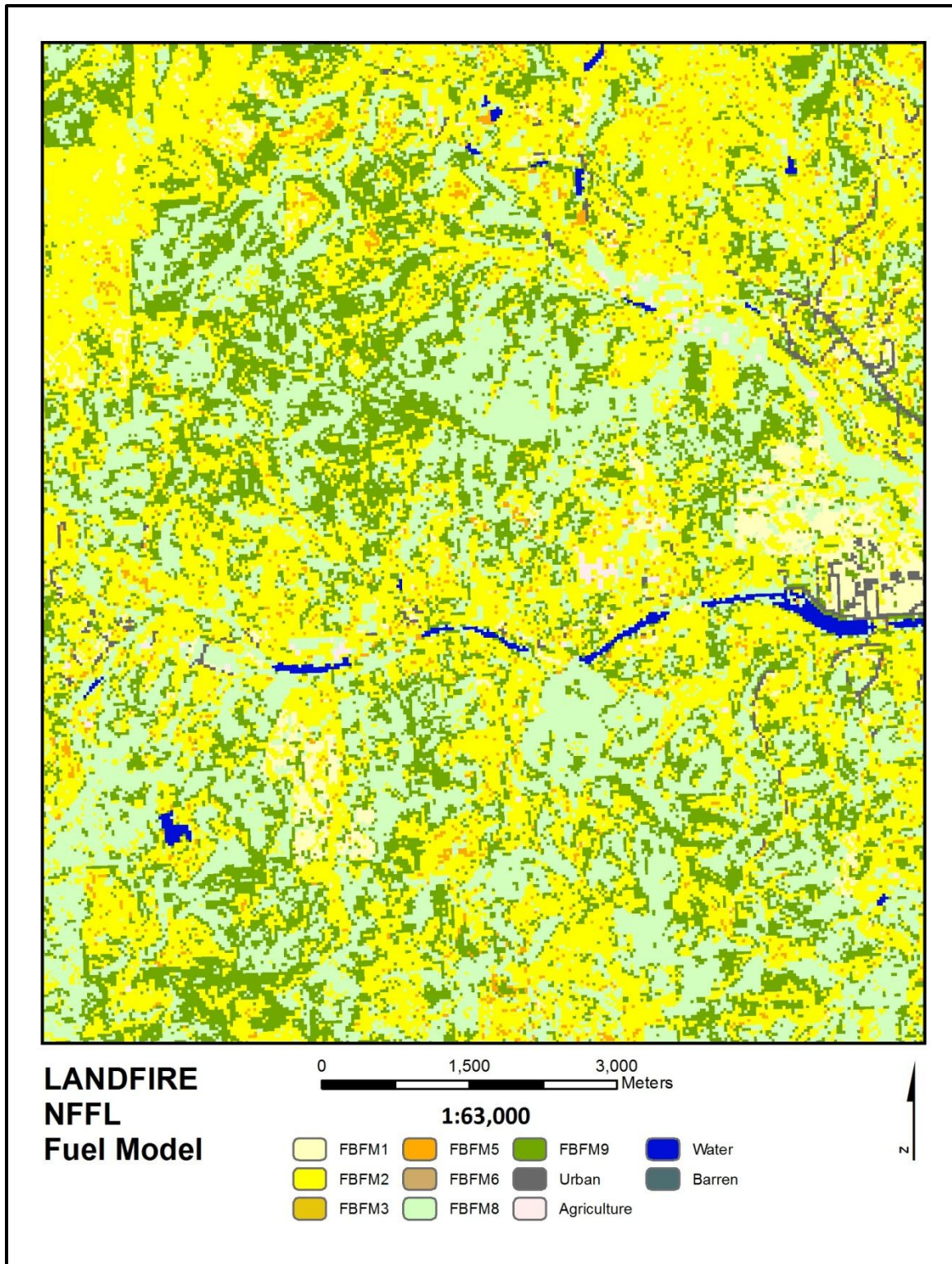


**Figure 13.** LANDFIRE NFFL Fuel Model. Pixel resolution is 30 meters. See Table 2 for data dictionary.

The 11 Excel files were then converted into points using the Add XY Data tool in ArcMap. The points were projected but not defined, so after a UTM projection definition was applied to each file they were merged into one large point file covering the entire Kerr study area. Since the CBD measurements exported from the CFE tool are actually the natural log of the CBD, expressed as  $\ln(x)$ , the values were converted using the formula:

$$\text{Canopy Bulk Density} = e^x$$

The float values converted from the natural log format represent kilograms per cubic meter, which matches the unit designation for the LANDFIRE dataset.

At this point, both the CBH and CBD values are still in the master point attribute table. This master point file was then converted first into a CBH raster in ERDAS .img format using the ArcMap Point to Raster tool and then to a CBD raster in ERDAS .img format. Each point represents the center of a raster cell and the raster resolution for each file was set at five meters.

Due to the complications from reducing file size to use the CFE tool, canopy/stand height was generated via another means. Canopy height can be calculated from the difference of the digital surface model (DSM) and the bare earth DEM (Zhao, Popescu and Nelson 2009). This was accomplished using MARS to generate a 5-meter DSM from all last-return lidar points in Class 2 Ground or Class 4 Vegetation. The 5-meter bare-earth DEM was already available. Using ArcMap's Raster Calculator, the DEM was subtracted from the DSM to create a difference raster representing canopy height.

Since canopy cover is not computed by the CFE tool but is required in FlamMap, it was necessary to create a custom methodology. Canopy cover derived from lidar is the ratio of vegetation points relative to all point returns expressed in percent (Lefsky et al. 1999). To achieve this ratio as percent canopy cover in raster form, it is necessary to generate a raster showing a count of vegetation points and another raster showing a count of all points for a given cell size (in this case 5-meter). ArcMap includes a tool to produce a raster from a point dataset with cell values showing point count, however ArcMap 10 does not recognize the LAS format.

To work around this limitation, all of the lidar was first converted into multipoint before the point count rasters were generated in Erdas IMG format. Although technically irrelevant as the final product is a ratio, each multipoint represented 100 lidar returns. To achieve the percent canopy cover as a ratio, the final output must be in floating point. Since it includes floating point as an output parameter, the ERDAS Imagine function Two Input Operators was used to divide the Vegetation Points raster by the All Points raster. The resulting product was canopy cover in IMG raster format.

Next, Esri's (2012) Spatial Analyst tool was used to calculate a 5-meter slope raster and a 5-meter aspect raster from the lidar-derived 1-meter DEM (Figure 14). The very last hurdle to prepare the data for input into FlamMap was to align all

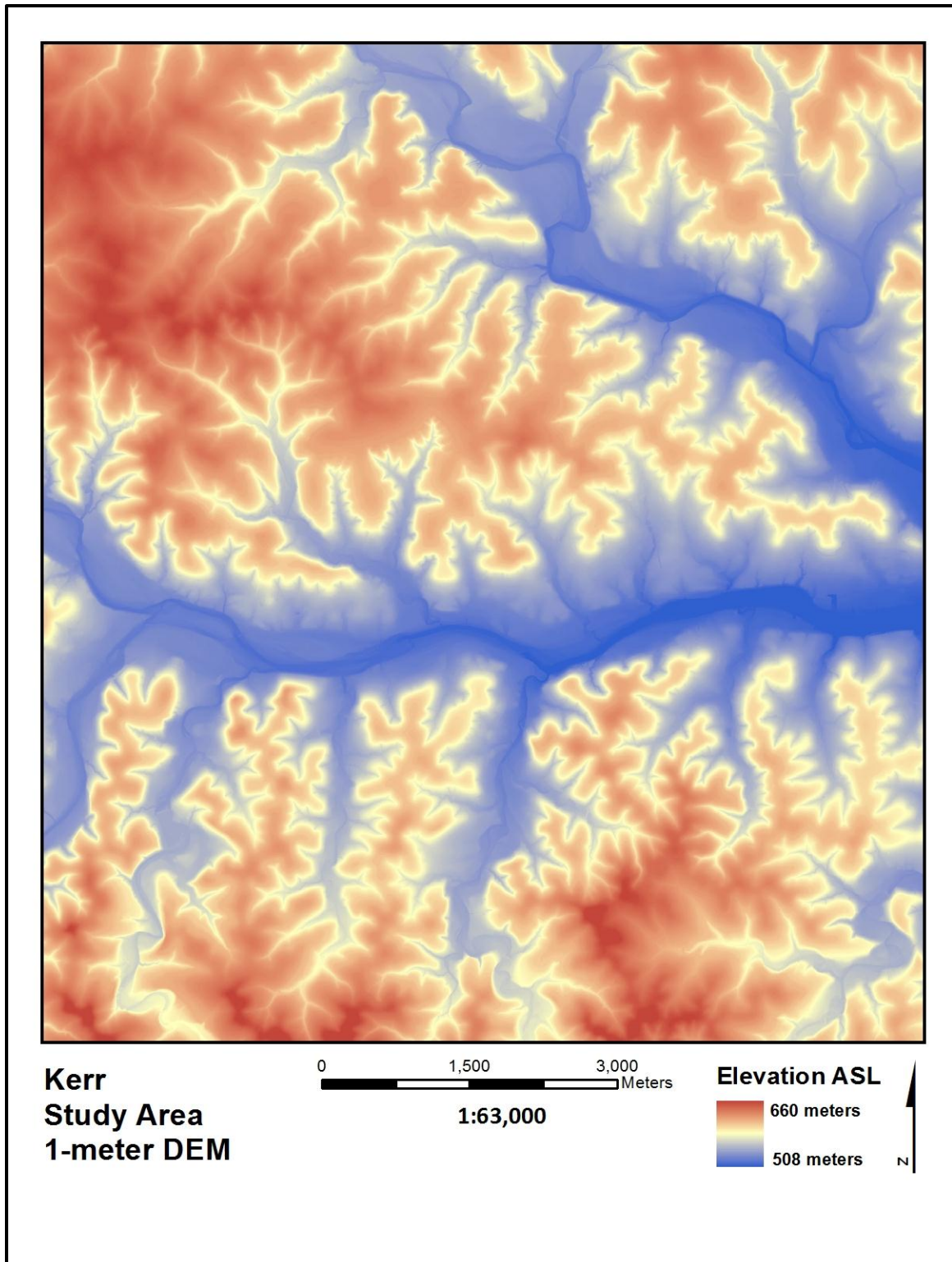


**Figure 14.** Kerr Study Area 1-meter DEM. Data obtained from Texas Natural Resources Information System (2011).

input rasters so that each pixel of each file was exactly coincident with the corresponding pixel in all other files. The rasters must also have the exact same spatial extent including an identical number of rows and columns. The elevation-based datasets – DEM, slope and aspect – already had a perfectly aligned extent because slope and aspect were both generated from the DEM file which had been clipped by the shapefile of the study area. However, the other files – NFFL fuel model, CBH, CBD, CH and CC – had pixels which were slightly shifted from the elevation files (Figure 15), usually only a few centimeters in any direction, and also may have had an extra row or two in either the X or Y direction.

The ArcMap Environment setting to snap rasters to a selected file did not work as anticipated, so another method was employed. The 5-meter slope file was chosen (randomly of the three elevation files) to generate a reference point file which would provide a means to spatially “correct” the other shifted rasters with the slope values being irrelevant. Using ArcMap’s Raster to Point tool, a point was generated representing the centerpoint of each slope raster pixel. This reference point file was then used in the ArcMap Extract Multi-Values to Point tool with each of the shifted rasters. The result is five new fields in the reference point file that contains values for NFFL, CBH, CBD, CH and CC. From the reference point shapefile, new rasters for each of these inputs were generated using ArcMap’s Point to Raster tool. The very last step to prepare the files for modeling was to convert all files from the interoperable IMG format into ASCII, the native format of FlamMap.

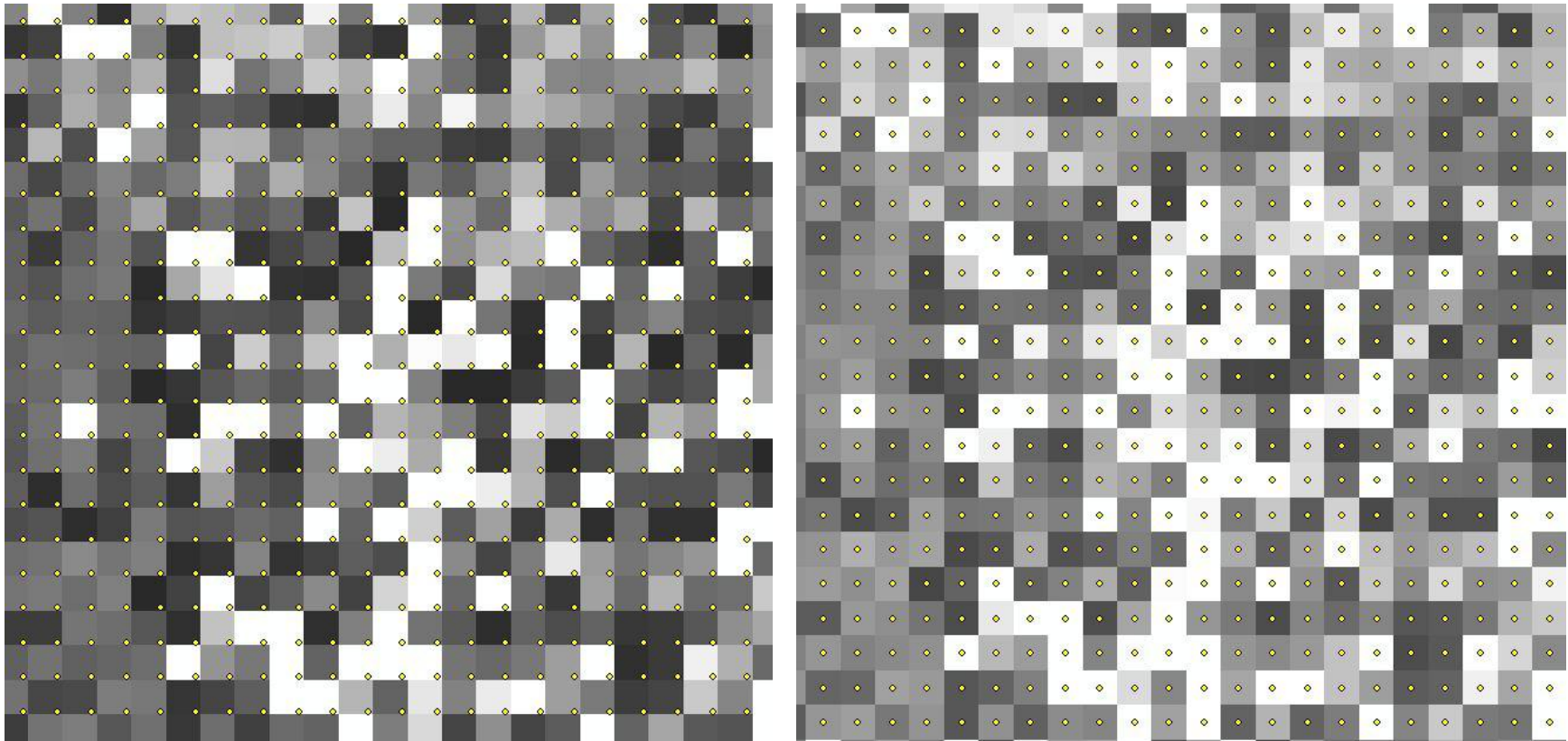


**Figure 15.** Rasters Aligned to Points. *Left*, Before alignment; *right*, After alignment.

### 3.3 Wildfire Modeling

#### *3.3.1 Model Setup for Research Question I*

To address the first research question, it is necessary to compare diverse wildfire modeling techniques in a wildland urban interface to determine differences in output from using lidar-derived input data compared to satellite imagery-derived data (LANDFIRE). These techniques are respectively referred to as the lidar method and the LANDFIRE method (Figure 16). To perform an accurate comparison of outputs derived from dissimilar inputs, the same software model was employed for both simulations. FARSITE and FlamMap are wildfire models which both produce data in a spatial raster output, compared to other modeling systems which export tables, graphs and charts (Missoula Fire Sciences Laboratory 2011). FARSITE and FlamMap have the exact same input parameter files, but FARSITE includes a temporal component so that conditions vary in both time and space. Since analysis of temporal changes in addition to spatial variation between iterations with different inputs is outside the scope of this project, FlamMap was used for the analysis. Each data input (from the lidar method and the LANDFIRE method) was inserted into the model along with other key model variables as listed in Table 1.

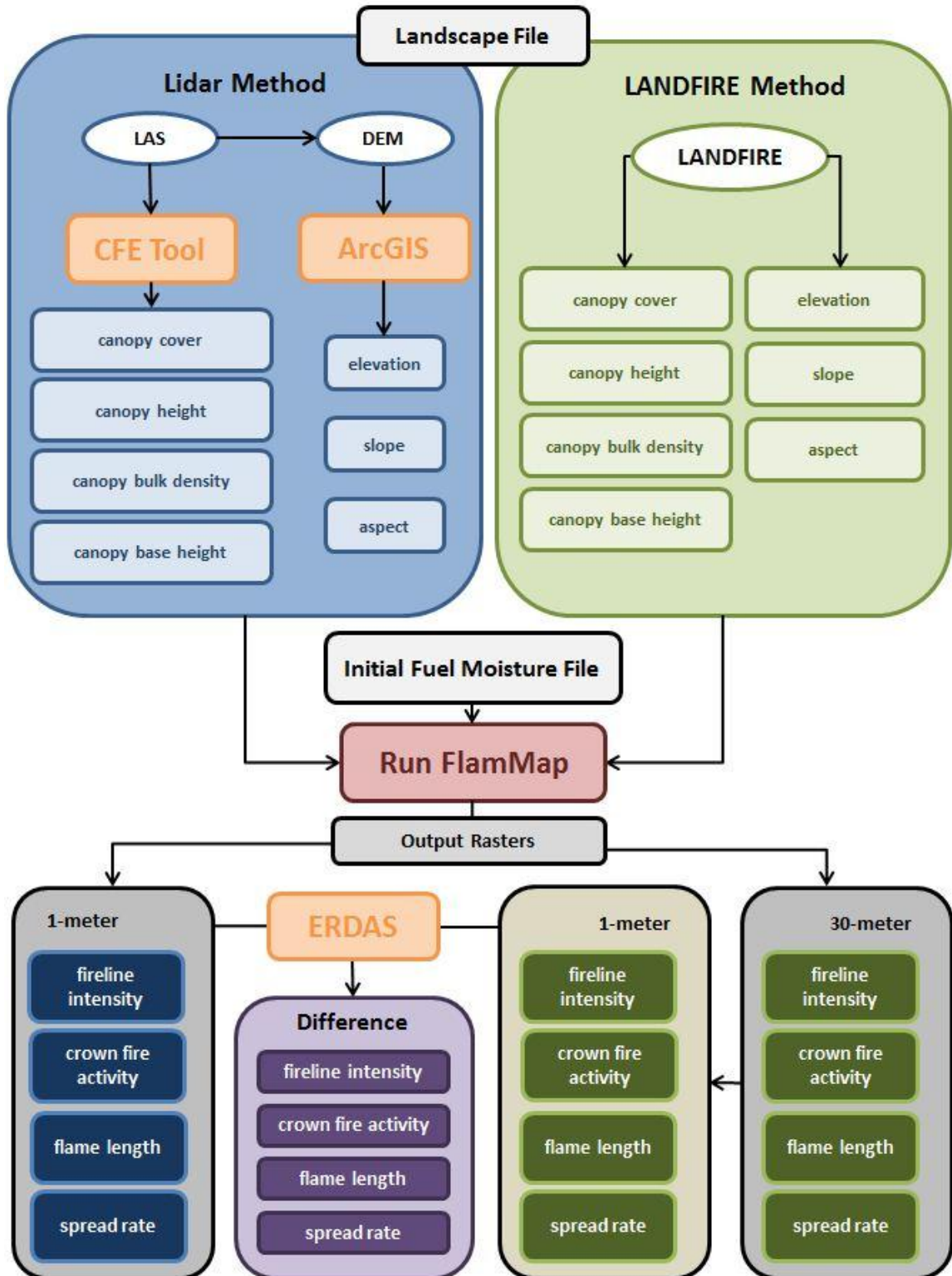


Figure 16. Work Process Diagram for Research Question I.

FlamMap natively refers to the thirteen Northern Forest Fire Laboratory (NFFL) fuel classifications as its fuel model and also requires two base input files (Table 3): a Landscape file (.LCP) which is in a GIS format, and an Initial Fuel Moisture file (.FMS), which is an ASCII text file. Optional tabular and spatial files include a Weather file (.WTR), Custom Fuel Model file (.FMD), Conversion file (.CNV), Wind file (.WND) and more. The Landscape file is a collection of several rasters, including the required fuel model, slope, aspect, DEM and canopy cover along with the optional crown bulk density (CBD), crown base height (CBH), stand/canopy height (CH), duff loading, and coarse woody themes. Even though LANDFIRE data can include fully-compiled Landscape files as required by FlamMap, only available component rasters were considered as individual inputs to maintain consistency with data inputs for the lidar simulation.

**Table 3.** Input Data Layers for Use in FlamMap.

<b>File Name</b>	<b>Extension</b>	<b>File Type</b>	<b>Required</b>	<b>Optional</b>
Landscape	.LCP	GIS	fuel model	crown bulk density
			slope	crown base height
			aspect	stand height
			elevation	<i>duff loading (not used)</i>
			canopy cover	<i>coarse woody (not used)</i>
			NFFL fuel model	
Initial Fuel Moisture	.FMS	Text		
Weather	.WTR	Text		
Wind	.WND	Text		

For both the lidar and LANDFIRE techniques, the mandatory Landscape file was compiled and stored separately, one for each (Figure 17). The other required file, Initial Fuel Moisture (Figure 18), accounts for dead fuel moisture by size class and live fuel moisture by type and is measured as a dry weight in terms of percent for each of the thirteen classes within the NFFL fuel model. The size classes for dead fuel moisture are considered in terms of time required for woody debris of different diameters to reach 63.2% equilibrium moisture content, measured in intervals of 1 hour, 10 hours, 100 hours and 1000 hours. The two types of live fuels are live herbaceous (LH) and live woody (LW).

Required Themes	Source	Use LCP	Source Units	Constants
Elevation:	C:\THEISIS\Lidar\Fla...\dem.asc	<input type="checkbox"/>	Meters	Constant: 0
Slope:	C:\THEISIS\Lidar\Fla...\slope.asc	<input type="checkbox"/>	Degrees	Constant: 0
Aspect:	C:\THEISIS\Lidar\Fla...\aspect.asc	<input type="checkbox"/>	Degrees	Constant: 0
Fuel Model:	C:\THEISIS\Lidar\FlamM...\nffl.asc	<input type="checkbox"/>	Class	Constant: 1
Canopy Cover:	C:\THEISIS\Lidar\FlamM...\cc.asc	<input type="checkbox"/>	Percent	Constant: 50

Crown Fuels	Source	Use LCP	Source Units	Constants
Include Crown Fuels:	<input checked="" type="checkbox"/>			
Stand Height:	C:\THEISIS\Lidar\FlamM...\ch.asc	<input type="checkbox"/>	Meters	Constant: 15
Canopy Base Height:	C:\THEISIS\Lidar\FlamM...\cbh.asc	<input type="checkbox"/>	Meters	Constant: 1
Canopy Bulk Density:	C:\THEISIS\Lidar\FlamM...\cbd.asc	<input type="checkbox"/>	kg/m3	Constant: 0.2

Ground Fuels	Source	Use LCP	Source Units	Constants
Include Ground Fuels:	<input type="checkbox"/>			
Duff Loading:	NA	<input type="checkbox"/>	Tons/Acre	Constant: 50
Coarse Woody Fuels:	NA	<input type="checkbox"/>	Class	Constant: 50

**Figure 17.** FlamMap Landscape File Parameters (U.S. Department of Agriculture 2011a).

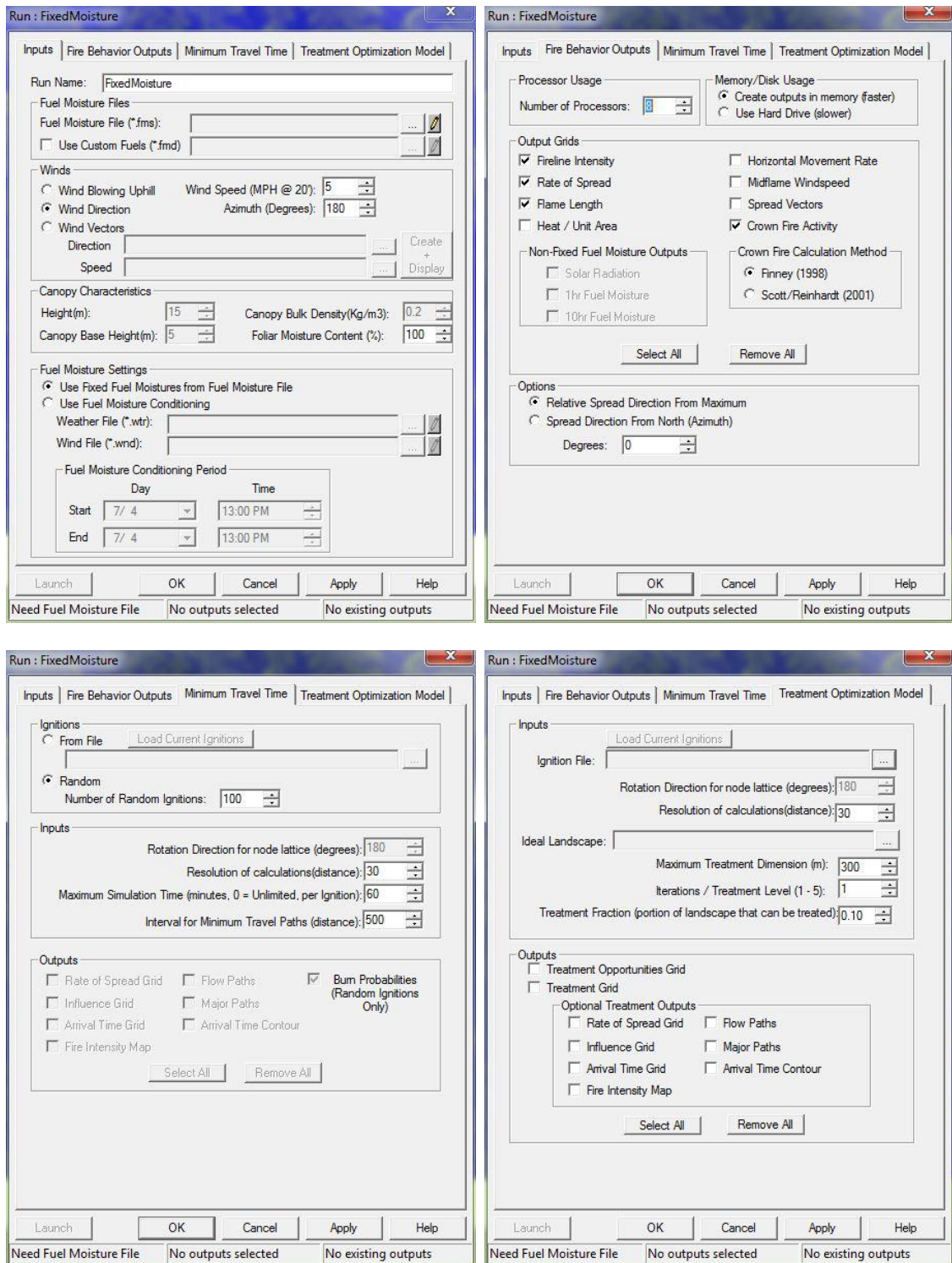


**Figure 18.** FlamMap Fuel Moisture File Parameters (U.S. Department of Agriculture 2011a).

FlamMap's sister model, FARSITE, also uses an Initial Fuel Moisture file but the moisture values change as the model runs through a set period of time. Both models can be set to run a pre-simulation "conditioning" period which incorporates local weather conditions with the terrain and vegetation variables to produce a realistic distribution of dead vegetation moisture content (live vegetation moisture content remains static). This time period can be set for any duration of time, but several days will allow for the dead fuel moistures to more accurately reflect local site conditions (Missoula Fire Sciences Laboratory 2011).

For FARSITE, this gives a more realistic moisture distribution platform on which the model can begin running. Since FlamMap does not incorporate time, there is no change in fuel moisture after the model runs. As such it is normally important to run a conditioning period when using FlamMap to get more realistic results which consider variability of dead vegetation fuel moisture. However, to effectively compare the FlamMap model results for the two different Landscape files for this study, it is crucial to hold all other variables constant. Instead, a conditioning period was not considered and the Initial Fuel Moisture file was identical for both the lidar and the remote sensing-based model runs. A value of 5% was input for each dead fuel size (1-hr, 10-hr, 10-hr and 1000-hr) and each fuel class (1-13) and a value of 50% was input for both LH and LW in all fuel classes. No other project files were included in the analysis. The FlamMap model was run one time with 100 randomly placed, simulated fires to produce output raster maps of fireline intensity, crown fire activity, flame length, and spread rate.

After a set of four output raster pairs (fireline intensity, crown fire activity, flame length and spread rate) from each of the two methodologies were processed (for example,

crown bulk density from remote sensing and crown bulk density from lidar), change detection was conducted to show discrepancies in output values between the two methods. However, before this could be accomplished, it was necessary that each file set being compared was of an identical spatial resolution and extent. Using the same methodology to spatially align the lidar-based inputs computed previously, a master point file was generated from lidar fireline intensity raster output with the ArcMap Raster to Point tool. As before, this particular file was chosen randomly since any of the lidar-based FlamMap outputs would have achieved the same end. The MultiValues to Point tool was again used for each of the LANDFIRE 30-meter output files to generate 5-meter rasters that align perfectly with the lidar FlamMap outputs yet retain the spatial patterns of the 30-meter products.

The raster-based Change Detection feature in ERDAS Imagine was used to generate two types of outputs: an image difference raster and a highlight change raster. Image differencing (subtracting one raster from the other) produces an output raster that shows a continuum of change with exact values in the units of the input rasters. For this study, it is not the output values that are of interest, it is the amount of change demonstrated by a range of values: higher values mean greater difference and low values or zero represent little or no change. The highlight change outputs are determined by values inserted by the user which represent significant inflection points – or values at a particular threshold considered to be critical. For this project, ten percent change in the positive or negative direction was considered significant. The output highlight change maps show values that have crossed the threshold in either direction (as “decreased” or

“increased”) or are close to the threshold (“some decrease” or “some increase”), or pixels that have not changed at all.

### *3.3.2 Model Setup for Research Question II*

The second research question visits the same Kerr County study area as the first, but now the focus is on vegetation moisture content, or foliar moisture content (FMC). When running the FlamMap model for the lidar and LANDFIRE methods, the Initial Fuel Moisture input to the FlamMap model was homogeneous across the study area because there was no conditioning period to allow for absorption of water by the dead vegetation. This time the LANDFIRE method was run in FlamMap again, but there was a conditioning period to allow for variable FMC of dead fuels across the landscape (Figure 19). To begin, the same homogeneous Initial Fuel Moisture input file was used as before, along with a Weather file and a Wind file for fuel moisture conditioning. The conditioning period lasted for seven days and the Weather and Wind files were created from weather data covering the week before the cloud-free Landsat 5 TM scene for the Kerr County study area, which was 17 August 2011.

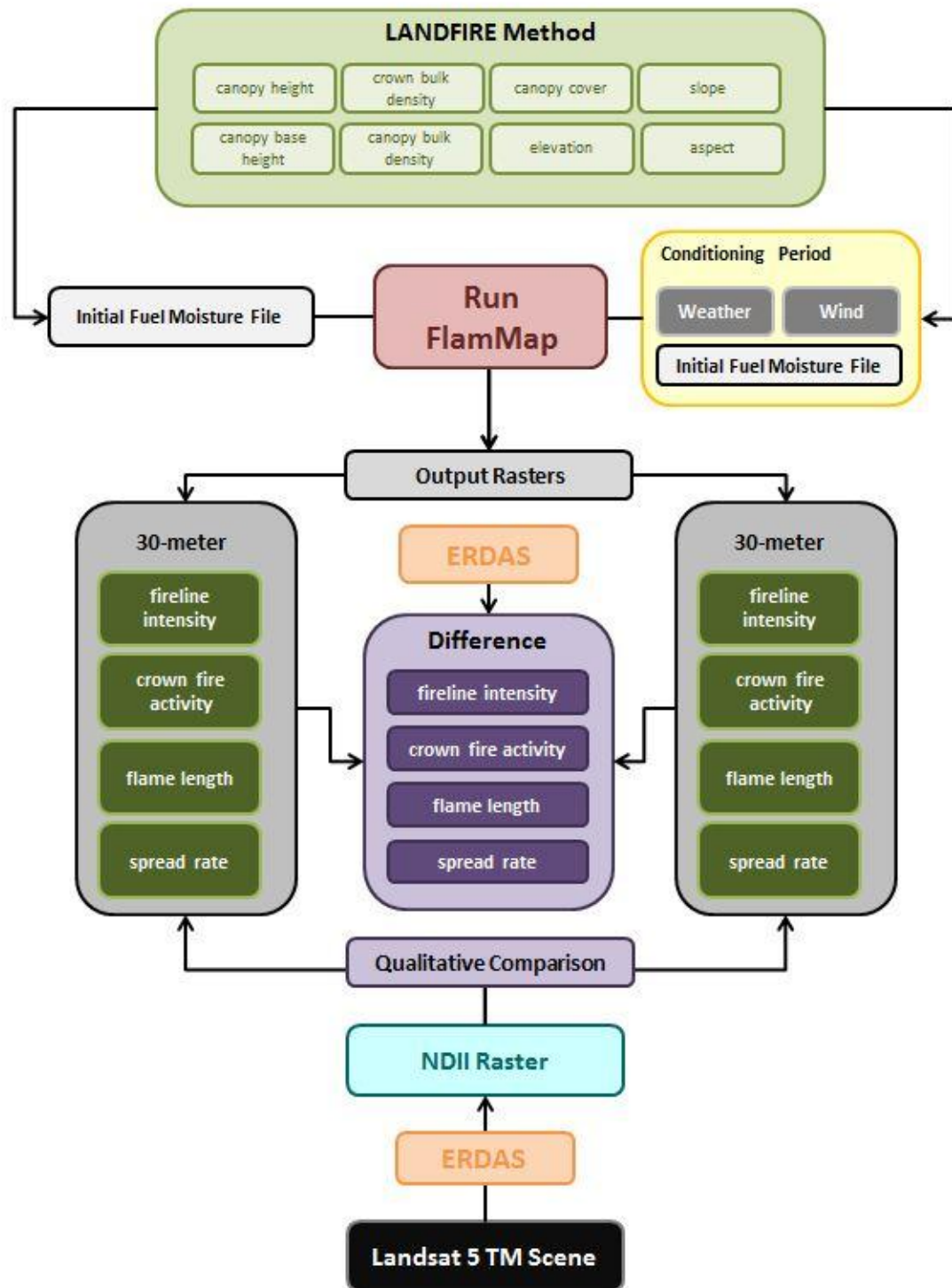
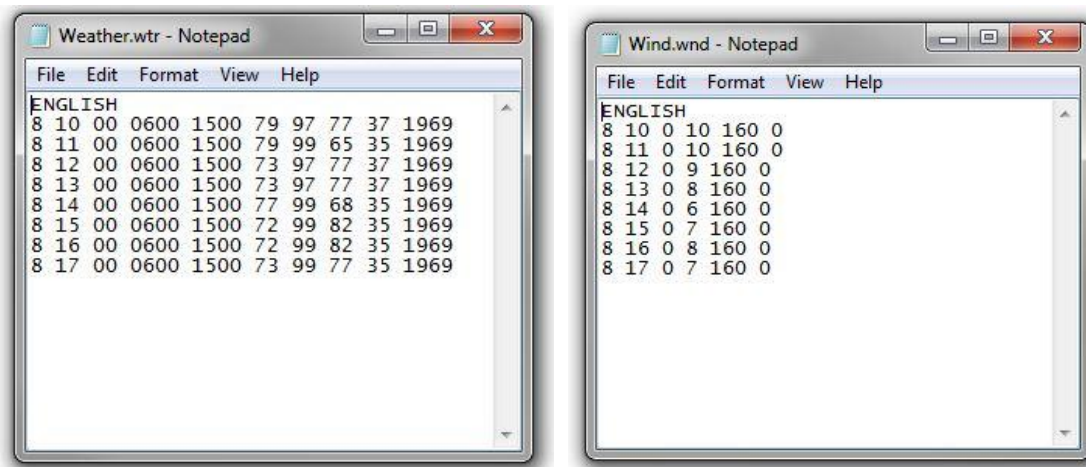


Figure 19. Work Process Diagram for First Component of Research Question II.

FlamMap requires that the Weather and Wind files follow a very specific template of numbers in columns stored in text files with .wtr and .wnd as the file extensions respectively. The columns in the Weather file are: month, day, total daily precipitation amount (hundredths of an inch), time of minimum temperature (GMT), time of maximum temperature (GMT), minimum daily temperature (F), maximum daily temperature (F), maximum daily relative humidity (%), minimum daily relative humidity (%), and elevation (feet) (Figure 20). The Wind file is comprised of: month, day, hour (GMT), wind speed (mph), wind direction (degrees from north), and cloud cover (%). The word 'ENGLISH' is included on the first line of each file to denote unit format.



**Figure 20.** *Left*, FlamMap Weather File; *right*, FlamMap Wind File.

Next, FMC was estimated from the 17 August 2011 30-meter Landsat 5 TM scene covering the Kerr County study area using the normalized difference infrared index (NDII) (Figure 21). A model was be created in Intergraph's ERDAS Imagine (Figure 22)

software to calculate NDII from Bands 4 and 5 of the Landsat 5 TM image (for Landsat 5 TM products, Band 4 is near-infrared and Band 5 is shortwave infrared) (Figure 23).

$$\text{NDII}_{(\text{Landsat TM})} = \frac{\text{NIR}_{(\text{Band 4})} - \text{SWIR}_{(\text{Band 5})}}{\text{NIR}_{(\text{Band 4})} + \text{SWIR}_{(\text{Band 5})}}$$

**Figure 21.** NDII Formula for Landsat 5 TM (Jensen 2000).

Change detection with the ERDAS Imagine Change Detection tool (described previously) was conducted between the four output rasters derived by the LANDFIRE method using homogeneous dead fuel moisture and the four output rasters created with the conditioning period to examine the effect of including dead fuel moisture in the model. Then, the NDII image of all vegetation moisture (live and dead combined) will be compared in the Results section of this document with each of the four output rasters using homogeneous moisture.

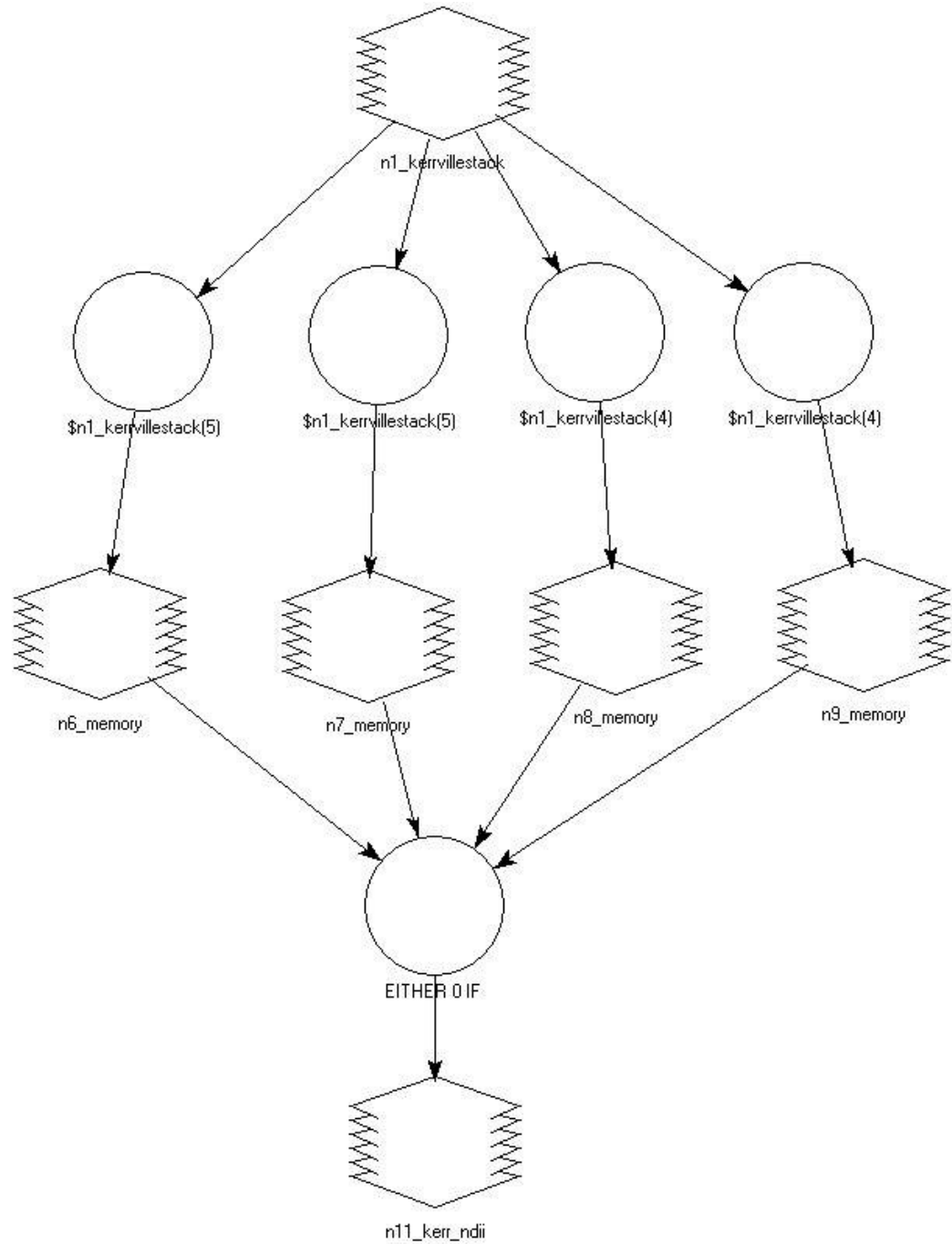


**Figure 22.** ERDAS Imagine NDII Model Layout.

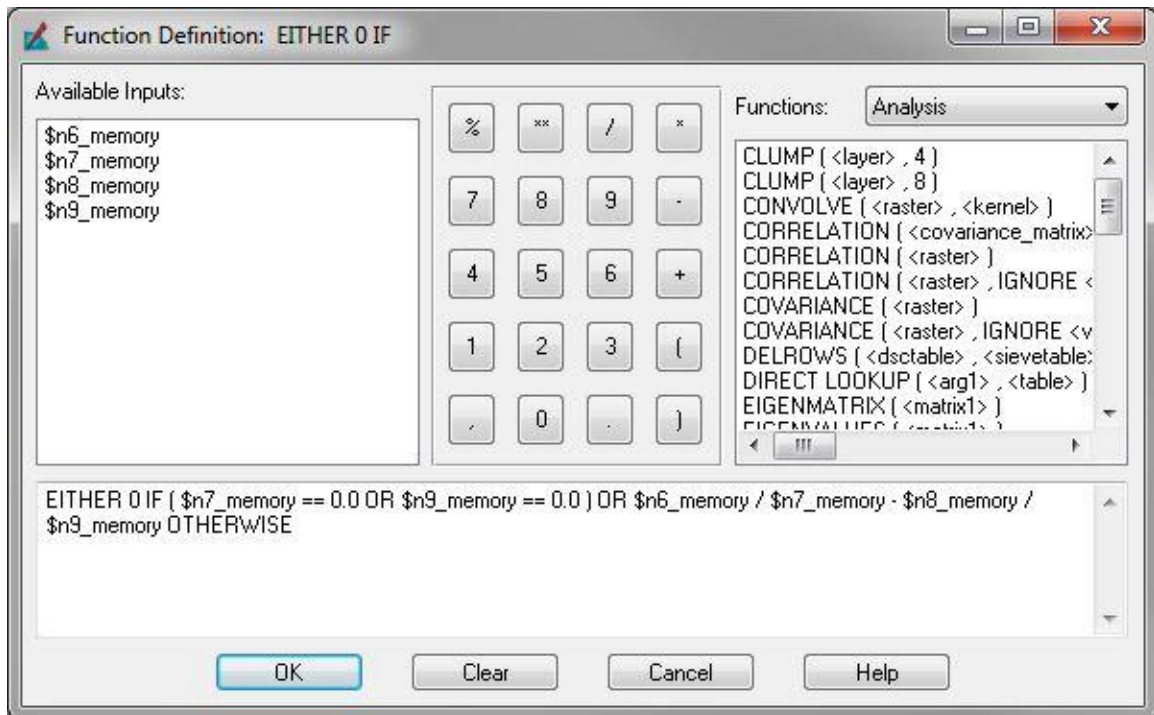


**Figure 23.** ERDAS Imagine NDII Model Parameters.

The other aspect of the second research question focuses on Possum Kingdom to investigate whether there is a significant relationship between FMC and extent of area burned (Figure 24). Fuel moisture content was estimated for the Possum Kingdom study area (PK Complex fire perimeter) from a Landsat 5 TM scene (Figure 25) captured before the April 2011 wildfire on 11 April 2011 using NDII. Then the NDII values for the scorched area (Figure 9) were compared to NDII values for the unburned remnant area in a test of statistical significance.

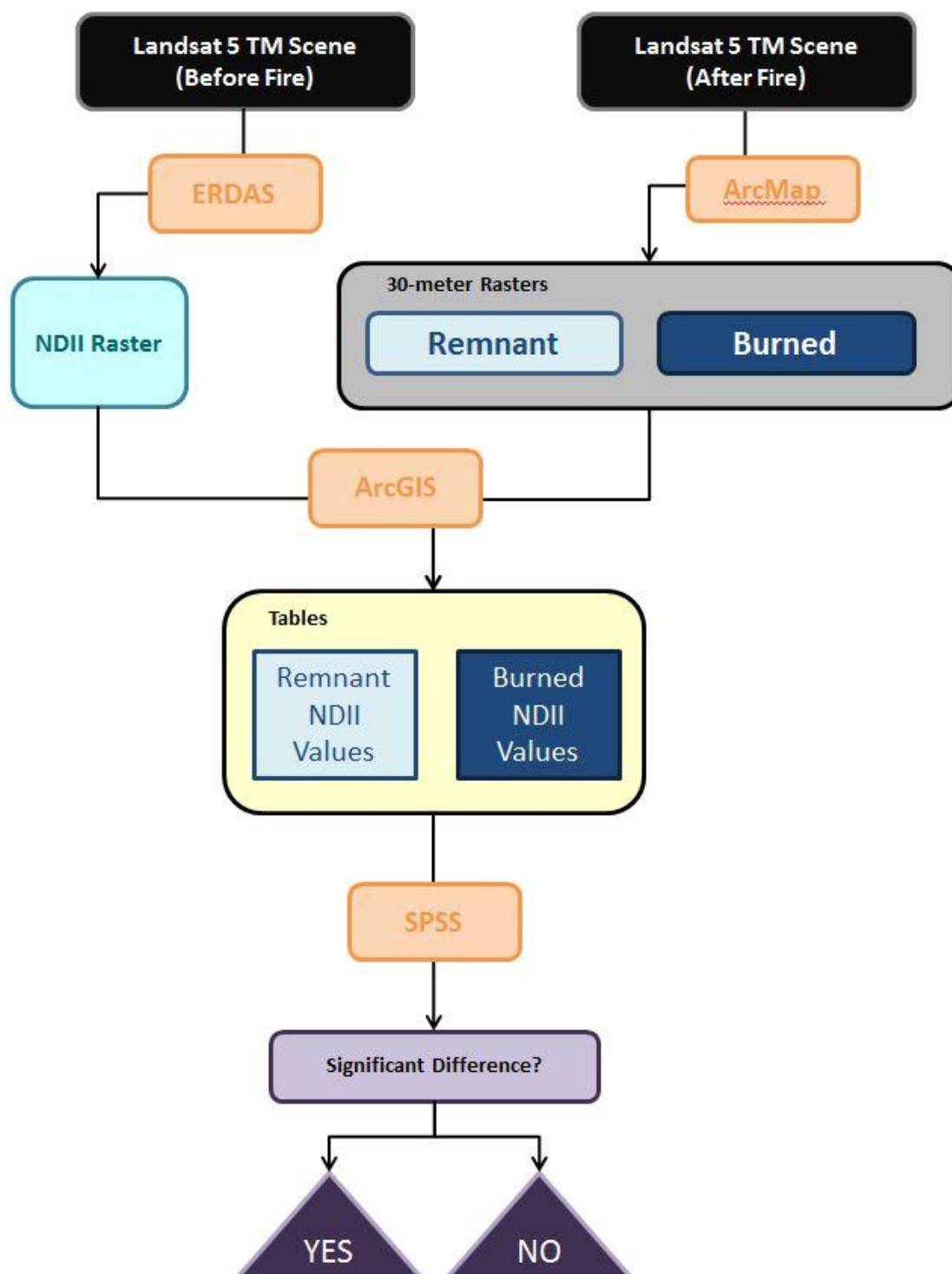
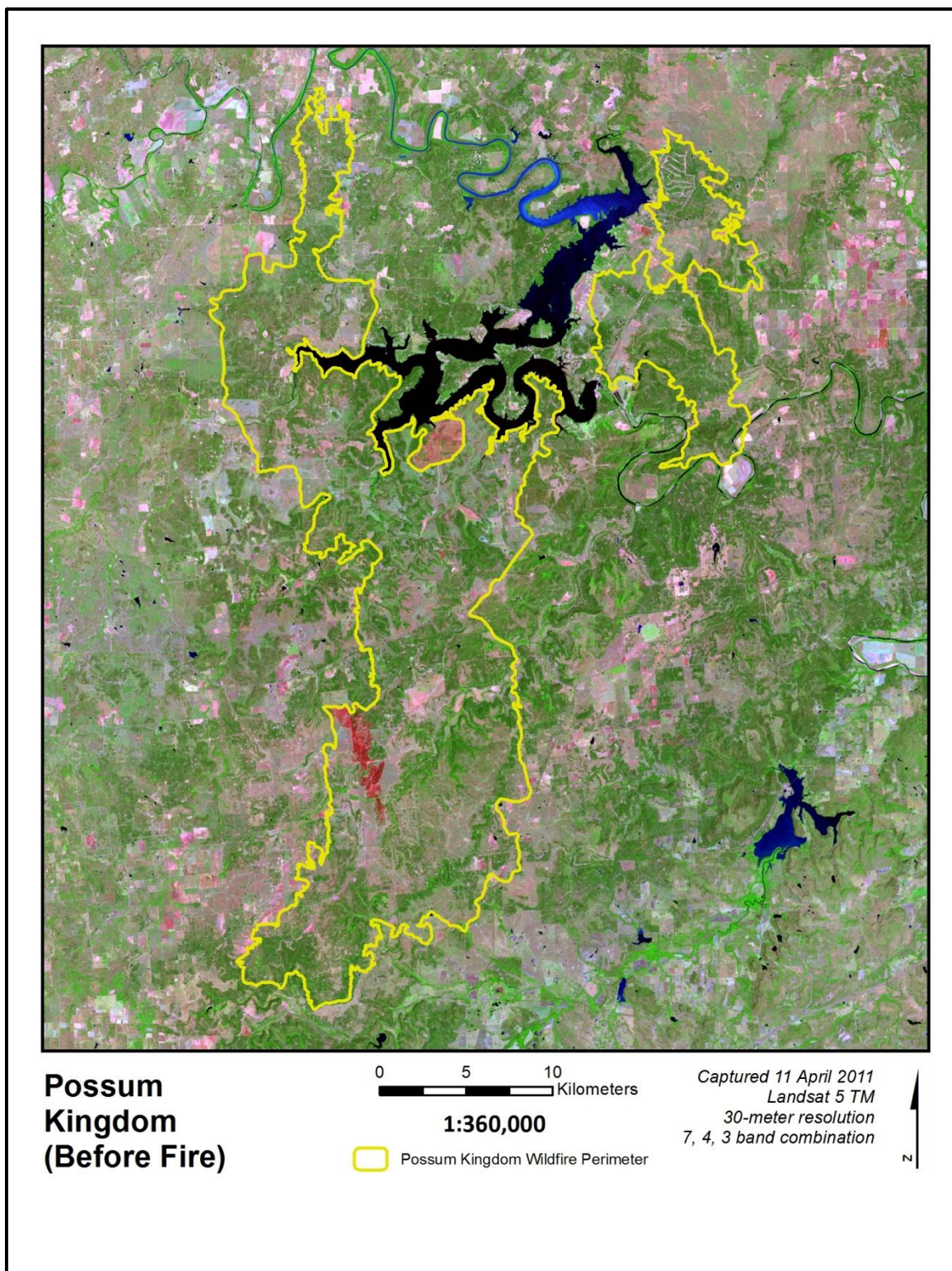


Figure 24. Work Process Diagram for Second Component of Research Question II.



**Figure 25.** Possum Kingdom Before Fire Image. Landsat 5 TM False color composite shown in 7,4,3 band combination. Image captured 11 April 2011 and obtained from U.S. Geological Survey (2011).

The null hypothesis states there is not a difference between the mean fuel moisture content (FMC), as measured by NDII, in the burned area compared to the mean fuel moisture content in the remnant area. The research hypothesis states there is a difference between fuel moisture content in the burned area compared to the mean fuel moisture content (FMC) in the remnant area.

$$H_0: FMC_{\text{burned}} = FMC_{\text{remnant}}$$

$$H_1: FMC_{\text{burned}} \neq FMC_{\text{remnant}}$$

$$\alpha = 0.05$$

After obtaining the fire perimeter, the next step is to determine if the fire patterns were influenced by fuel moisture content. NDII was calculated for the Before Fire image only. Once again, ERDAS Imagine was utilized to generate and run the NDII model for the study area. To distinguish the burned area from the unburned remnant area of the After Fire image, an NDVI (normalized difference vegetation index) calculation was performed to isolate pixels likely to have been burned (which would have exceptionally low NDVI) from the remnant areas (Figure 26). The results were polarizing enough that an unsupervised classification (ISODATA algorithm) (Figure 27) with only two classes produced reliable results: pixels in one class cover areas that had burned (orange pixels) while pixels in the other class were cover areas that had not (blue pixels).

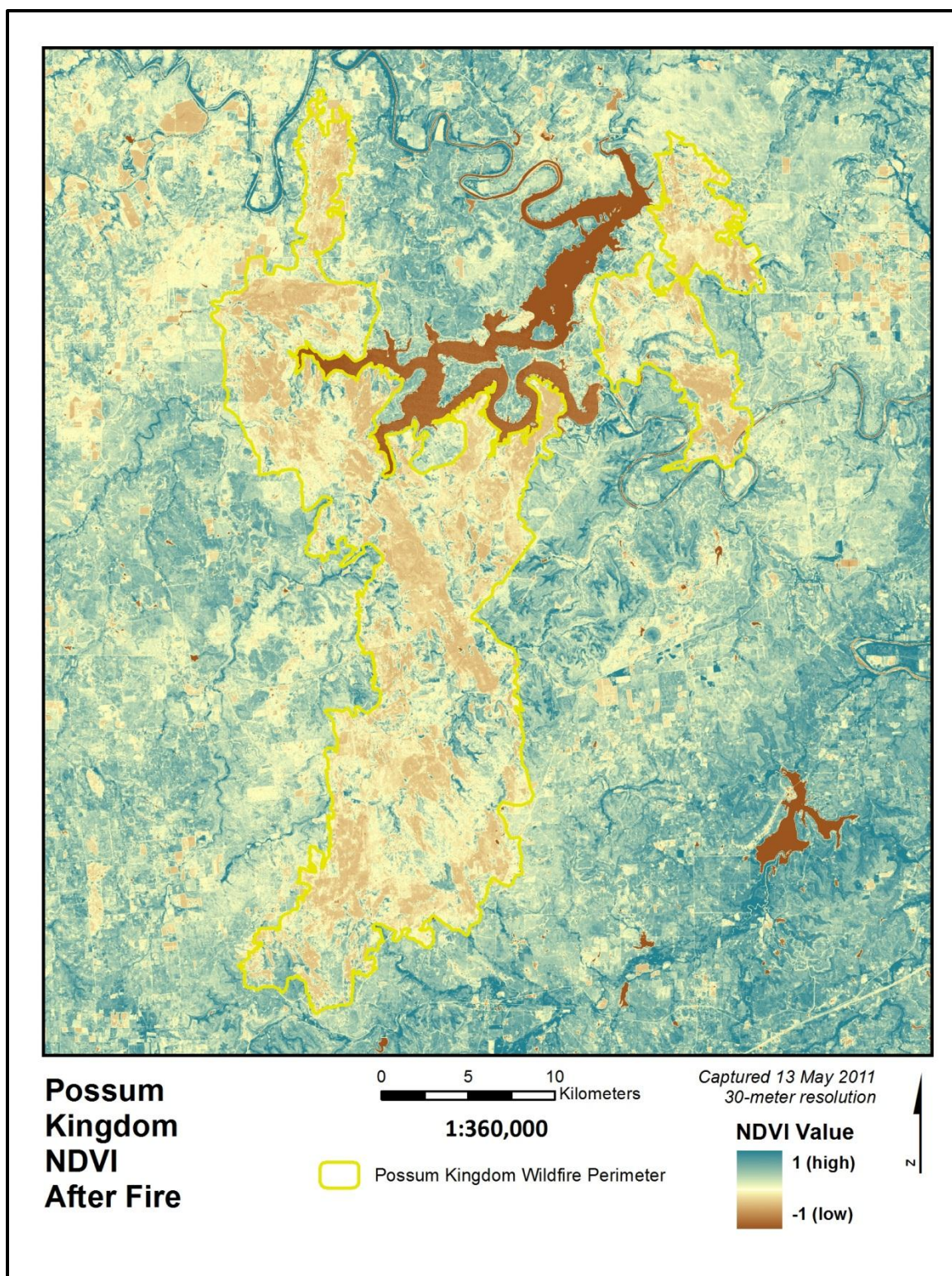


**Figure 26.** Possum Kingdom NDVI Map. Map generated by author from image captured 11 April 2011 and obtained from U.S. Geological Survey (2011).

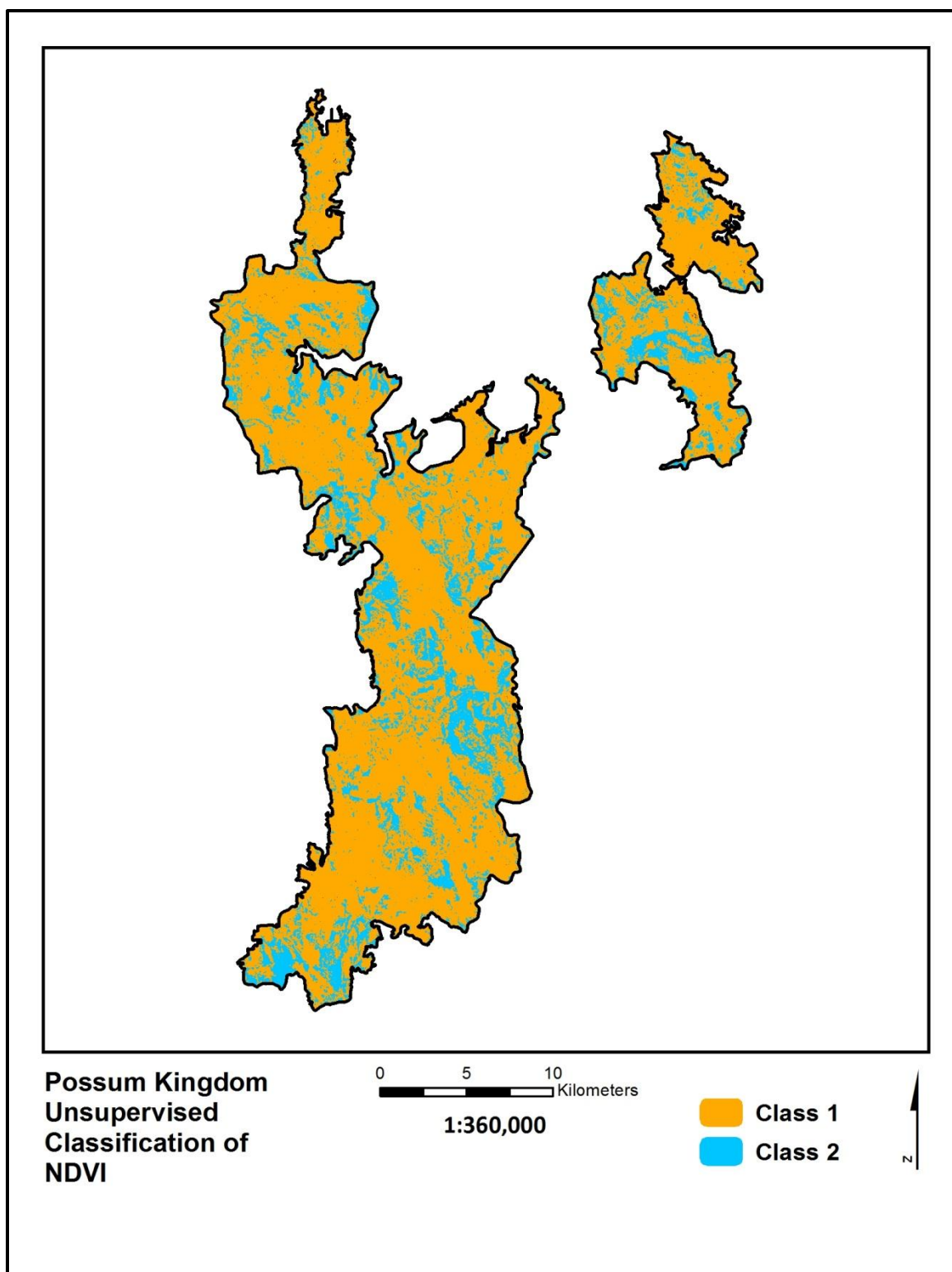


**Figure 27.** Possum Kingdom Unsupervised Classification Map. Class 1 represents area burned; Class 2 represents remnant unburned area.

When the burned and unburned areas were clearly defined, the NDII values from the Before Fire image were extracted from each section and exported as a table using the Extract Multi-Values to Point tool in ArcMap. Before choosing a statistical testing method, the variance for the burned area was compared against the variance for the unburned area in Microsoft Excel using an F test to determine whether equal variances are to be assumed. Then resulting mean NDII values for burned and remnant areas were tested for statistical significance at a 95% confidence interval using the statistical software package SPSS.

## CHAPTER IV

### RESULTS

#### 4.1 Research Question I

The first research question explores the use of high resolution lidar for wildfire modeling as compared to Landsat-based LANDFIRE data. The wildfire model FlamMap was selected to produce map outputs that when compared for each methodology can highlight the impacts of using one method or the other.

The LANDFIRE data collected for model input was pre-compiled by the U.S. Department of Agriculture (2011b) and will be discussed first. Next, the same type of inputs generated from the lidar data will be described and compared relative to their LANDFIRE counterparts. The results of the LANDFIRE model run and the lidar model run can then be introduced along with maps displaying the results of change detection analysis. When all of the results have been showcased, then finally a section for notes and discussion will add context and meaning to the analysis portion of this study.

##### *4.1.1 LANDFIRE Inputs*

Three fundamental tenants of elevation are considered in the FlamMap model: slope, aspect and orthometric height above sea level (referred to as the generic “elevation”). The digital elevation model, or DEM, clearly defines the river and stream patterns cutting through the hilly terrain (Figure 28). The gradient peaks around 700

meters ASL in the highest hills to the northwest of the study area and slopes down to about 400 meters ASL alongside the Guadalupe River and Johnson Creek. The 30-meter resolution gives a sufficient amount of detail to describe the terrain features; however the DEM image does not provide sharp definition.

The slope map (Figure 29) highlights the steepest hillsides which will be a contributing factor to the model results since fire catches quickly along steep terrain (Lein and Stump 2009). The aspect map displays the direction a particular hillside is facing, which is of course determined on a pixel-by-pixel level analysis (Figure 30). For example, in the 30-meter LANDFIRE map hillsides appear blocky and there is some definition, but the result here is more abstract. FlamMap will use this information to help determine which direction fire will spread – similar values present less of a barrier than a peak or a cliff.

In addition to the elevation-based inputs are the vegetation metrics which include canopy height (CH), canopy base height (CBH), canopy cover (CC) and canopy bulk density (CBD). Canopy height, which measures the total height of the vegetation from base to canopy, is shown to be mostly 5-15 meters with a few trees reaching closer to 20 or 25 meters high (Figure 31). The middle shade of green denotes areas where there is no canopy present such as urban, water, grass and bare ground and the lightest shade of green is likely capturing some bushland or scrubby trees.

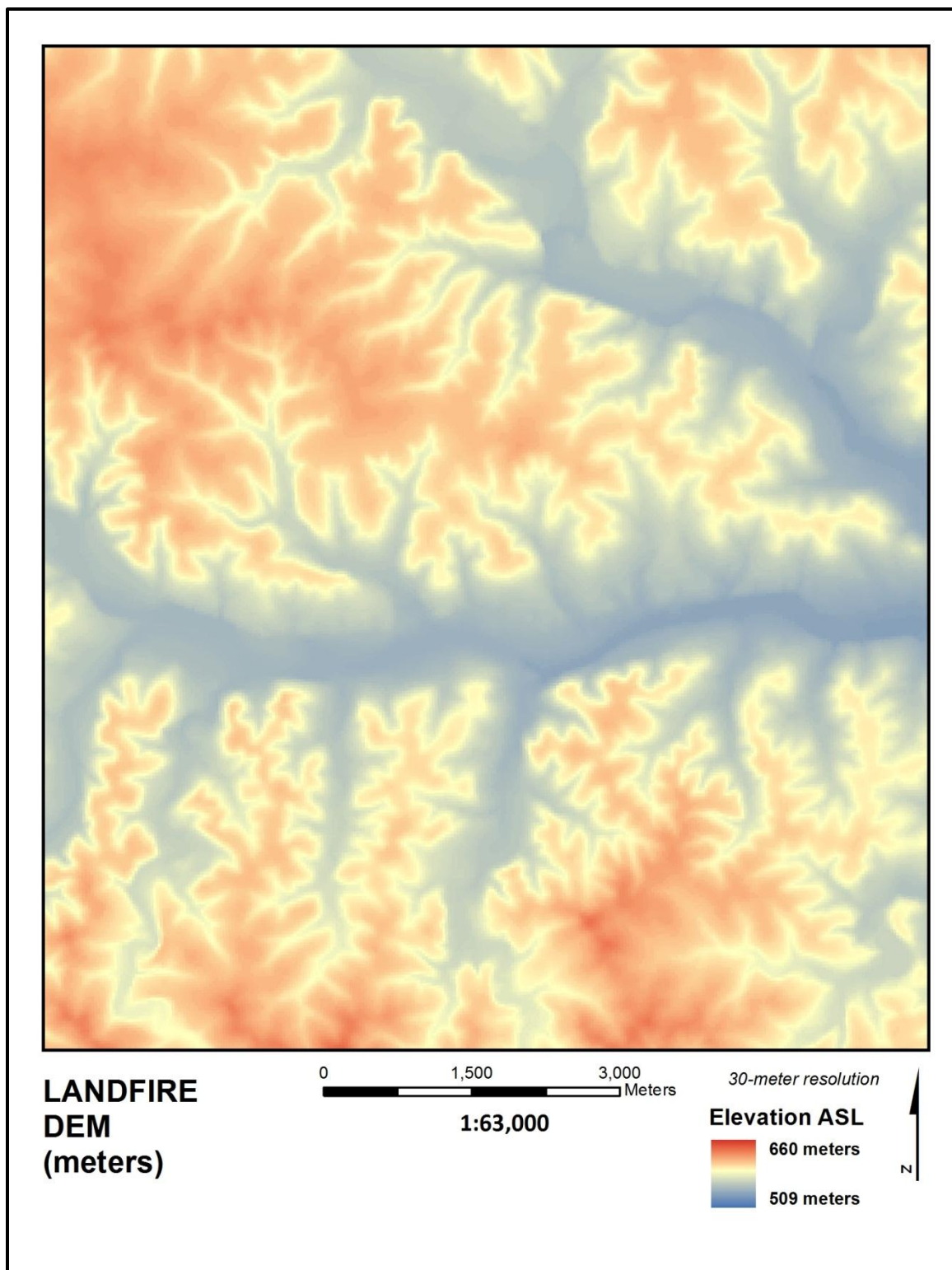


**Figure 28.** LANDFIRE 30-meter DEM in Kerr Study Area.

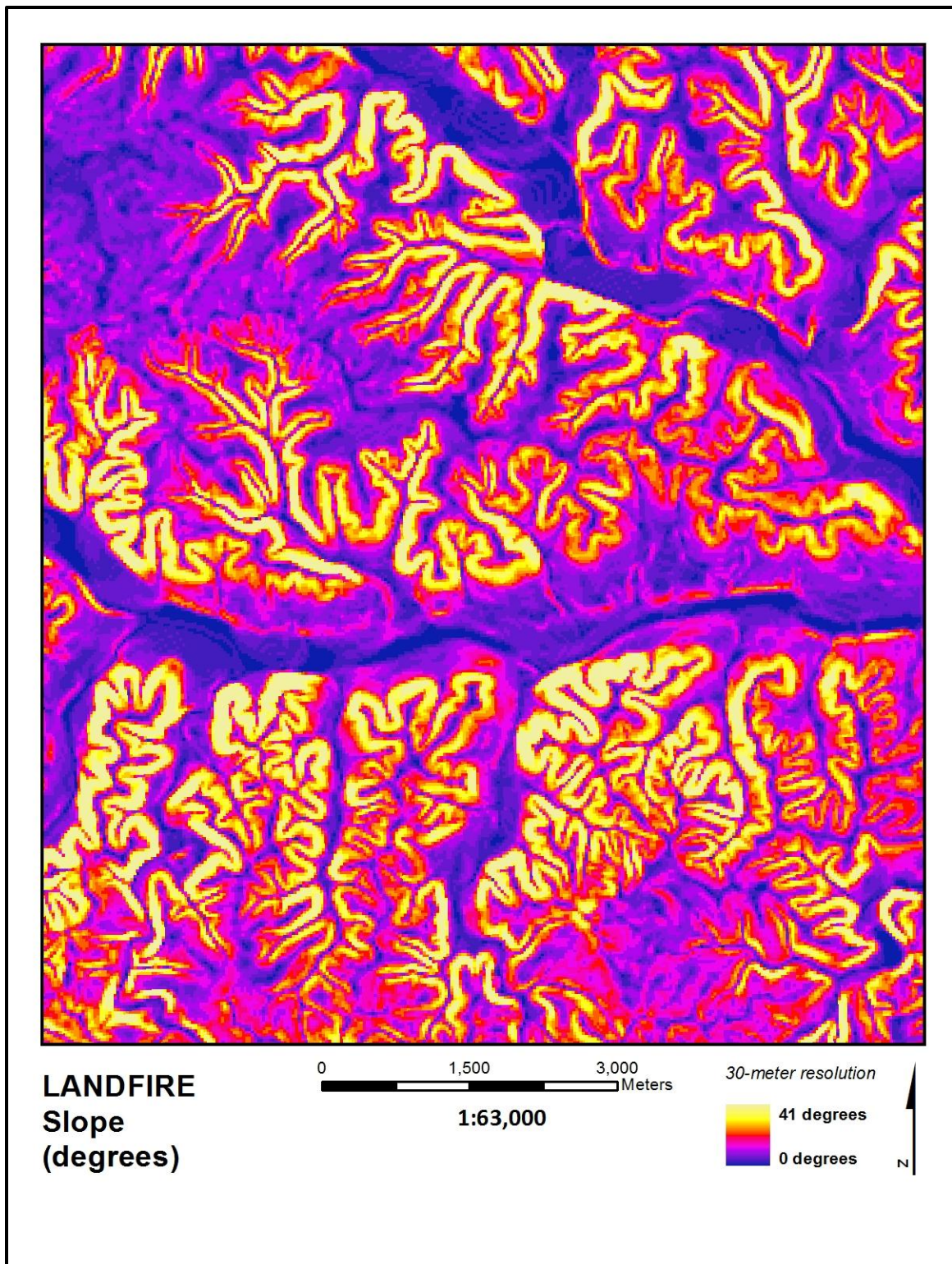


Figure 29. LANDFIRE Slope in Kerr Study Area.

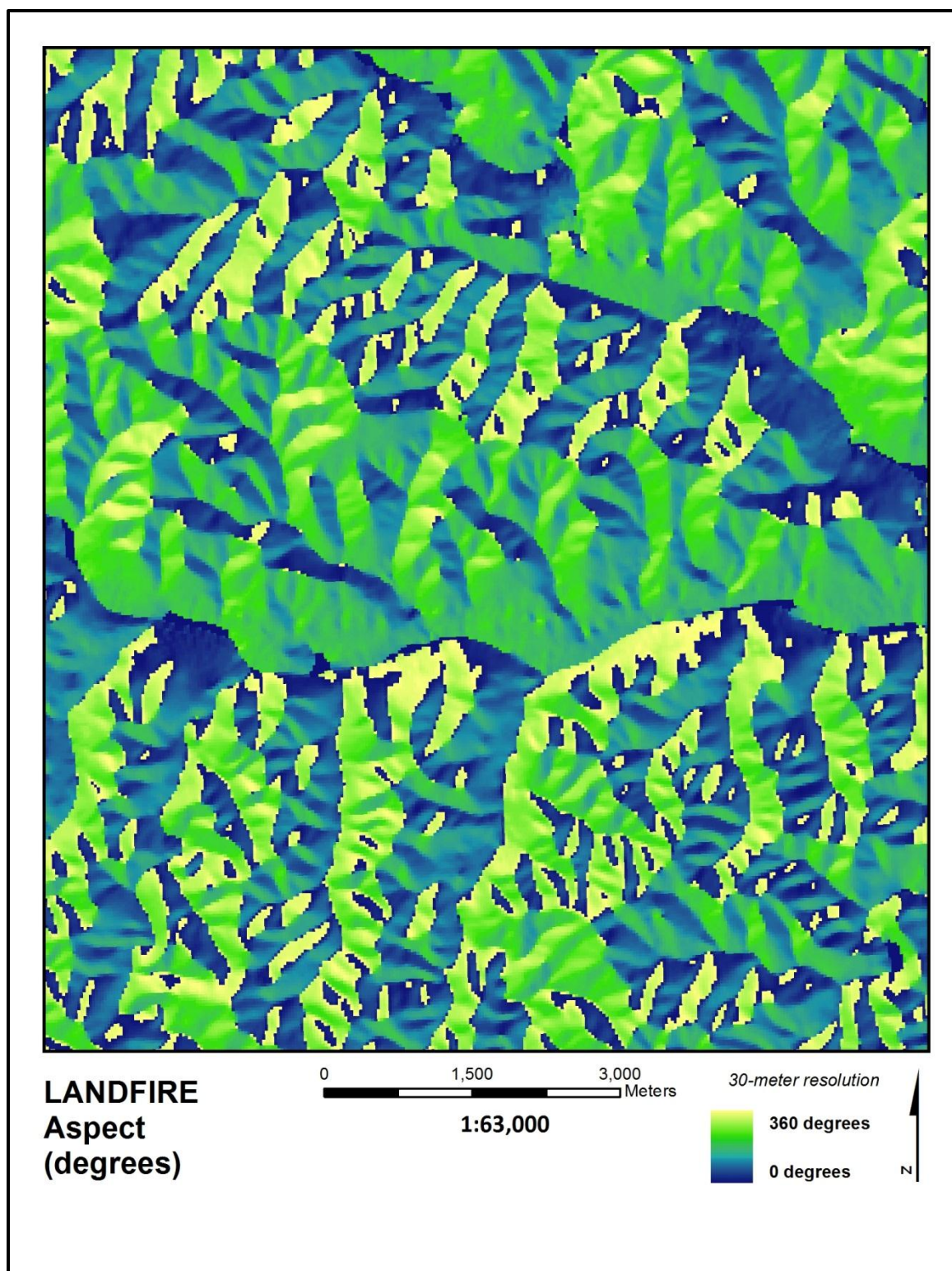


Figure 30. LANDFIRE Aspect in Kerr Study Area.

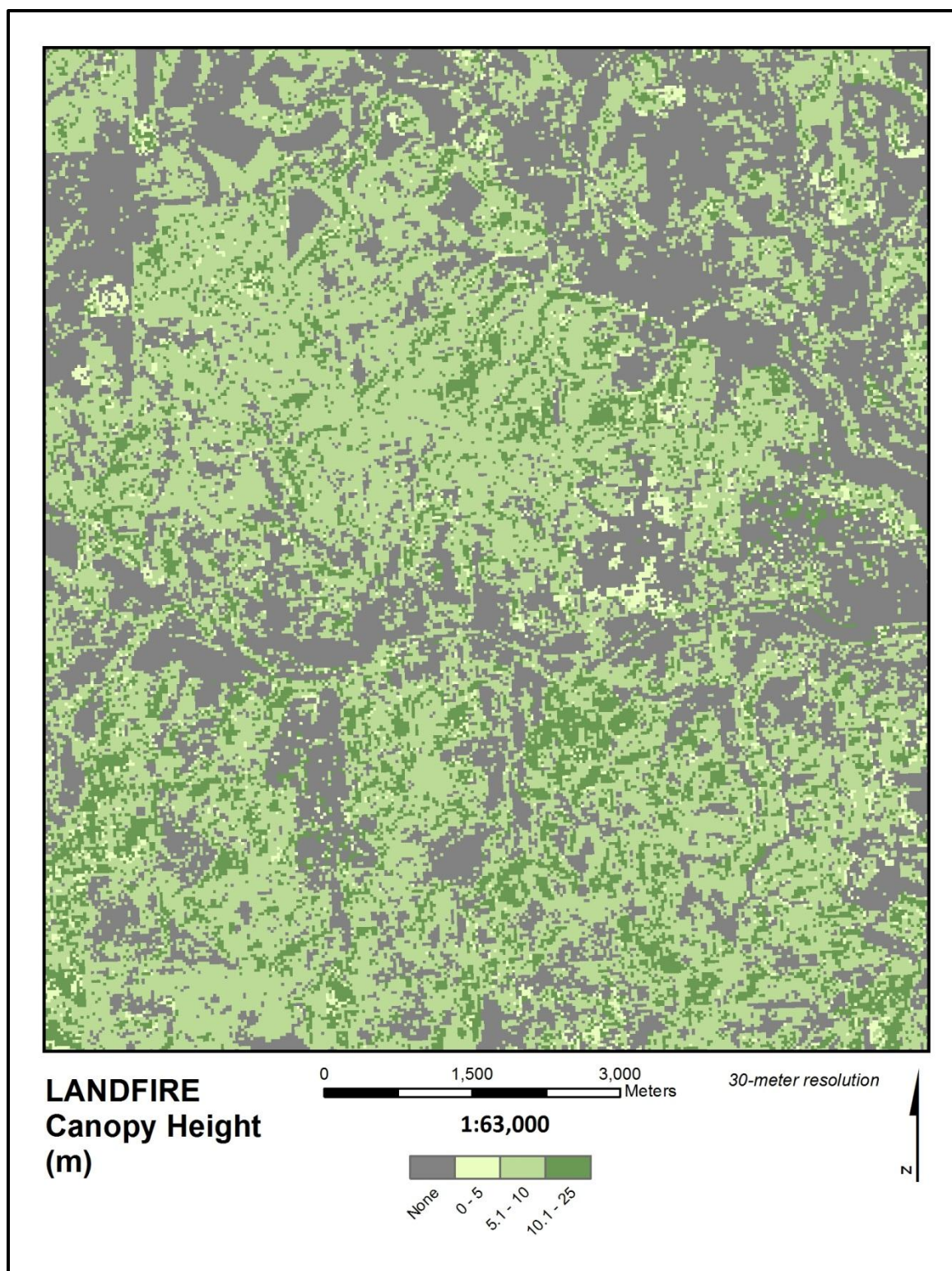


Figure 31. LANDFIRE Canopy Height in Kerr Study Area.

Canopy base height, or the average height from the ground to the base of the canopy, shows a completely different story than CH from the LANDFIRE maps (Figure 32). Here, CBH values are highest in the northwestern portion of the study area between the river and the creek and are coincident with the uninterrupted evergreen forests covered in Texas live oak and Ashe juniper (mountain cedar). Most CBH values are about 1-5 meters high.

Canopy cover is measured in percent and shows where the thickest tree stands are found (Figure 33). The highest values from LANDFIRE approach 90% with most of the range being somewhere between 50% and 90%. From this map it is possible to see interruptions in stand continuity such as right of way (ROW) cleared for utilities.

The last vegetation metric, canopy bulk density, measures available canopy mass per unit of canopy volume that would burn in a crown fire and the units are kilograms per cubic meter (Figure 34). The LANDFIRE CBD map multiplies the units by 100 converted to integer notation. The CBD map follows the same patterns seen in the CC map since a denser canopy volume covering the sky would logically result in more canopy mass.

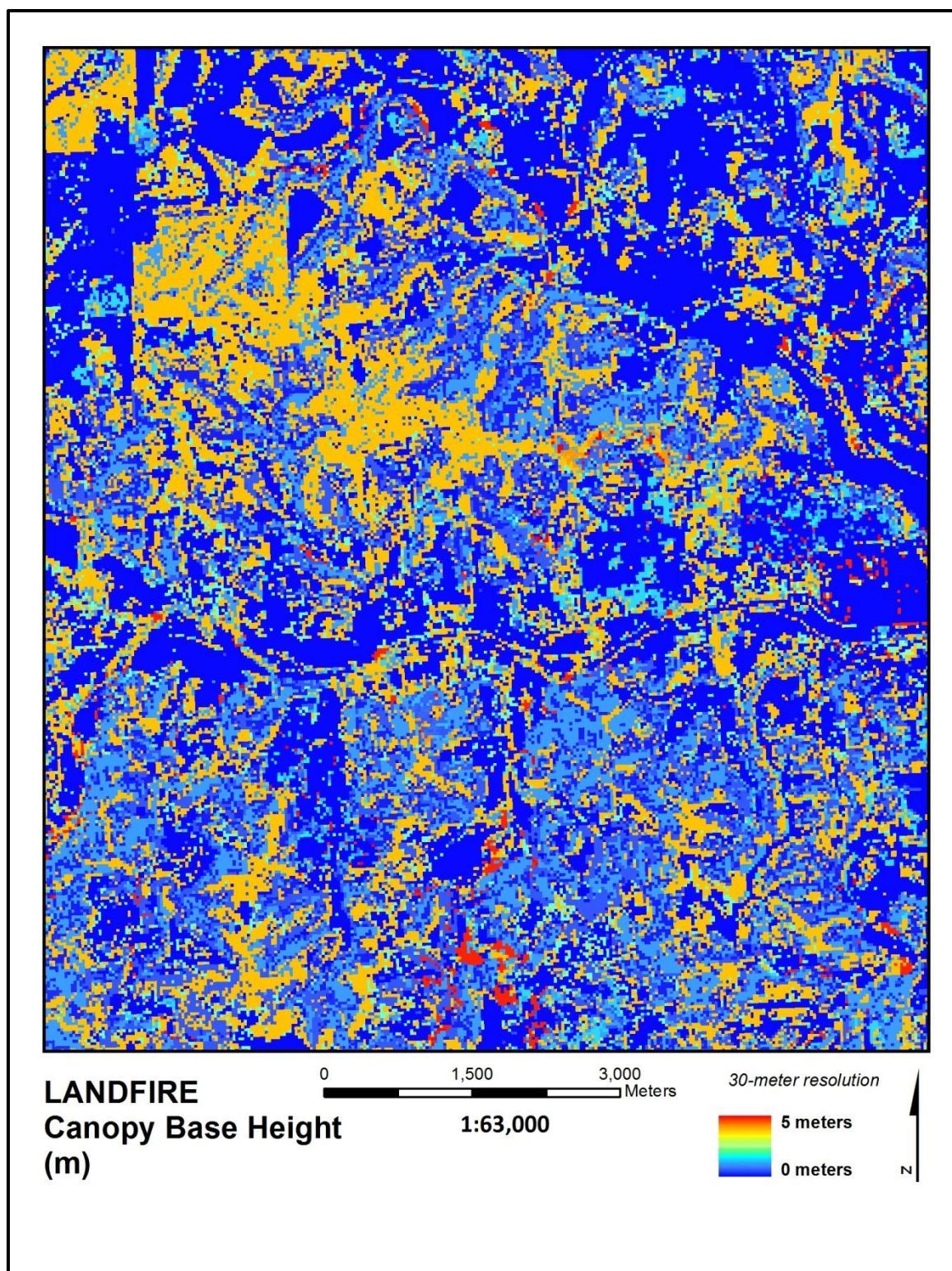
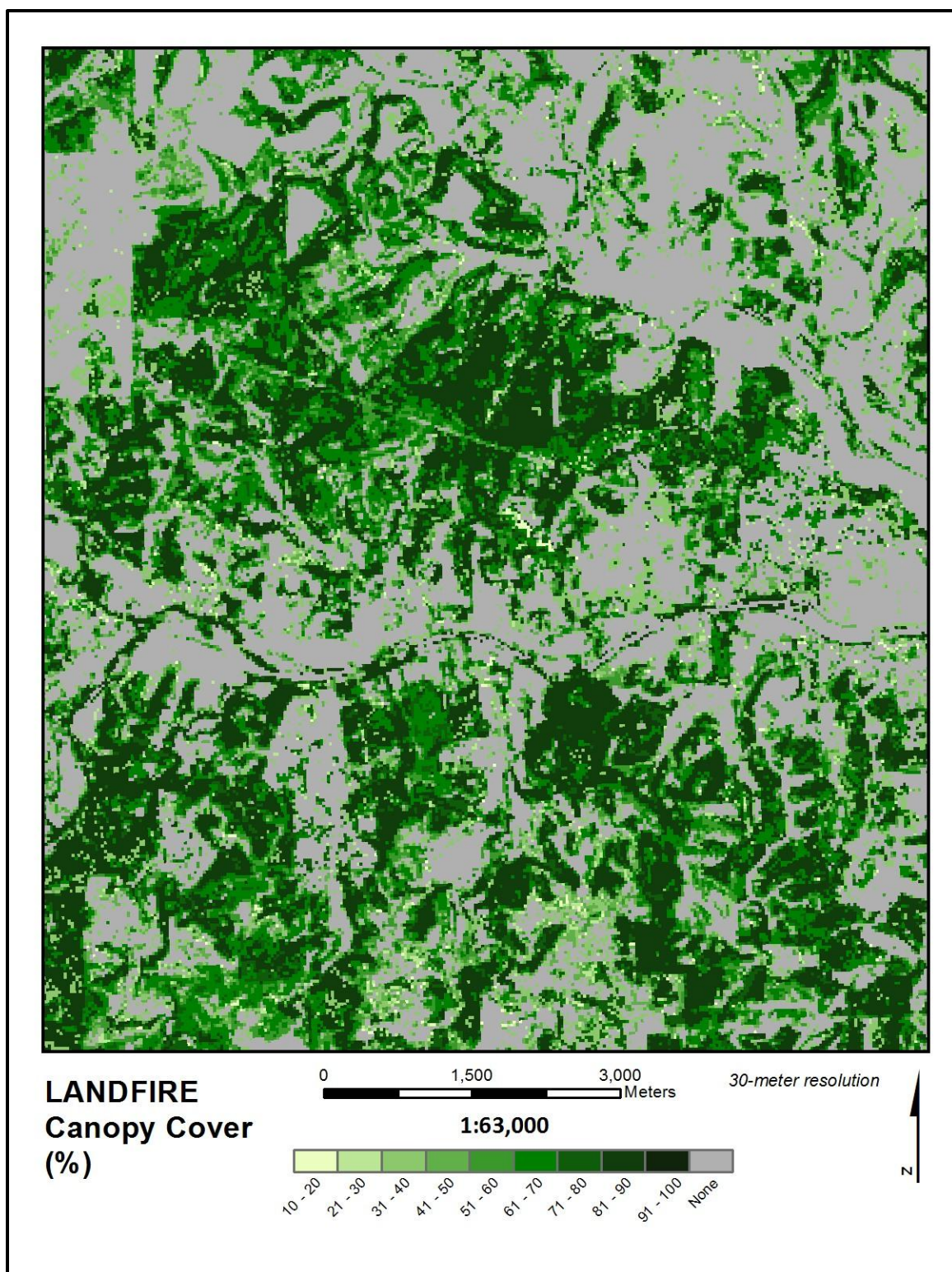


Figure 32. LANDFIRE Canopy Base Height in Kerr Study Area.



**Figure 33.** LANDFIRE Canopy Cover in Kerr Study Area.

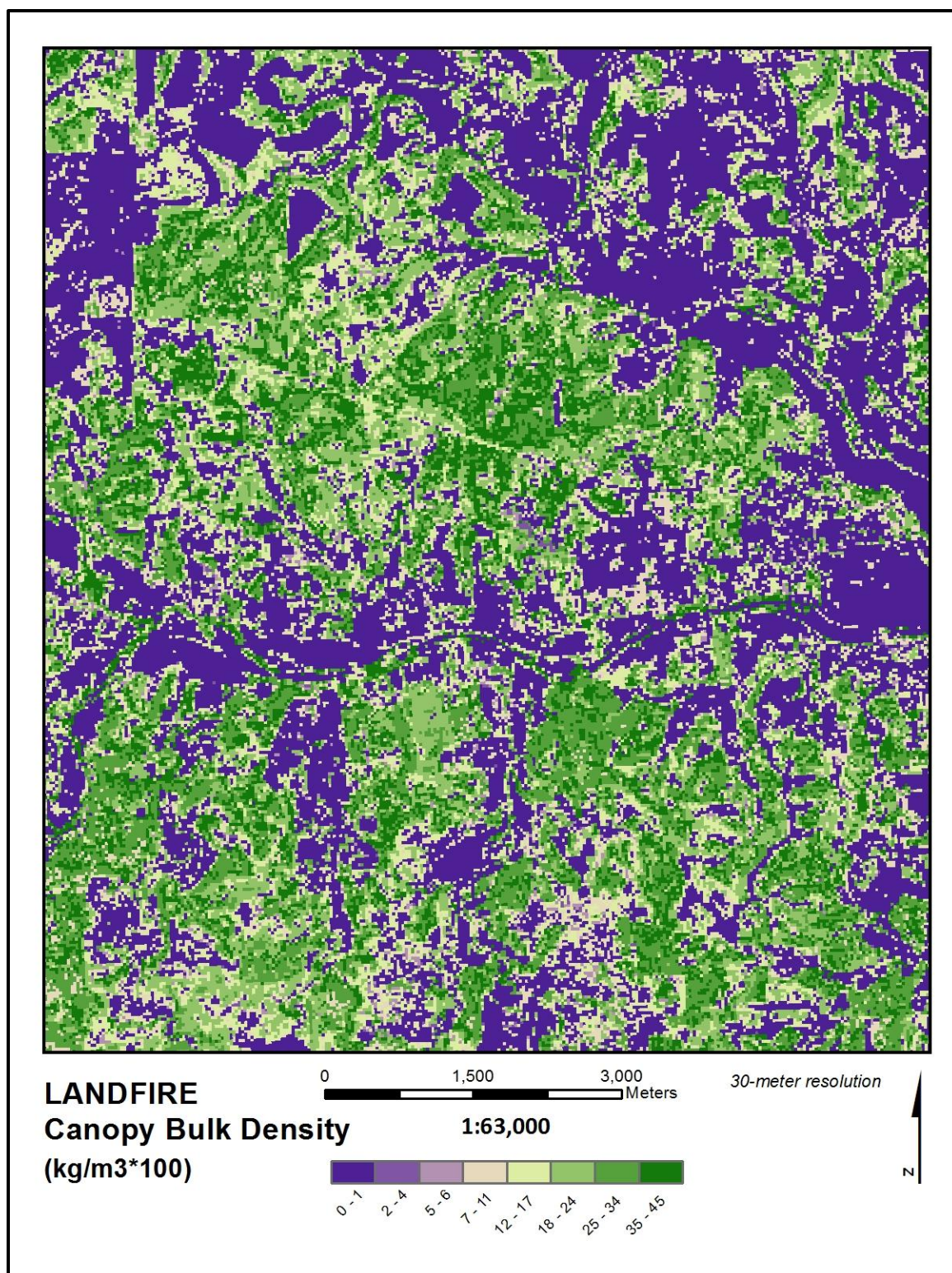


Figure 34. LANDFIRE Canopy Bulk Density in Kerr Study Area.

#### *4.1.2 Lidar Inputs*

The elevation-based datasets derived from lidar refine the landscape from a 30-meter perspective (Figure 28) to a 5-meter resolution (Figure 35). The 5-meter DEM reveals much more detail in the river and stream channels and defines the hillsides with a sharper focus. Overall the patterns displayed in each are consistent and while the lidar does add more context in some areas, it is unlikely these minor differences would significantly impact the wildfire model.

However, the lidar-based slope map (Figure 36) is significantly different than the 30-meter product (Figure 29). Initially the two maps may appear quite similar since the same patterns are evident in each, yet the value ranges tell a different story. The LANDFIRE slope map indicates that areas of maximum slope here are 41 degrees, yet the lidar slope map shows terrain with up to 85 degrees of slope. This is most likely due to the fact that as pixel size gets larger, more and more features are normalized into abstraction. Each pixel represents the average slope across a 900 square meter area and the terrain can vary greatly in that amount of space. There may be a few steeper slopes, but many times this is being averaged by the flat ground around it.

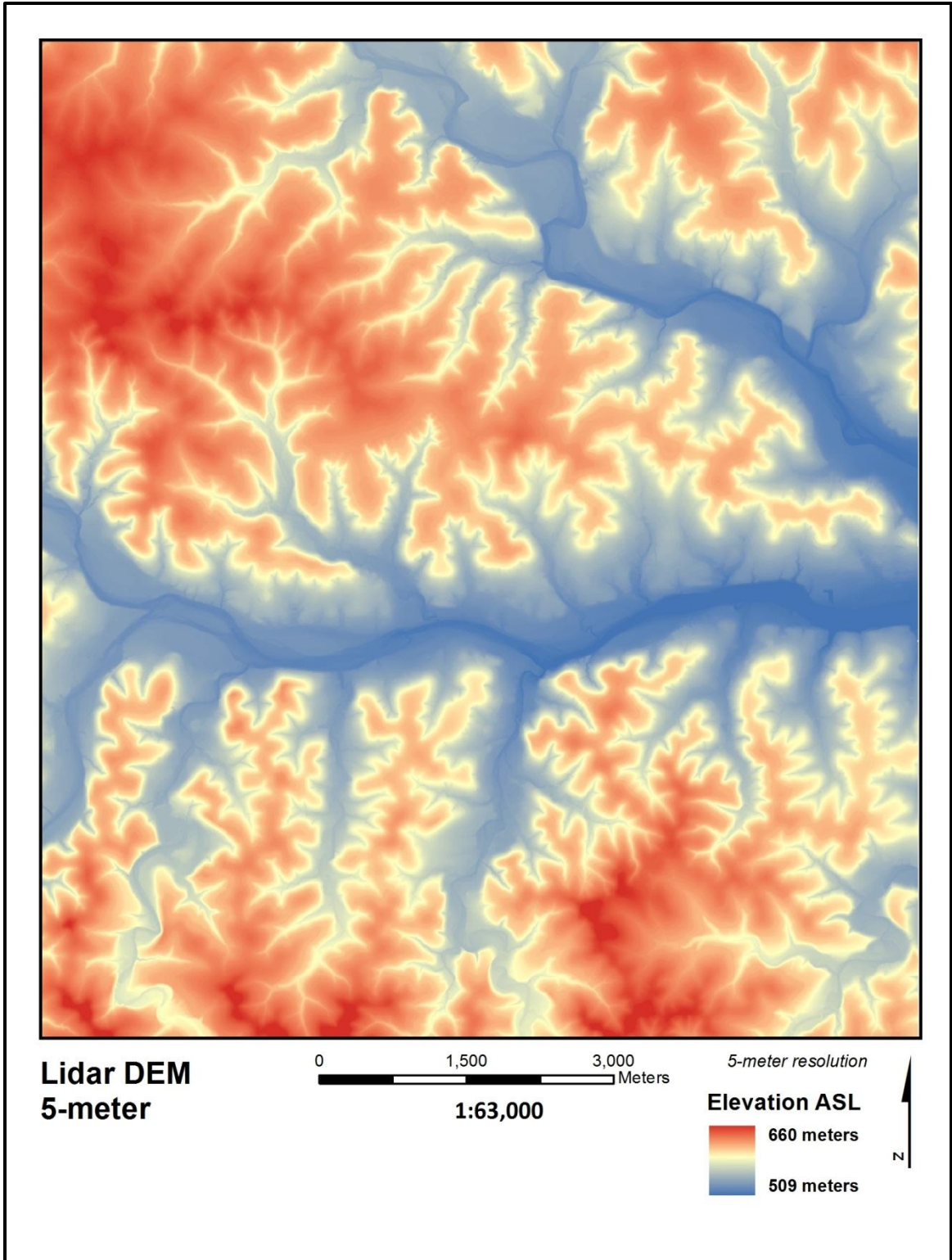


Figure 35. Lidar 5-meter DEM in Kerr Study Area.

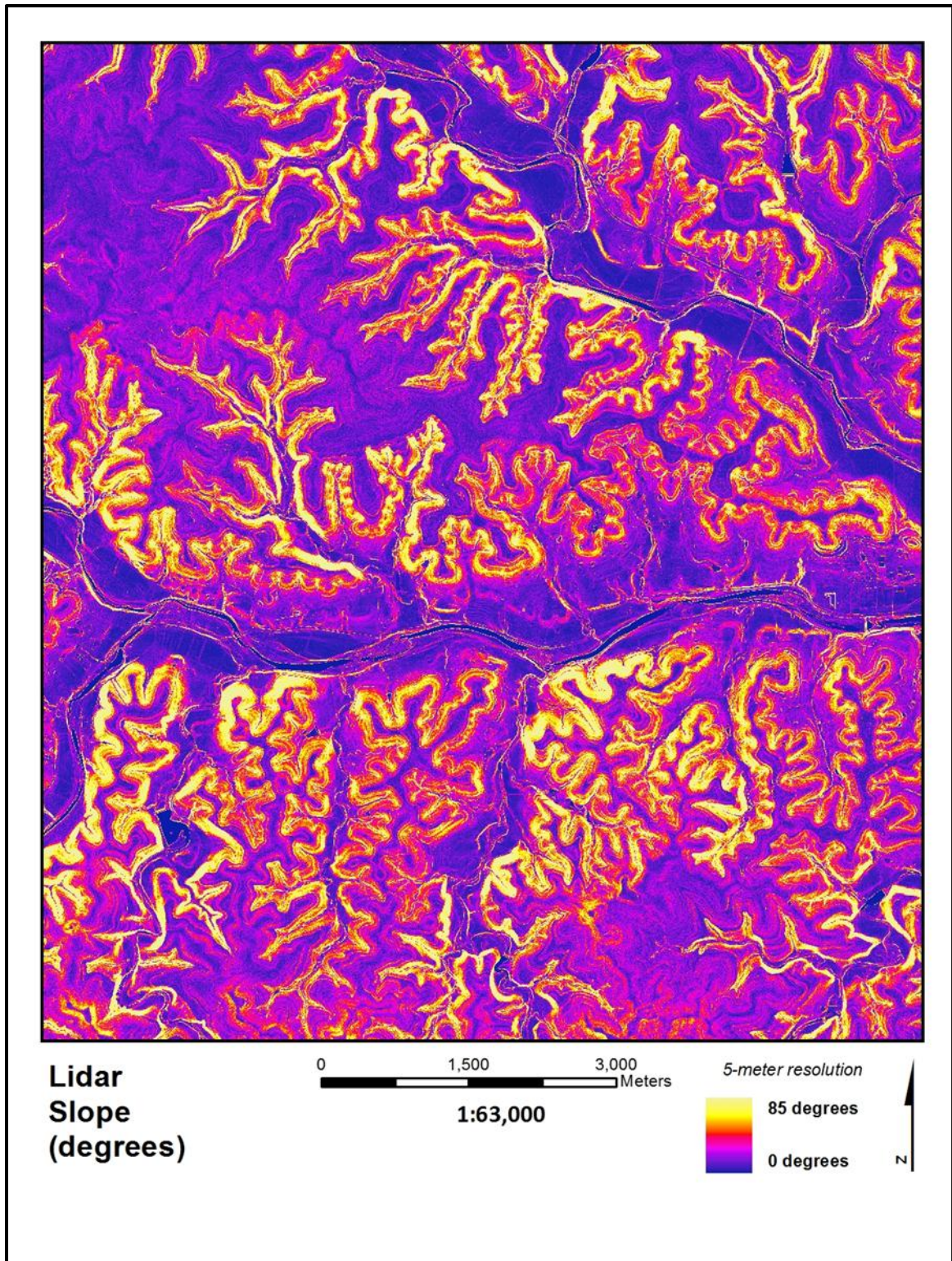


Figure 36. Lidar Slope in Kerr Study Area.

The result is a much lower average slope across the study area than is actually present. The lidar slope map reduces each pixel area to only 25 square meters ( $5 \text{ m}^2$ ), and within this threshold slope will be less undulating and will capture finer-scale variation. As such, it is possible that a given pixel will show a much higher slope value than would be found for the exact same spot on the 30-meter map. The identification of steeper slopes is important because as mentioned in the LANDFIRE section above, fire propagates much more quickly over steep terrain. Modeling with information that is not only accurate but also precise will stand to improve the results, although it should be noted that these are differences at a highly localized scale which could be easily irrelevant when considering the broader picture.

Similar to the differences in slope maps, there is a marked increase in resolution between the LANDFIRE aspect map (Figure 30) and the lidar aspect map (Figure 37). The general trends are similar, but the 5-meter map appears quite pixelated. Within the lidar-based aspect map, the steeper hillsides show much more consistency than in the riparian corridors where the effect is noisy. This indicates that perhaps five meters is too fine a resolution for aspect since the general trends are being diluted by the noisy pixels.

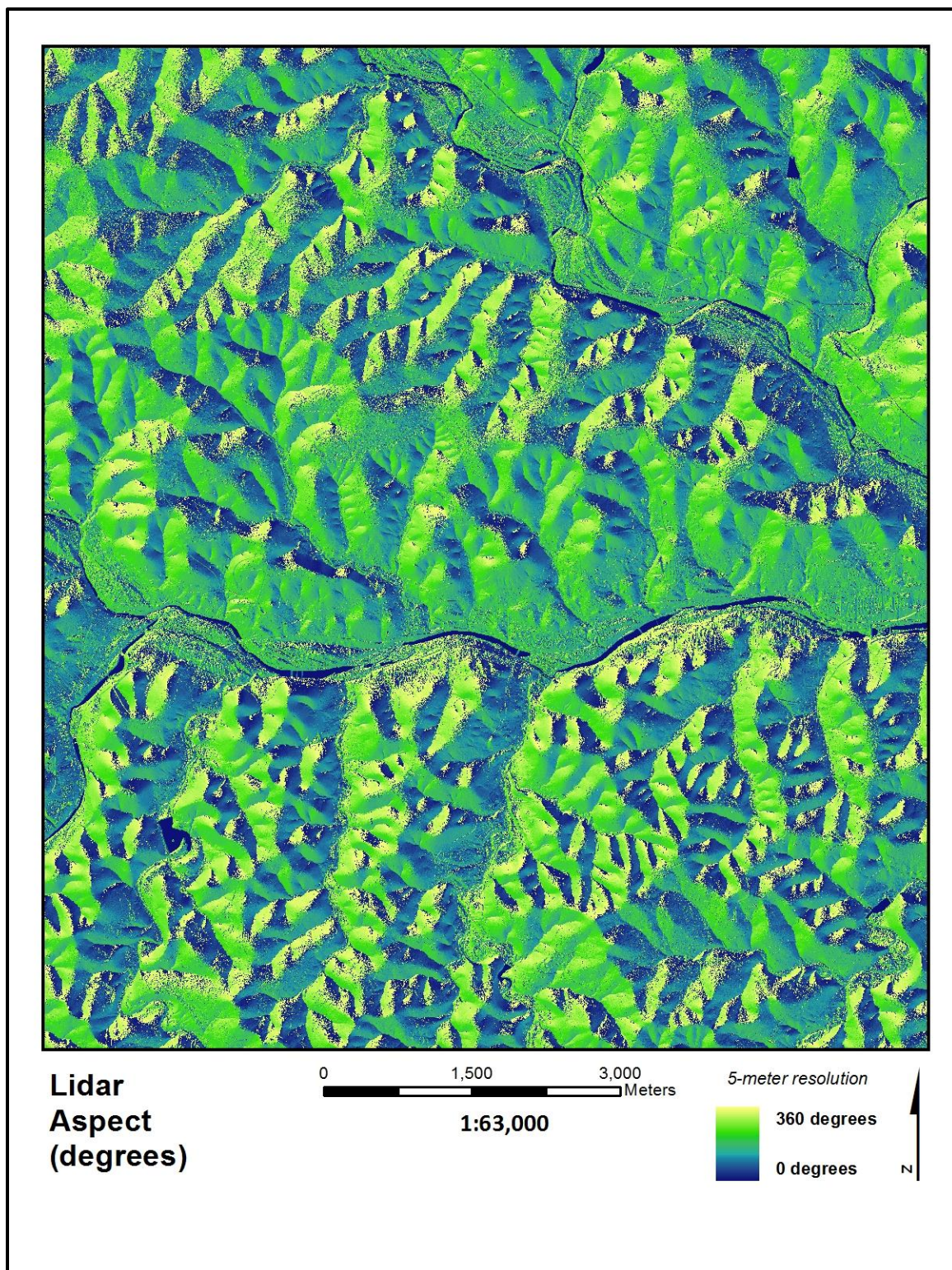


Figure 37. Lidar Aspect in Kerr Study Area.

The lidar-based canopy height model gives a highly detailed picture of the vegetation patterns found within the study area (Figure 38). While the 30-meter product captures the broad strokes of vegetation height (Figure 31), the 5-meter version displays an ornate landscape with ribbons of taller trees twisting around the hills and (as in the LANDFIRE CC map) utility ROW's cutting through the terrain. One anomaly is the presence of erroneously large height values in the river bed. These values are an artifact from the CH calculation methodology and though it is possible this will negatively affect the model results, the impact is unlikely to be severe since other inputs (such as NFFL) will identify those pixels as water.

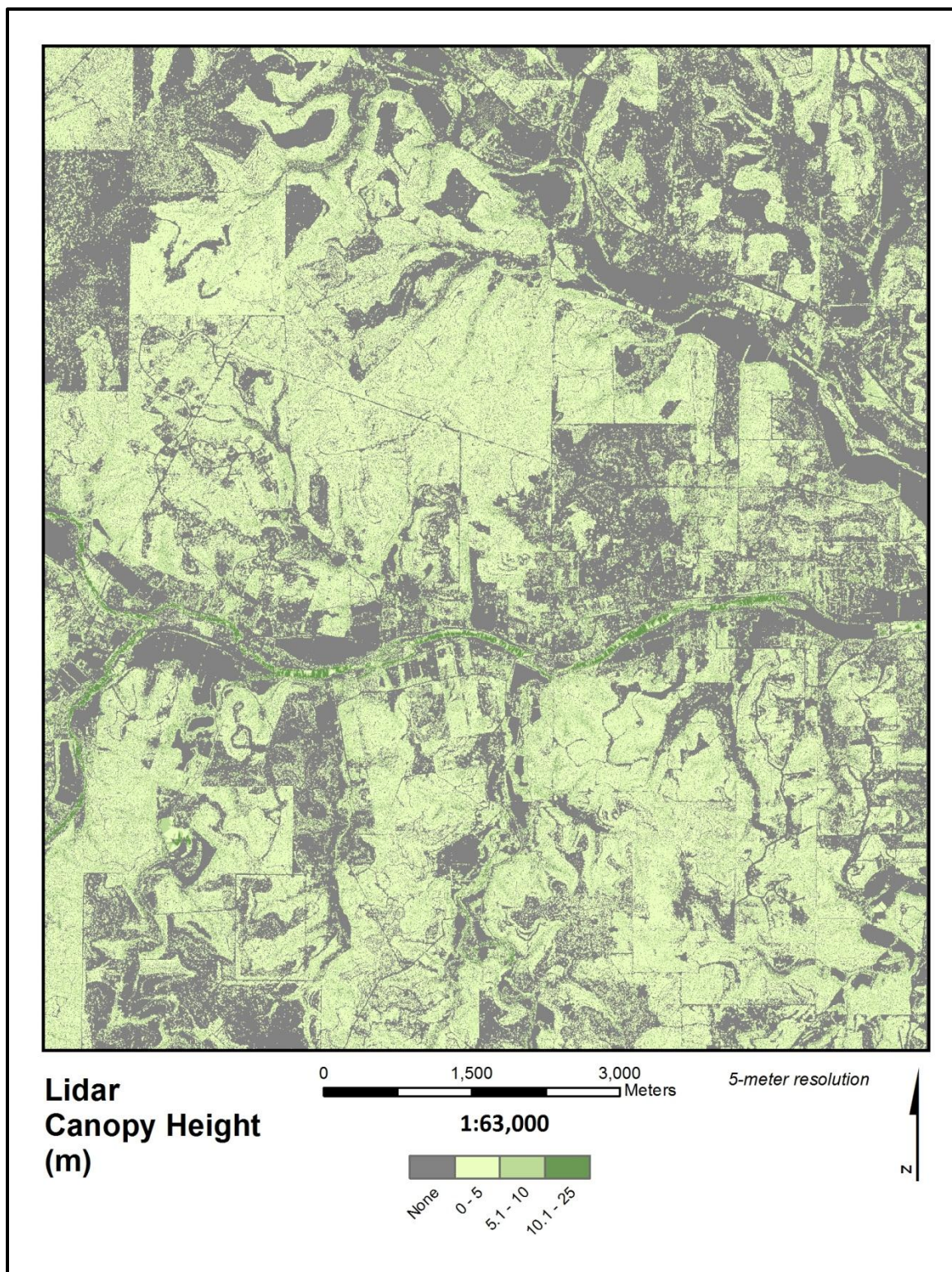
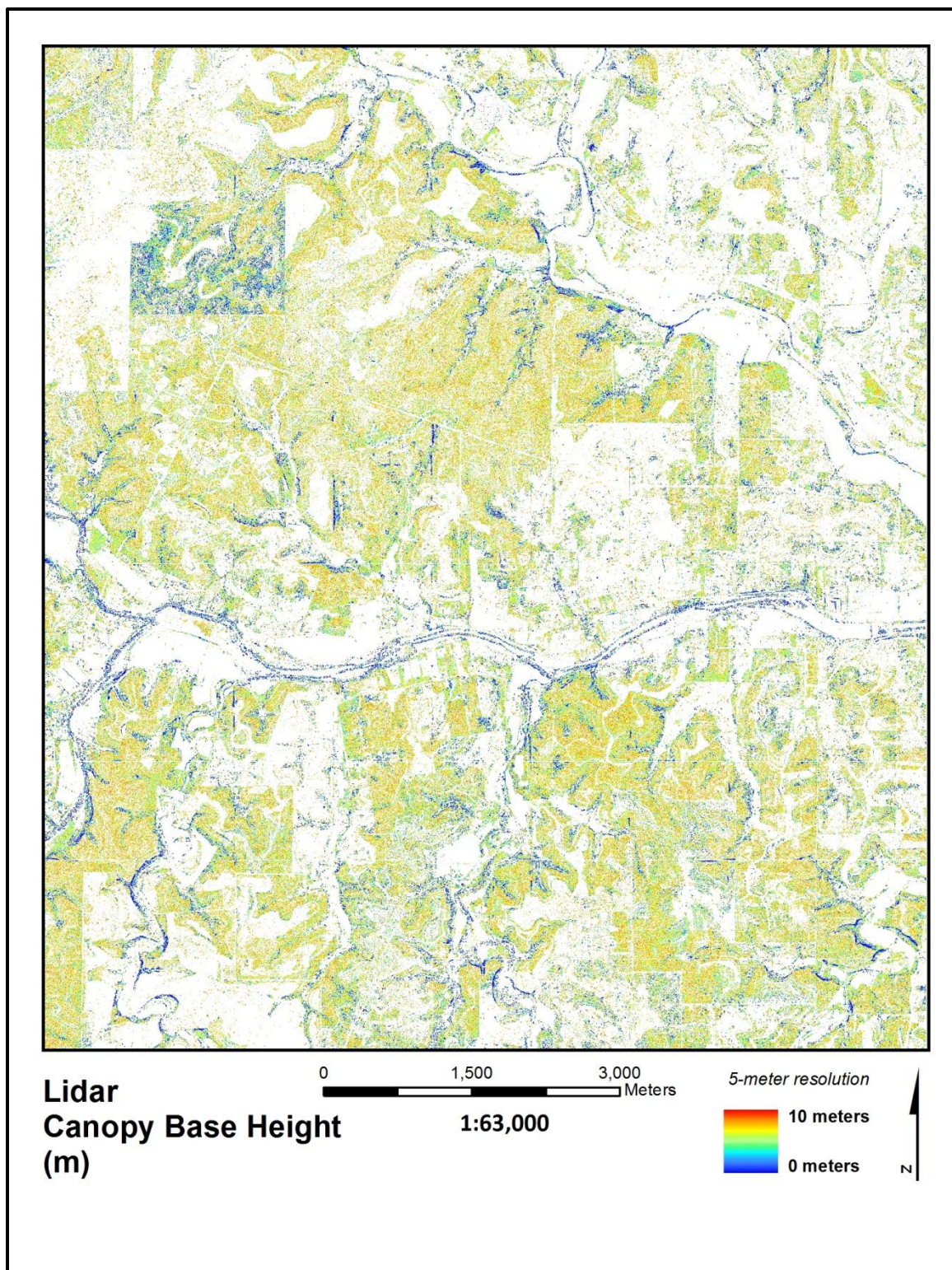


Figure 38. Lidar Canopy Height in Kerr Study Area.

Similar to the relationship between the LANDFIRE and lidar-based CH models, the CBH model becomes significantly more detailed in the 5-meter iteration but the range in values is shifted slightly higher (Figure 39). This likely resolves the effect of higher CBH values being averaged down due to large 30-meter pixels (which could include a dozen trees) (Figure 32). Also, it is more likely that gaps between trees are captured, which is the likely explanation for the peppered effect seen in the heavily vegetated portions of the lidar CBH map. By rescaling the LANDFIRE CBH map to match the lidar map it is easier to see the increase in CBH (Figure 40).



**Figure 39.** Lidar Canopy Base Height in Kerr Study Area.

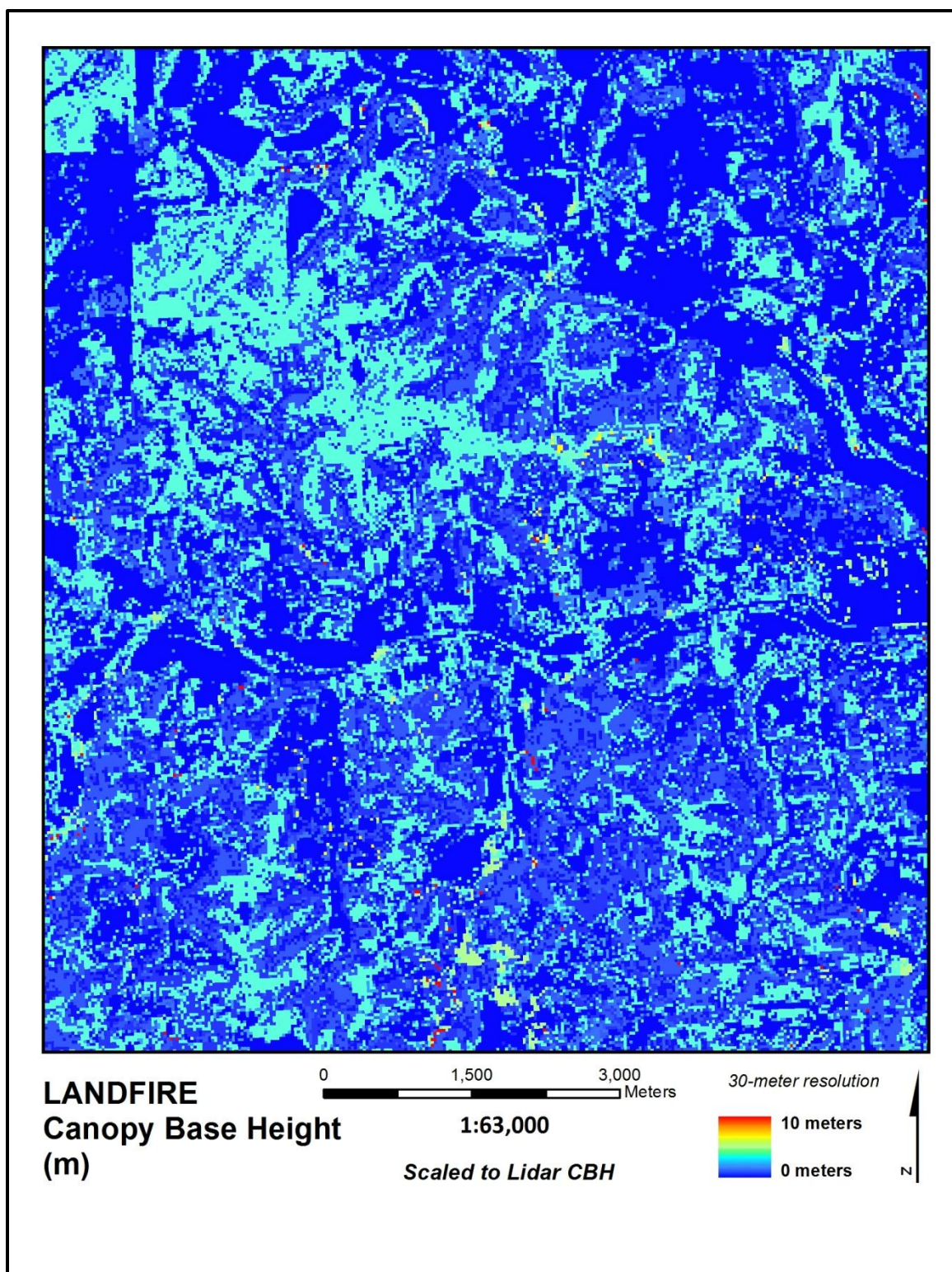
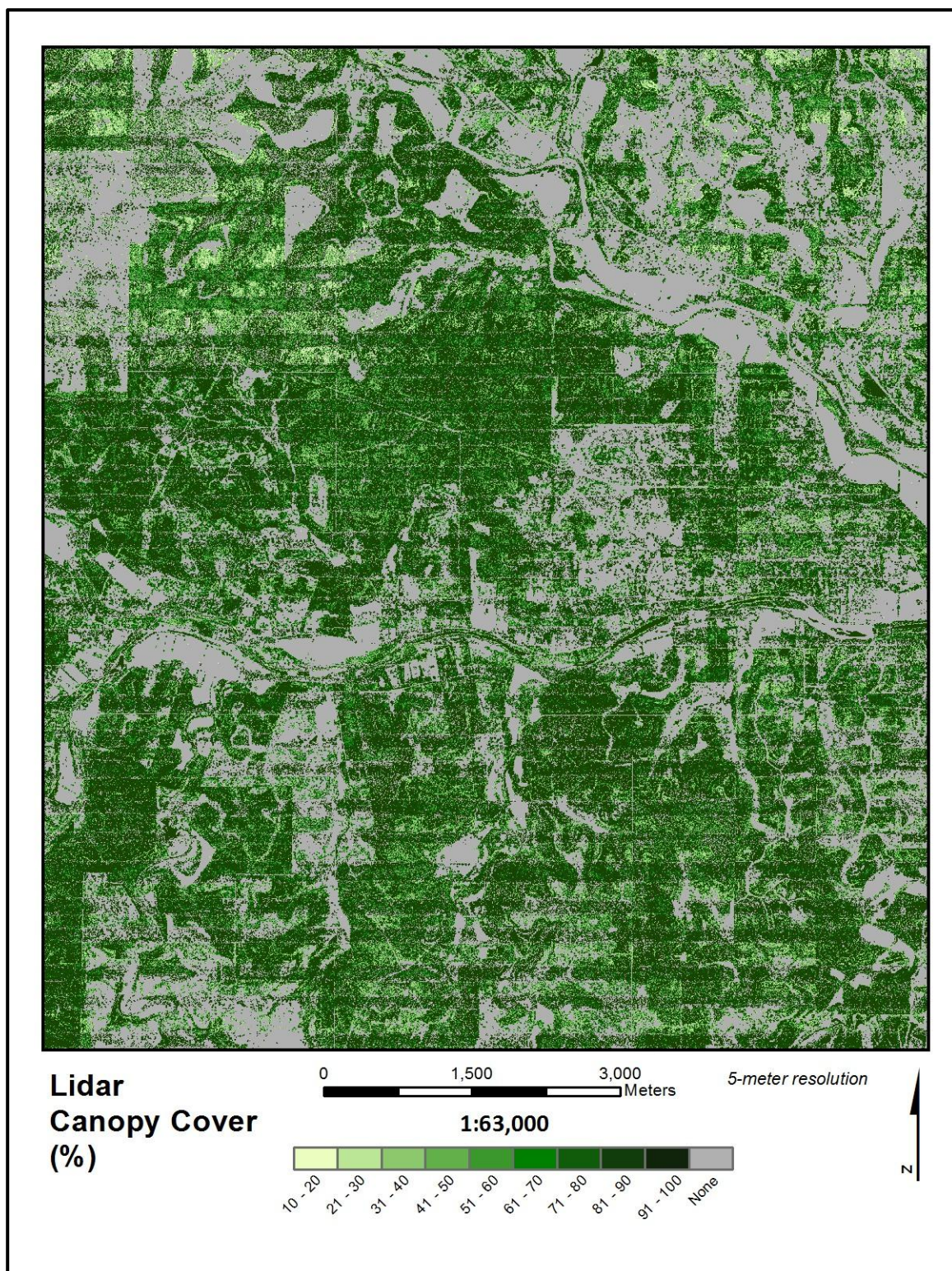


Figure 40. LANDFIRE Canopy Base Height Scaled to Lidar Data Range.

The canopy cover map generated from lidar (Figure 41) appears to show substantially more canopy cover than in the LANDFIRE counterpart (Figure 33). Also there is a notable horizontal striping effect throughout the study area. Both anomalies are the result of a particular characteristic of the parent lidar data that has been propagated through the data creation process. In lidar collection, overlapping flight lines cause double the amount of point returns than areas with only one flight line. Since canopy cover was generated from the lidar by recording the ratio of vegetation points relative to all collected points, the variation in point density persisted to the final product, albeit slightly. Also, the parent lidar did not distinguish between low, medium, and high vegetation and so all vegetation was considered for calculation of canopy cover, including some areas that were likely just tall grass. This result should not significantly impact the wildfire model since the extra “erroneous” canopy cover is technically still vegetation.



**Figure 41.** Lidar Canopy Cover in Kerr Study Area.

The canopy bulk density map produced from the CFE tool (Figure 42) is remarkably different than its LANDFIRE counterpart (Figure 34). The lidar CBD map shows a faint scattering of higher CBD values with one concentration of high values in a plot of land to the northwest of the study area. While the location of the highest values matches the general pattern found in the LANDFIRE map, the latter shows much more continuous coverage. Using the Kerrville study area Landsat 5 imagery for comparison, it is apparent that the LANDFIRE CBD representation more closely matches the distribution and density of vegetation than the lidar.

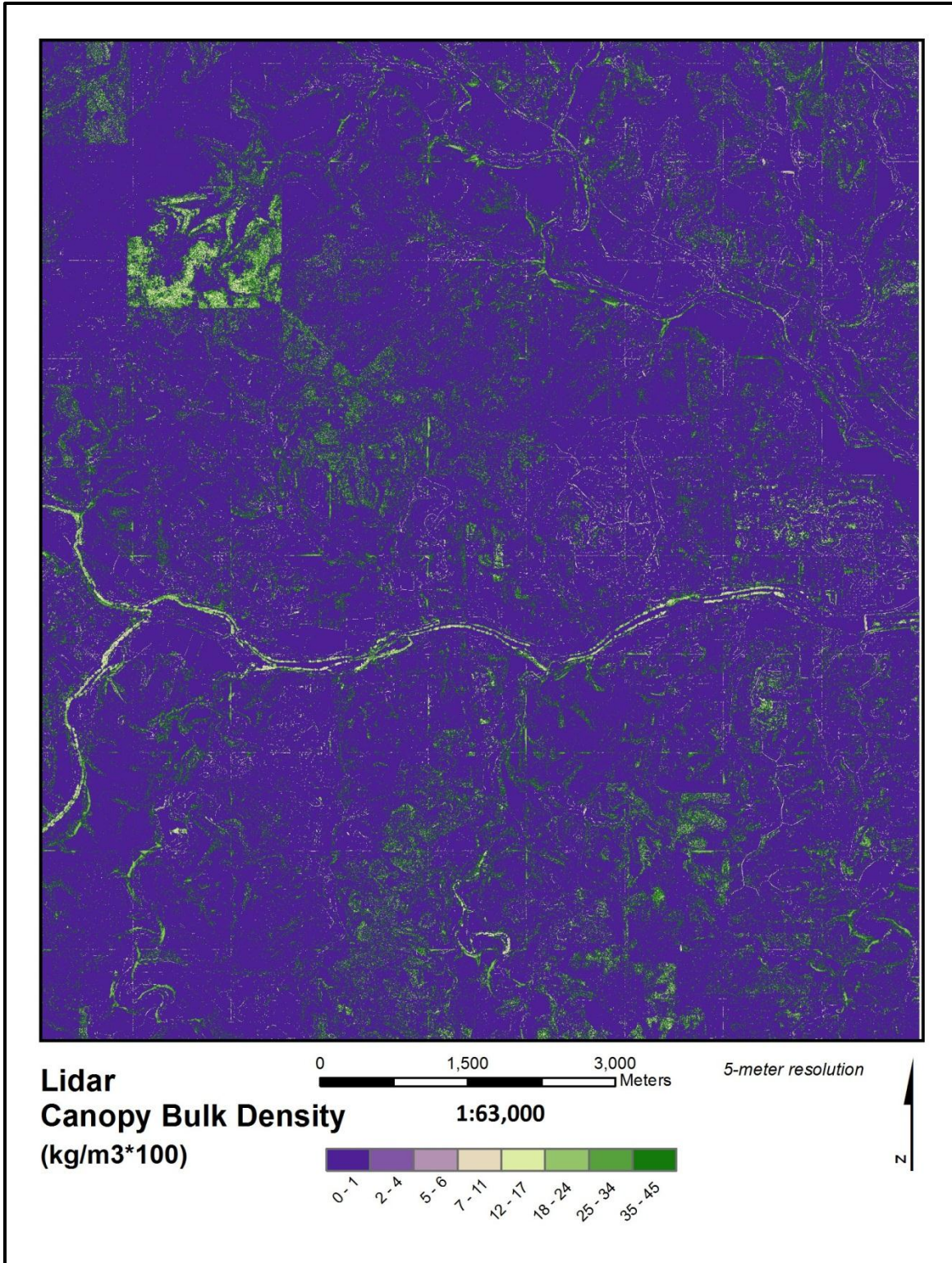
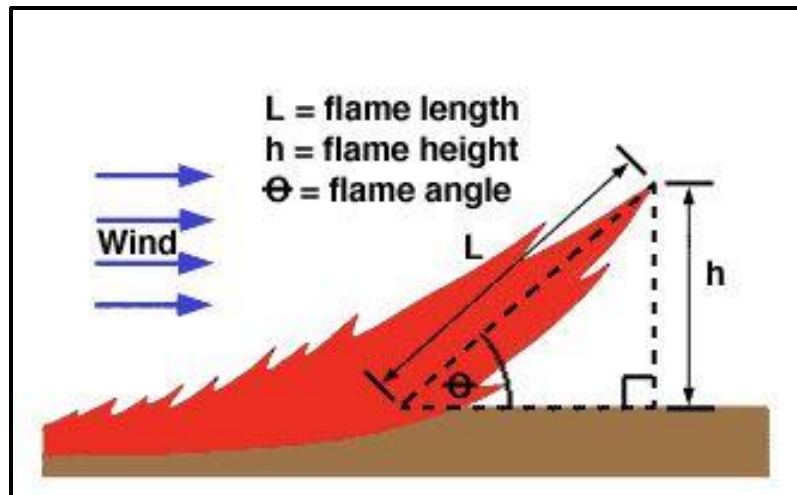


Figure 42. Lidar Canopy Bulk Density in Kerr Study Area.

### *4.1.3 FlamMap Output*

The following fire behavior characteristic maps were selected to be generated by FlamMap: Flame Length, Spread Rate, Fireline Intensity and Crown Fire Activity. This study was developed on the premise that high-resolution, high-precision inputs to a wildfire model based on lidar data would result in fire behavior maps that are also of a higher resolution and exhibit a finer degree of precision compared to lower-resolution satellite imagery-derived LANDFIRE data. The change detection maps (including both Image Difference maps and Highlight Change maps) were created on the basis that the LANDFIRE method maps represent “before” and the lidar method maps represent “after”. For example, an increase in values from one map to the other indicates that the LANDFIRE values were lower than the lidar values. The image difference maps show gradation of change from the LANDFIRE method to the lidar method while the highlight change maps identify pixels which have experienced at least a 10% change in value (increase or decrease). Pixels that have changed slightly (less than 10%) are denoted by “some increase” or “some decrease”.

The first map, Flame Length, is a measure of fire intensity and can estimate the level of challenge to extinguish. Technically speaking, flame length is the distance from the fuel surface to the point on the flame axis where the carbon monoxide concentration is 5000 parts per million (Long 2012) (Figure 43).



**Figure 43.** Flame Length Diagram (Long 2012).

Both flame length output maps show similar patterns, although the lidar map (Figure 44) shows a wider range of values than the LANDFIRE map (Figure 45), particularly in the grass/shrubland areas. The Image Difference map (Figure 46) highlights these discrepancies as dark patches distributed across these lower-lying areas. The Highlight Change map in the same figure shows a widespread amount of subtle increase and decrease. Most of the areas denoted as “some decrease” are located in the higher elevations where the densest vegetation is located while “some increase” values are stronger in the northern portion of the study area, where grassland or bare earth is more prevalent.

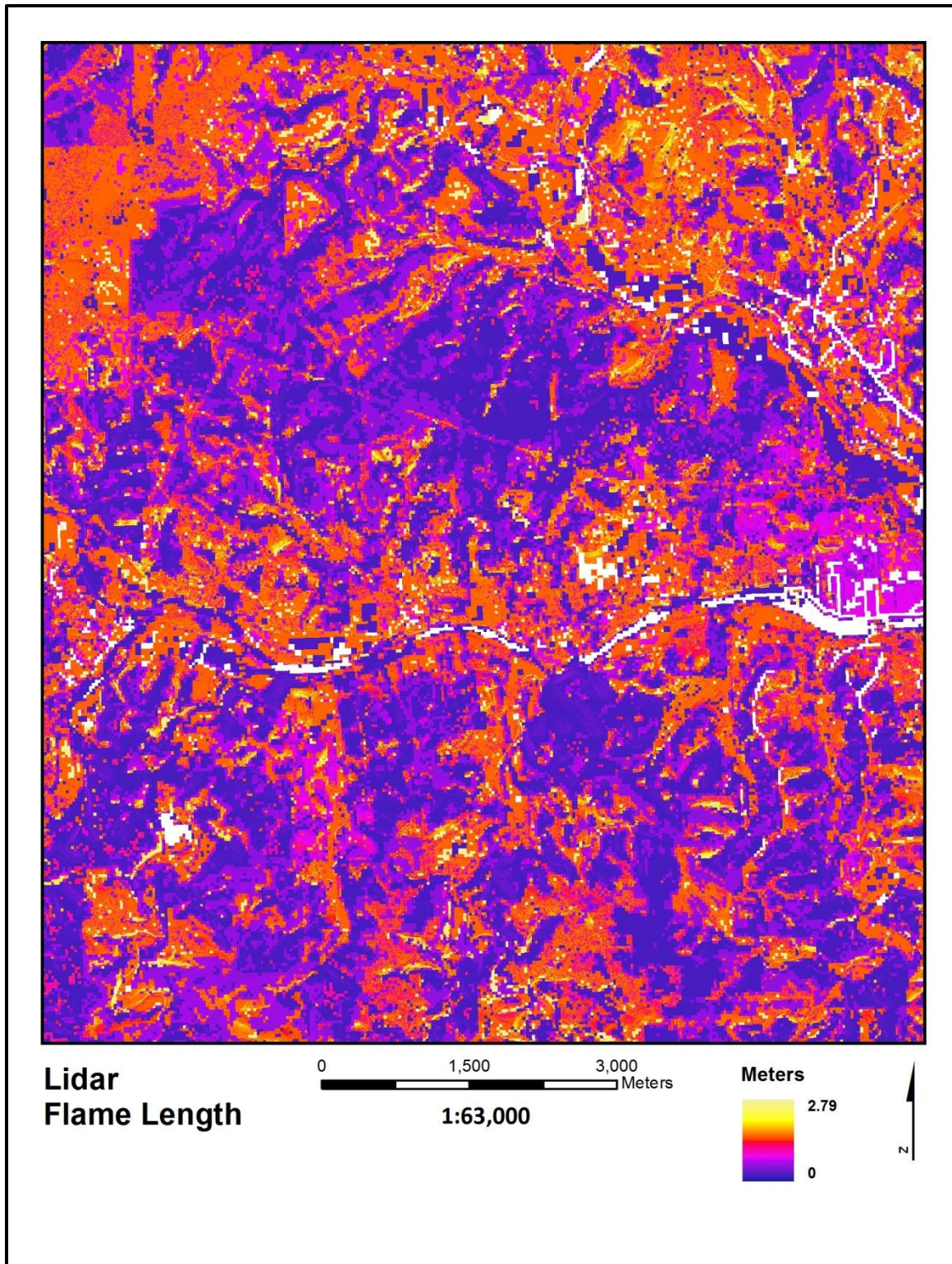


Figure 44. Lidar Flame Length Output.

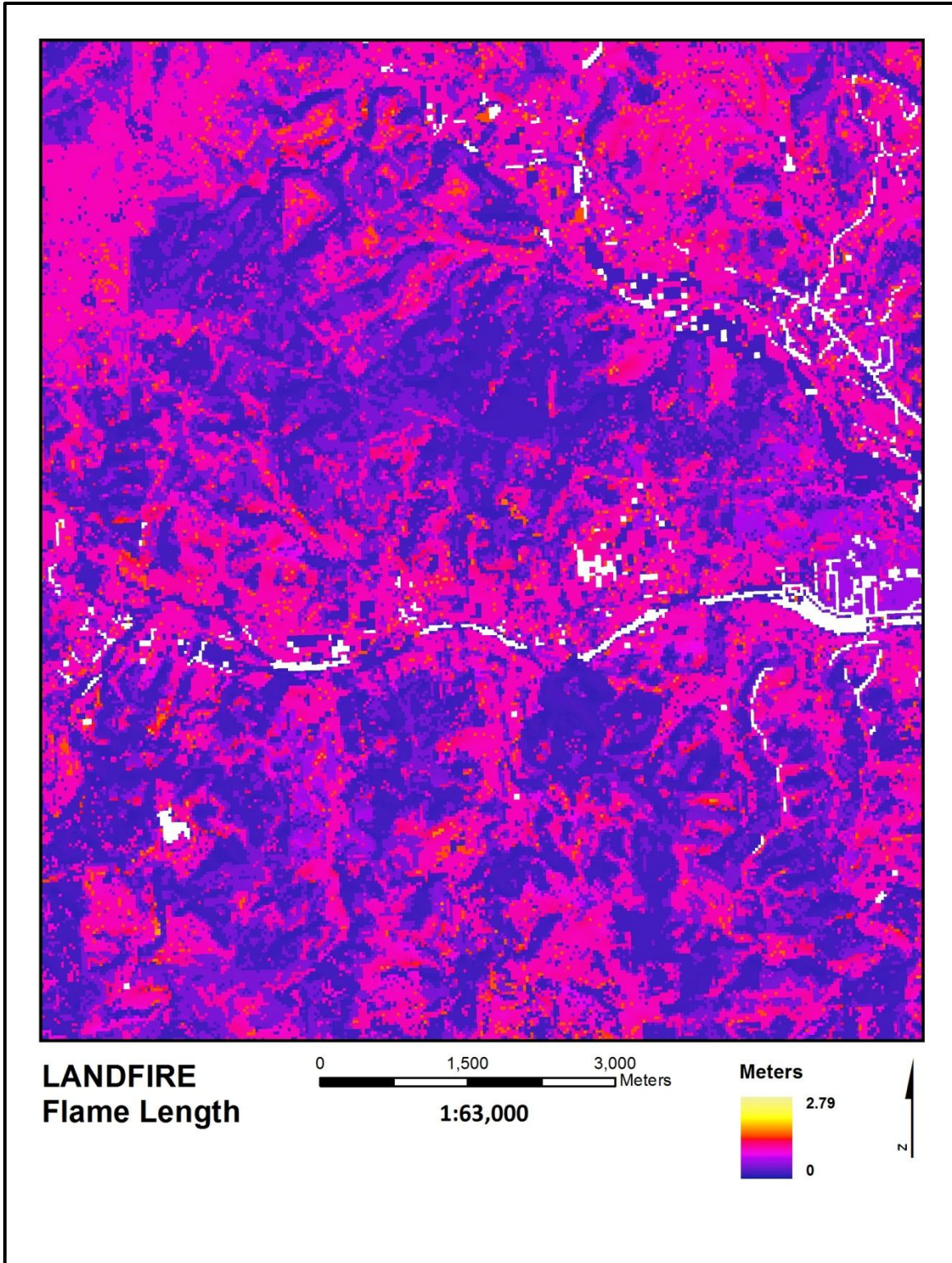


Figure 45. LANDFIRE Flame Length Output.

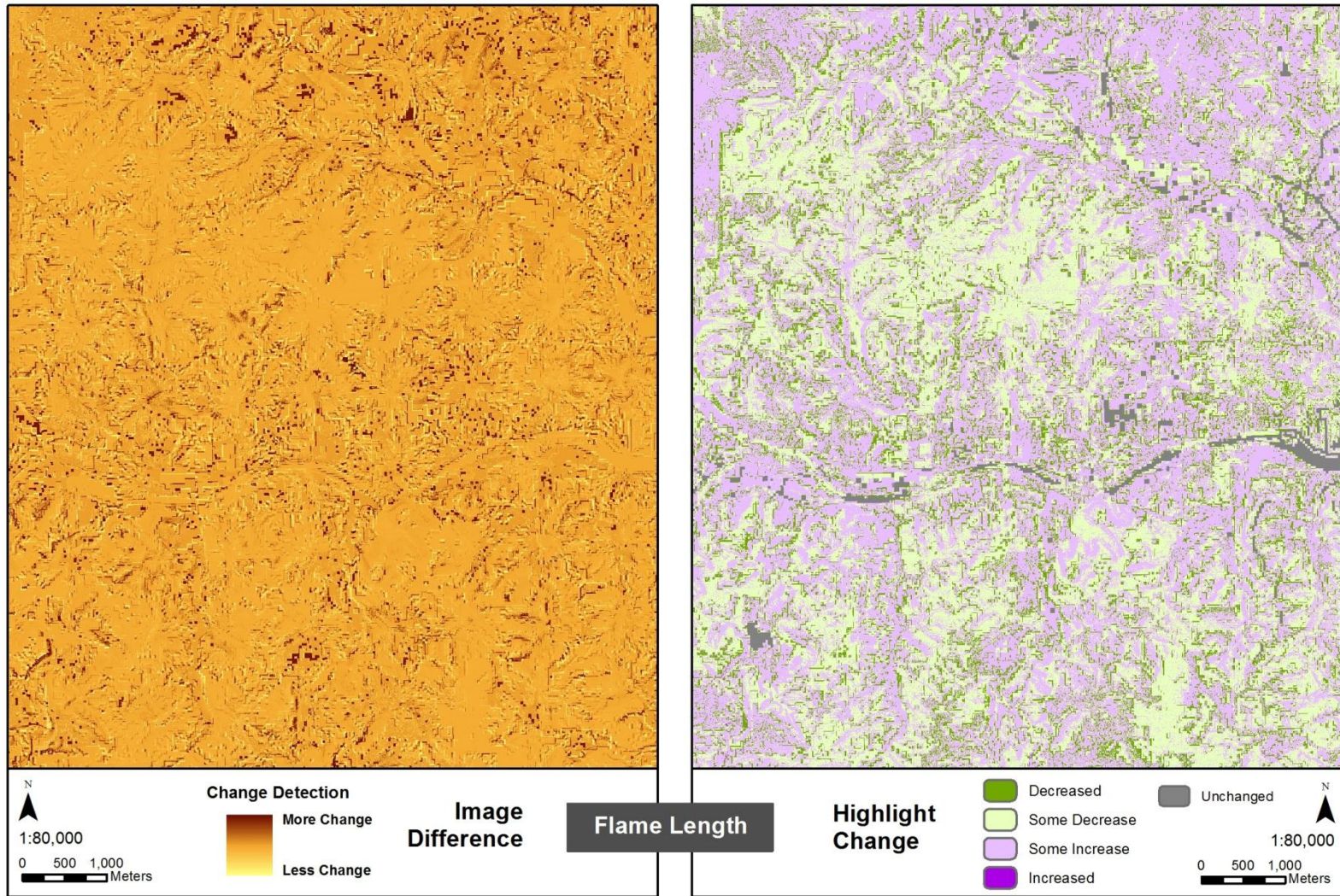


Figure 46. Flame Length Change Detection.

Fireline intensity can be used to compare fires, assess the effects of prescribed burns, or to assess the difficulty of wildfire containment (Long 2012). The metric “is the rate of heat energy released per unit time per unit length of fire front, regardless of the depth of the flame zone” and “is calculated as the product of available fuel energy and the fire’s rate of advance” (Long 2012):

$$I = Hwr$$

Where:

I = Byrams fireline intensity (kW/m)

H = fuel low heat of combustion (kJ/kg)

w = weight of fuel consumed per unit area in the active flaming zone (kg/m<sup>2</sup>)

r = rate of spread (m/s)

Fireline intensity can be highly variant with low intensity fires being less than 550 kW/m and high intensity fires exceeding 4000 kW/m. The results from FlamMap show a somewhat similar set of outputs from the LANDFIRE and lidar inputs. The LANDFIRE fireline intensity values range from zero to a high just shy of 1000 kW/m (Figure 47). The spatial pattern predicts a higher intensity fire would take place where there is open grassland vegetation interspersed with a few trees, as opposed to the heavily vegetated areas where values are lowest.

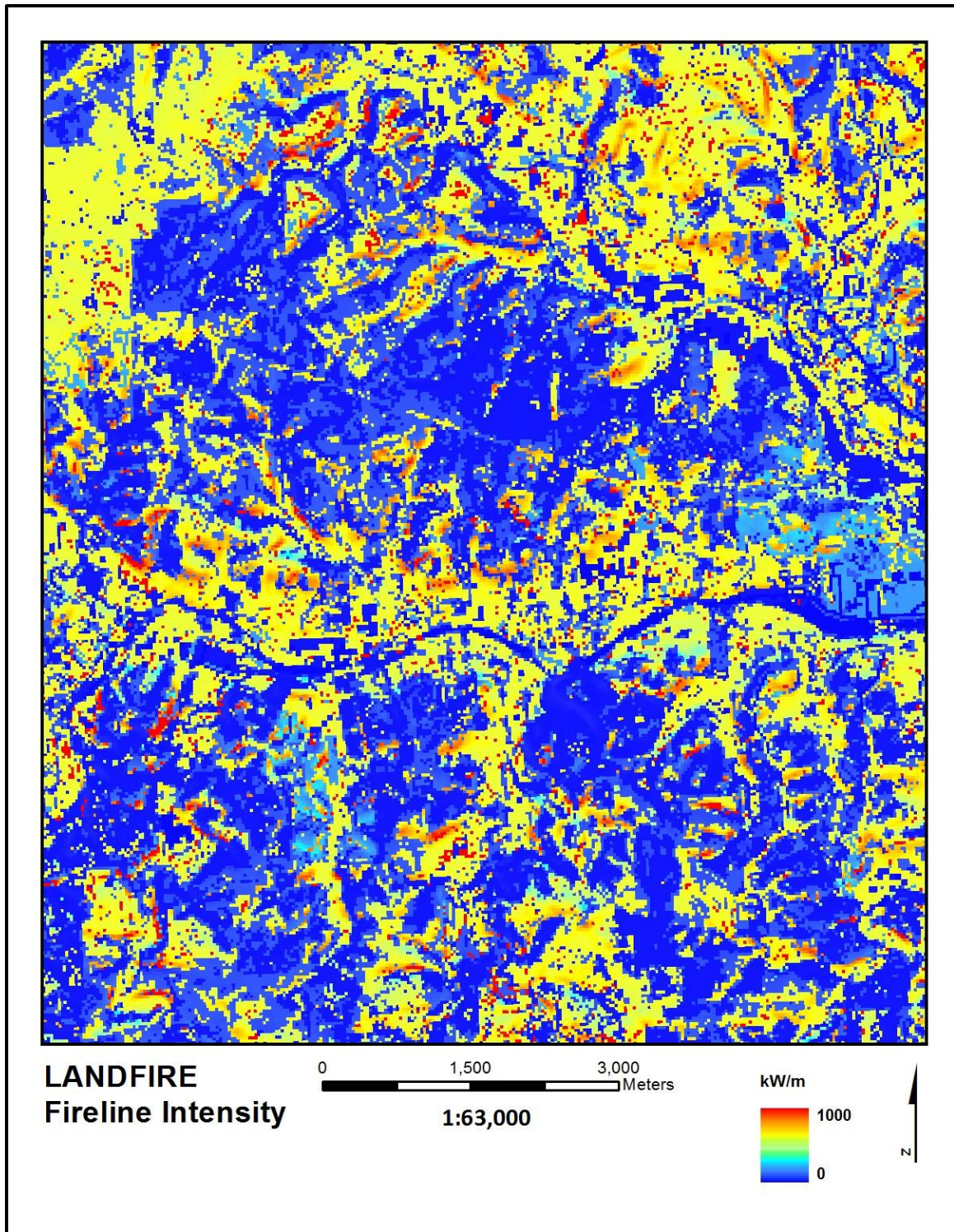


Figure 47. LANDFIRE Fireline Intensity Output.

By comparison, the lidar fireline intensity map shows very similar patterns, but with values that have shifted higher where there is grassland vegetation (Figure 48). The spatial pattern here also appears to be correlated with the lidar method canopy bulk density map (Figure 42) which as mentioned above is sparsely populated with CBD values. The Image Difference map shows very little severe change and the Highlight Change map is quite similar to that above for flame length – lots of moderately increased values in the grassy areas with moderately decreased values in the forested areas (Figure 49).

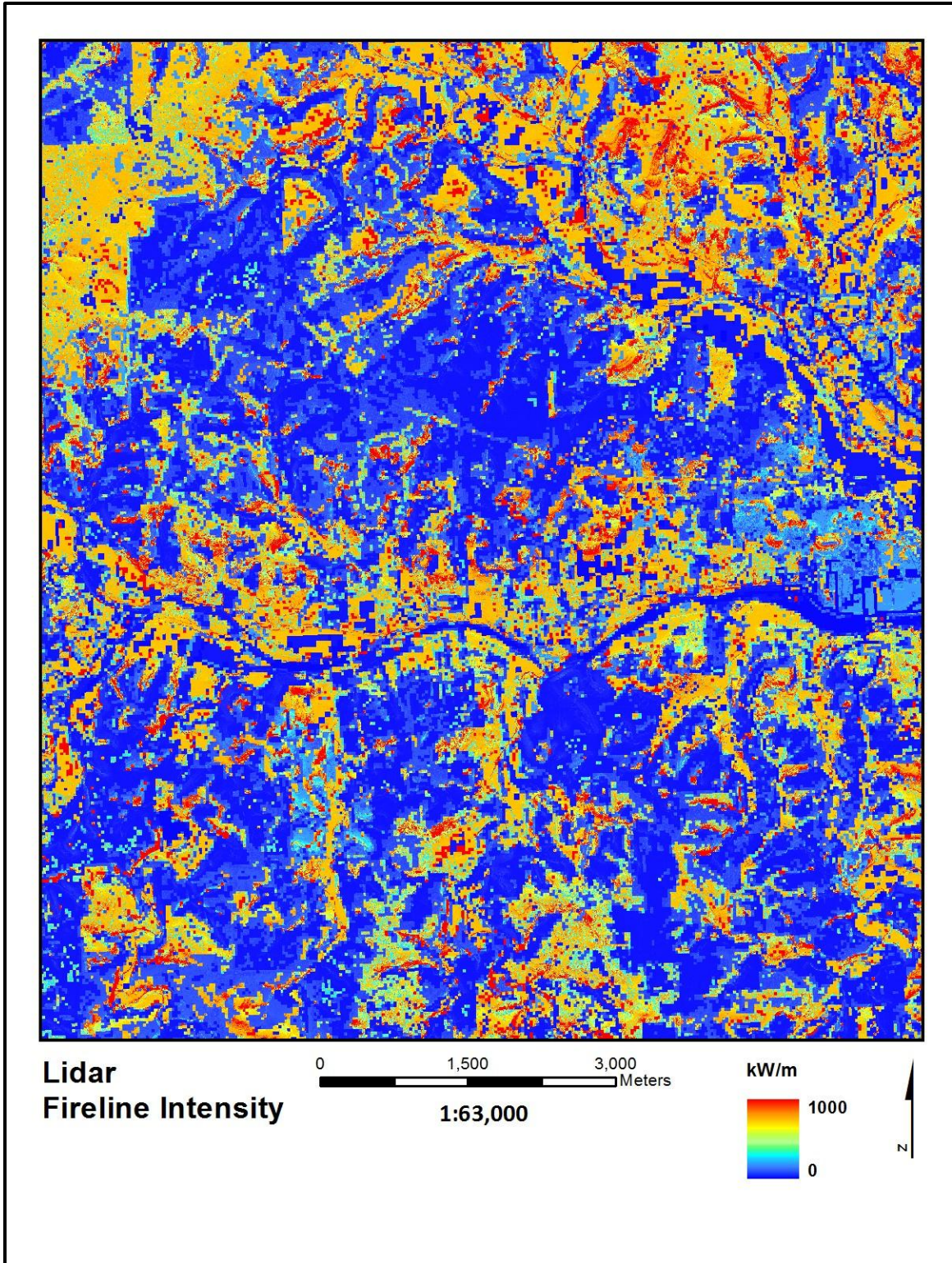
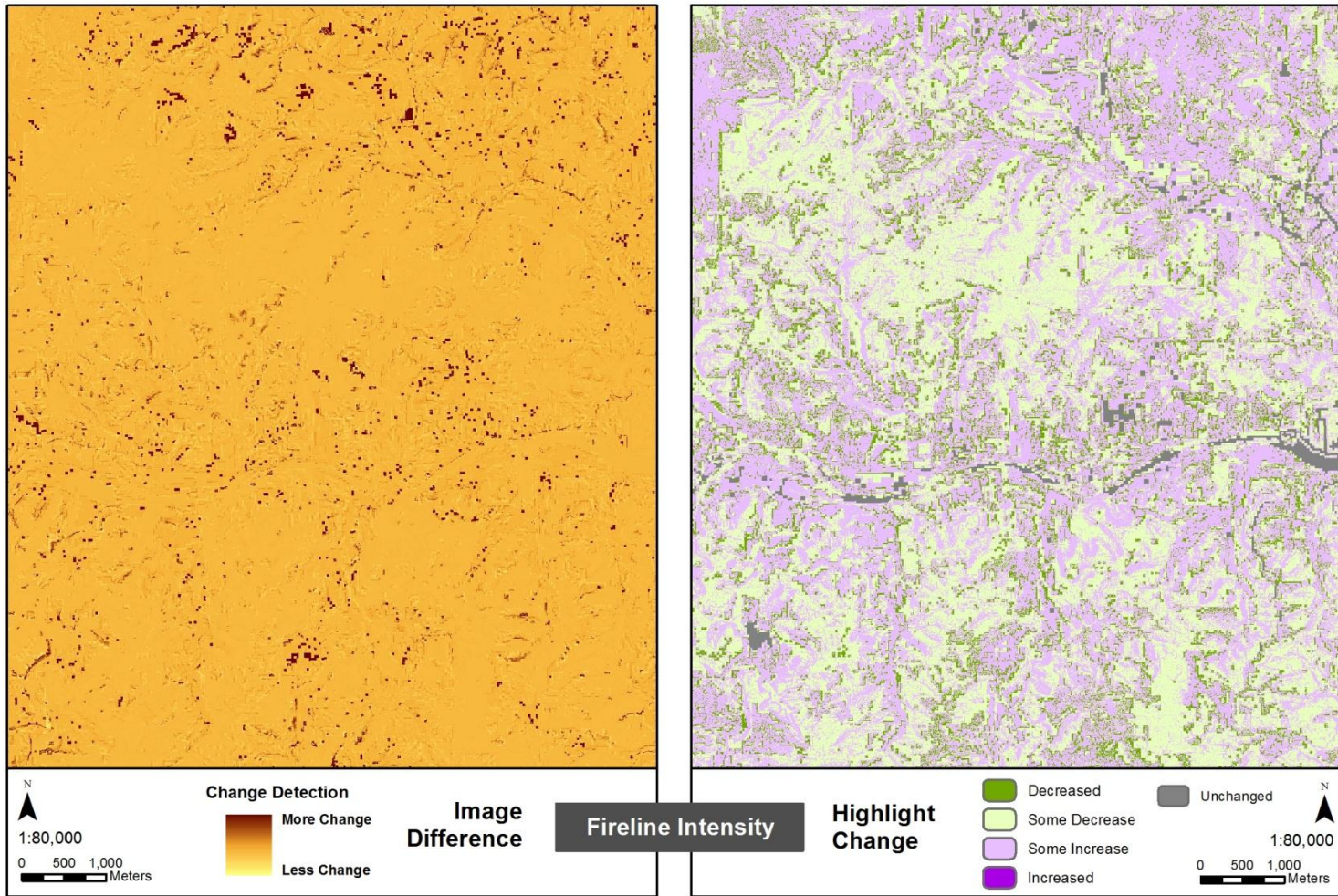


Figure 48. Lidar Fireline Intensity Output.



**Figure 49.** Fireline Intensity Change Detection.

Crown fire activity is a more discrete description with values representing one of three scenarios: No Fire, Surface Fire, and Crown Fire. The FlamMap results for crown fire activity gave no values for Crown Fire from either LANDFIRE (Figure 50) or lidar results (Figure 51). Instead, almost the entire study area is shown as Surface Fire with the water, urban and bare earth features shown as No Data.

The Image difference output between the two methods only picks up on a few pixels along the riparian corridors which were significantly different from the 30-meter iteration to the 5-meter version (Figure 52). Almost all of these pixels are shown in the Highlight Change map to have experienced an increase. This is very likely due to the fact that larger 30-meter mixed pixels along the water features were better defined in the lidar input and so the crown fire activity output pixels moved from a No Data value to a Surface Fire value.

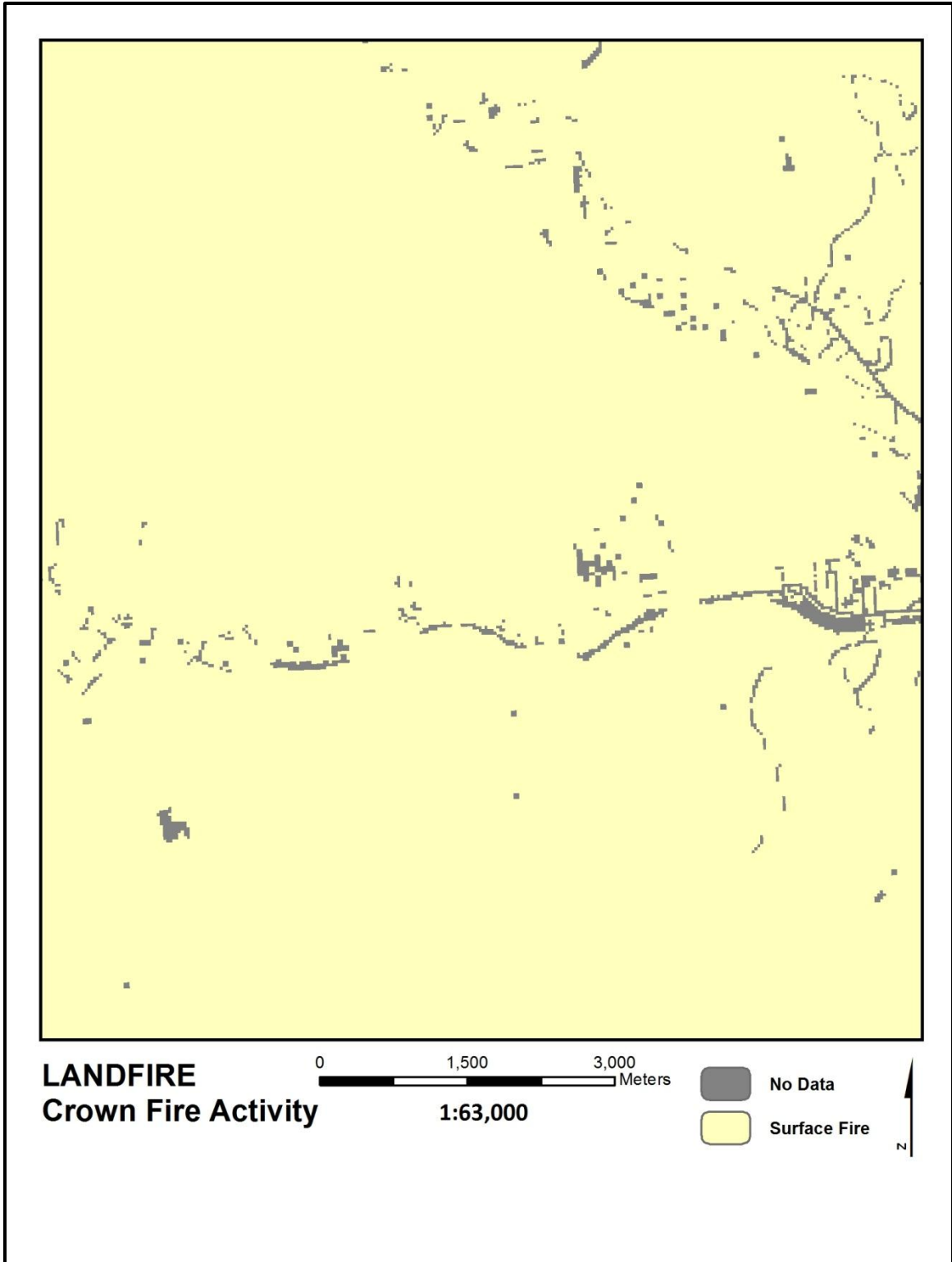


**Figure 50.** LANDFIRE Crown Fire Activity Output.

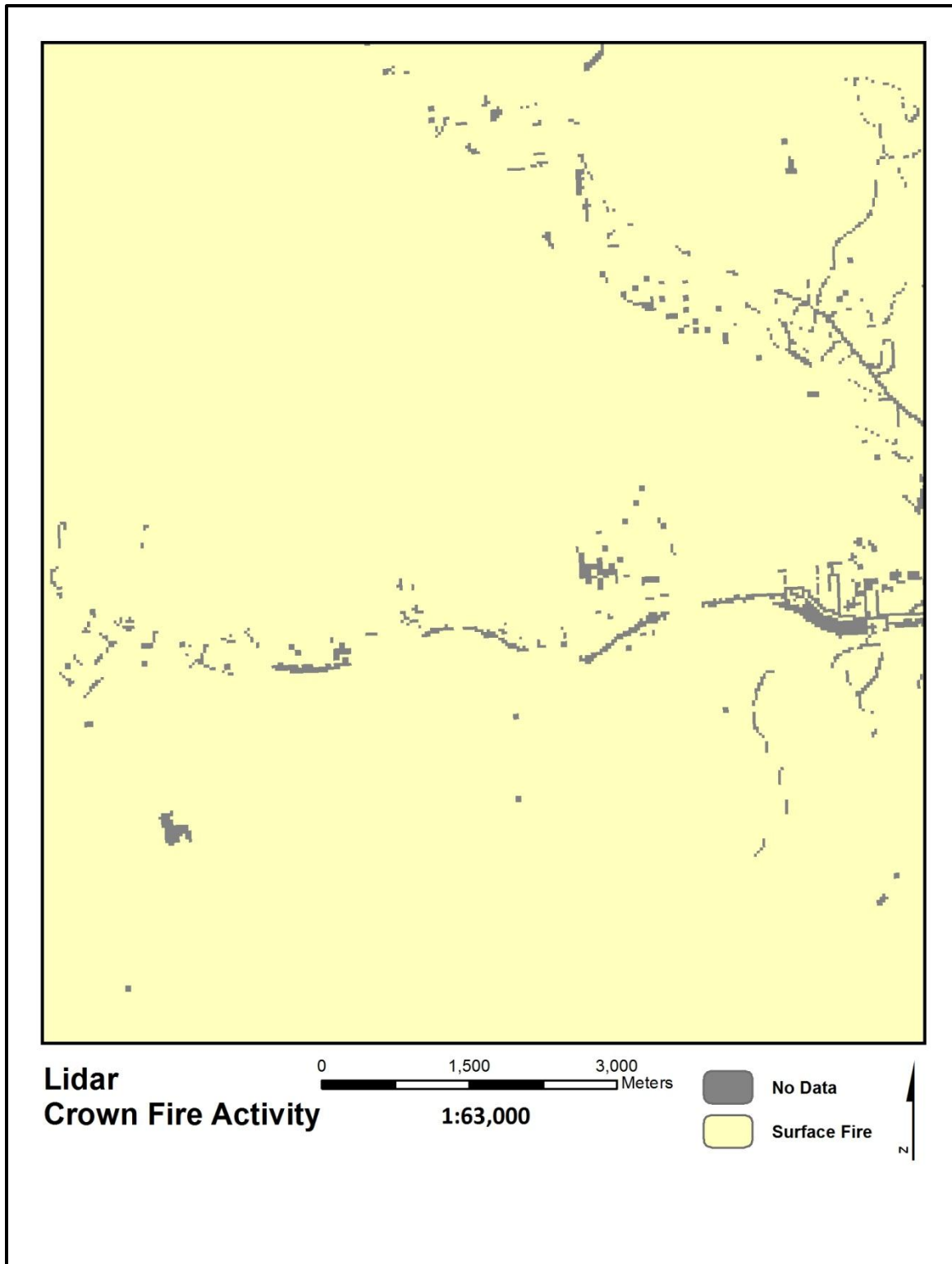


Figure 51. Lidar Crown Fire Activity Output.

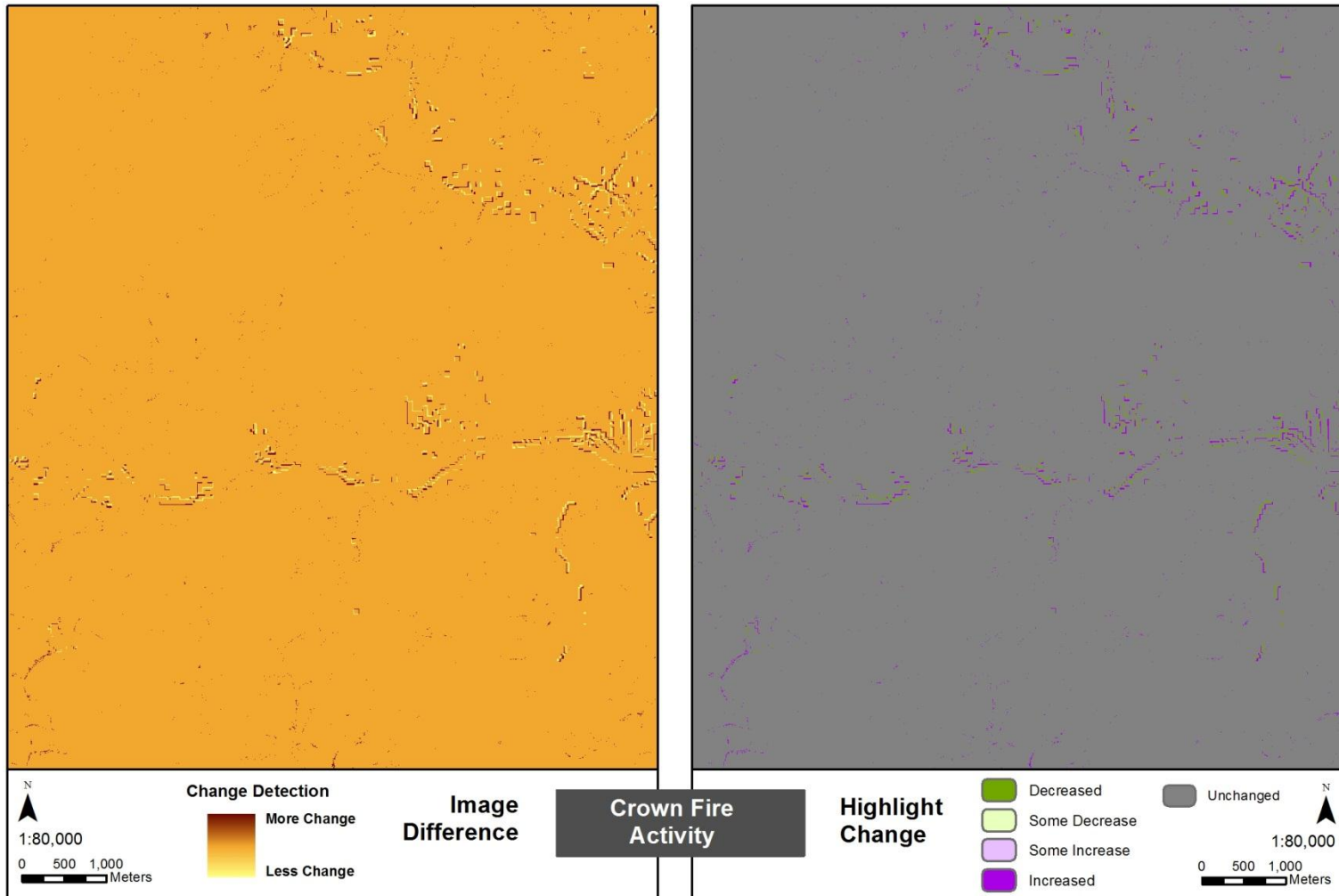


Figure 52. Crown Fire Activity Change Detection.

The last FlamMap output map is spread rate. Rate of spread is closely related to fireline intensity and according to Long (2012):

“Rate of spread is the horizontal distance that the flame zone moves per unit of time and usually refers to the head fire segment of the fire perimeter... (it) can be measured from any point on the fire perimeter in a direction that is perpendicular to the perimeter. Because rate of spread can vary significantly over the area of the fire, it is generally taken to be an average value over some given period of time. The fastest rate of spread is along the forward moving perimeter located at the head of the fire. The slowest rate of spread will be found on the windward (back) side of the perimeter. The rate of spread along the flanks will be intermediate between the head and backing rates of spread. Rates of spread can easily be estimated by timing the passage of the flaming front between two landmarks of known distance apart. To determine rate of spread within the interior of a fire, firecrackers placed at known intervals along a transect perpendicular to the flame front have also been used. More technical techniques of measuring rates of spread involve videography or the use of thermocouples to record the passage of the flaming front.”

The two spread rate outputs from FlamMap are remarkably similar, with the lidar-based map (Figure 53) showing the same spatial patterns as the LANDFIRE version (Figure 54) but with the extra resolution from being 5-meter. The only major difference appears to be the treatment of hydrologic features, which are NoData values in the LANDFIRE map (white) and are displayed as zero in the lidar map (yellow). The Image Difference map follows the same patterns as in the fireline intensity and flame length

maps, although there are many more pixels showing “more change” than in either of those two (Figure 55). Likewise, the Highlight Change map shows the majority of the decreased values to be located in the forested areas and the grasslands show some increase from the LANDFIRE model run relative to the lidar run.

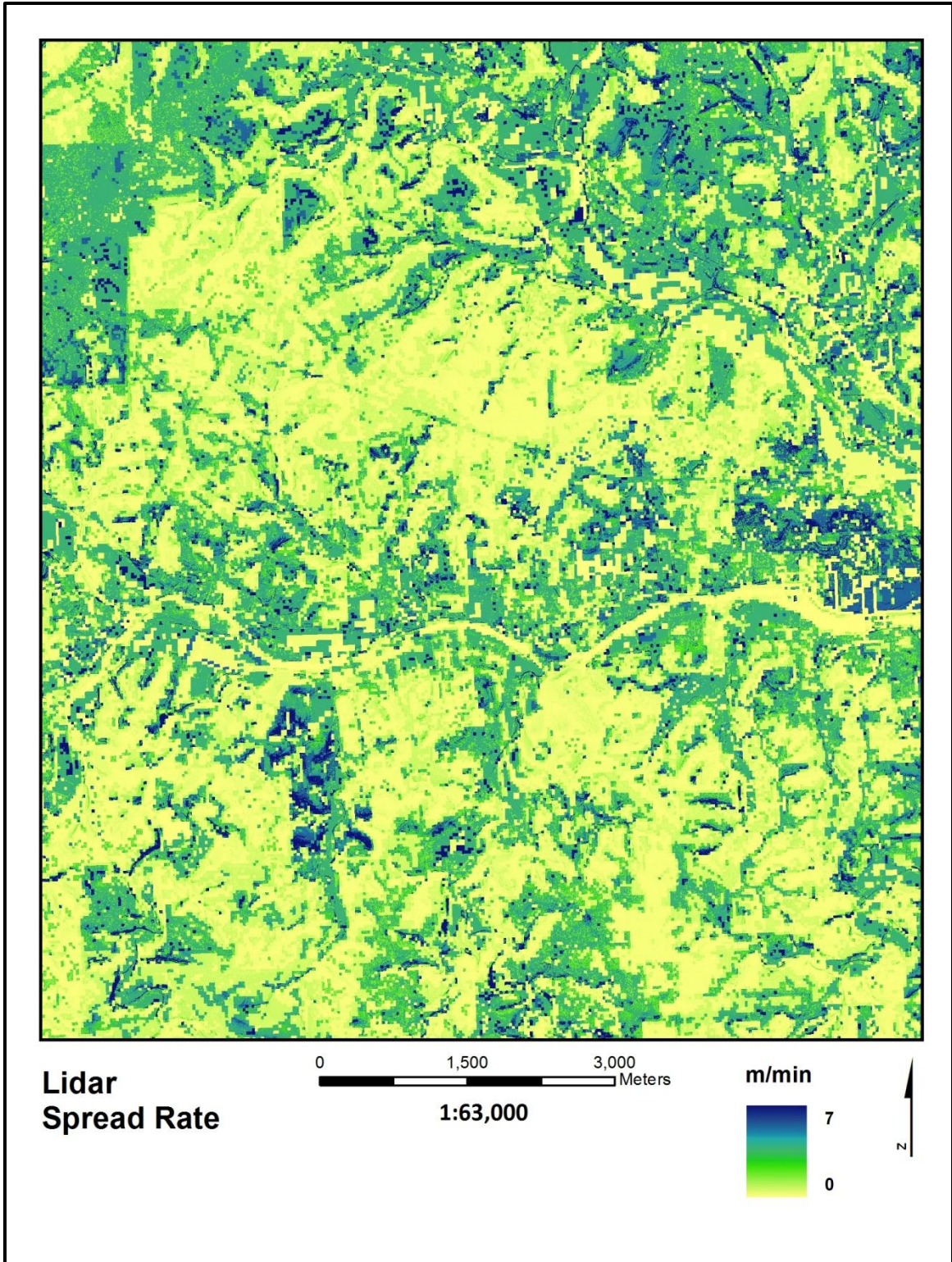


Figure 53. Lidar Spread Rate Output.

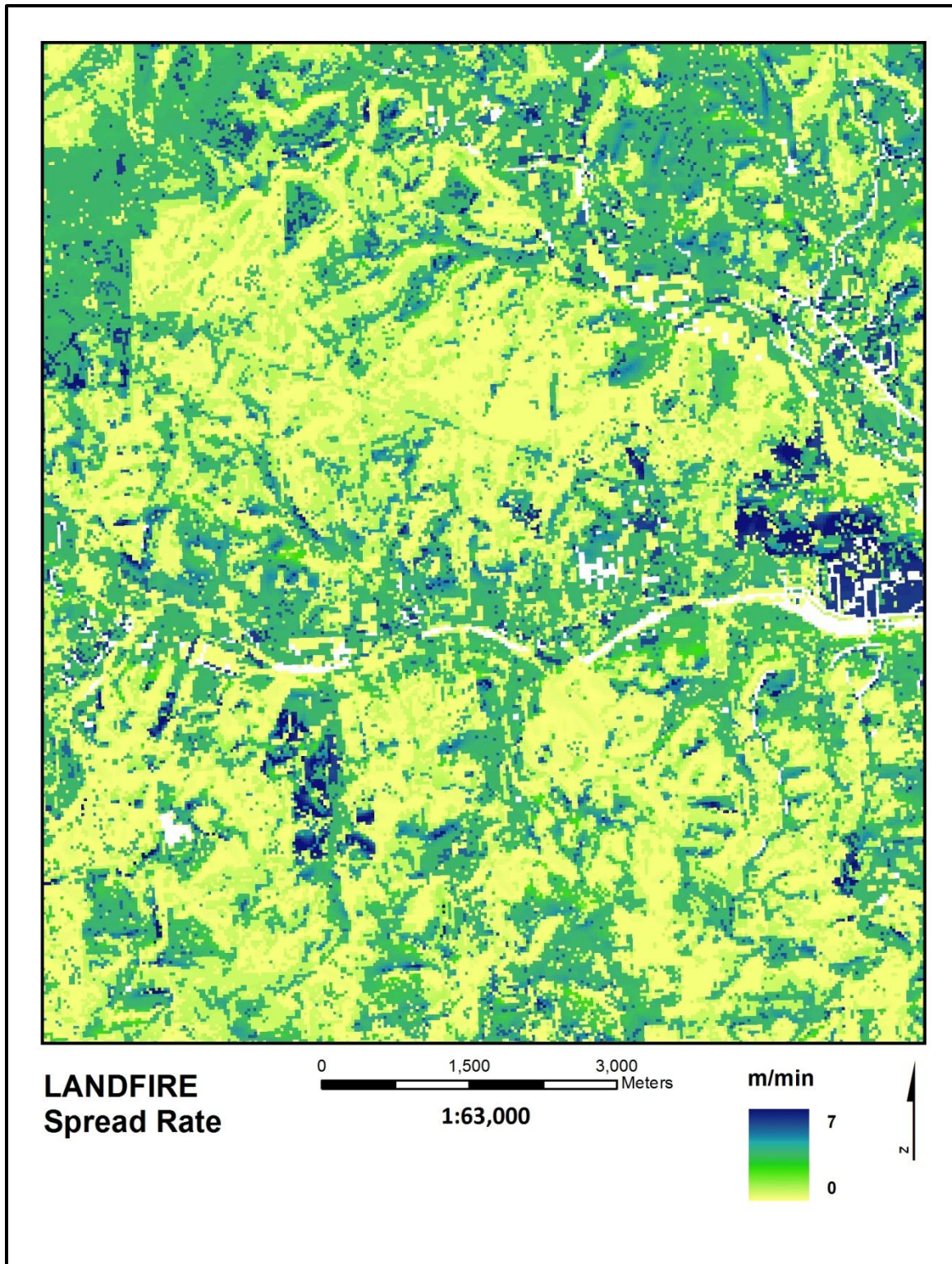
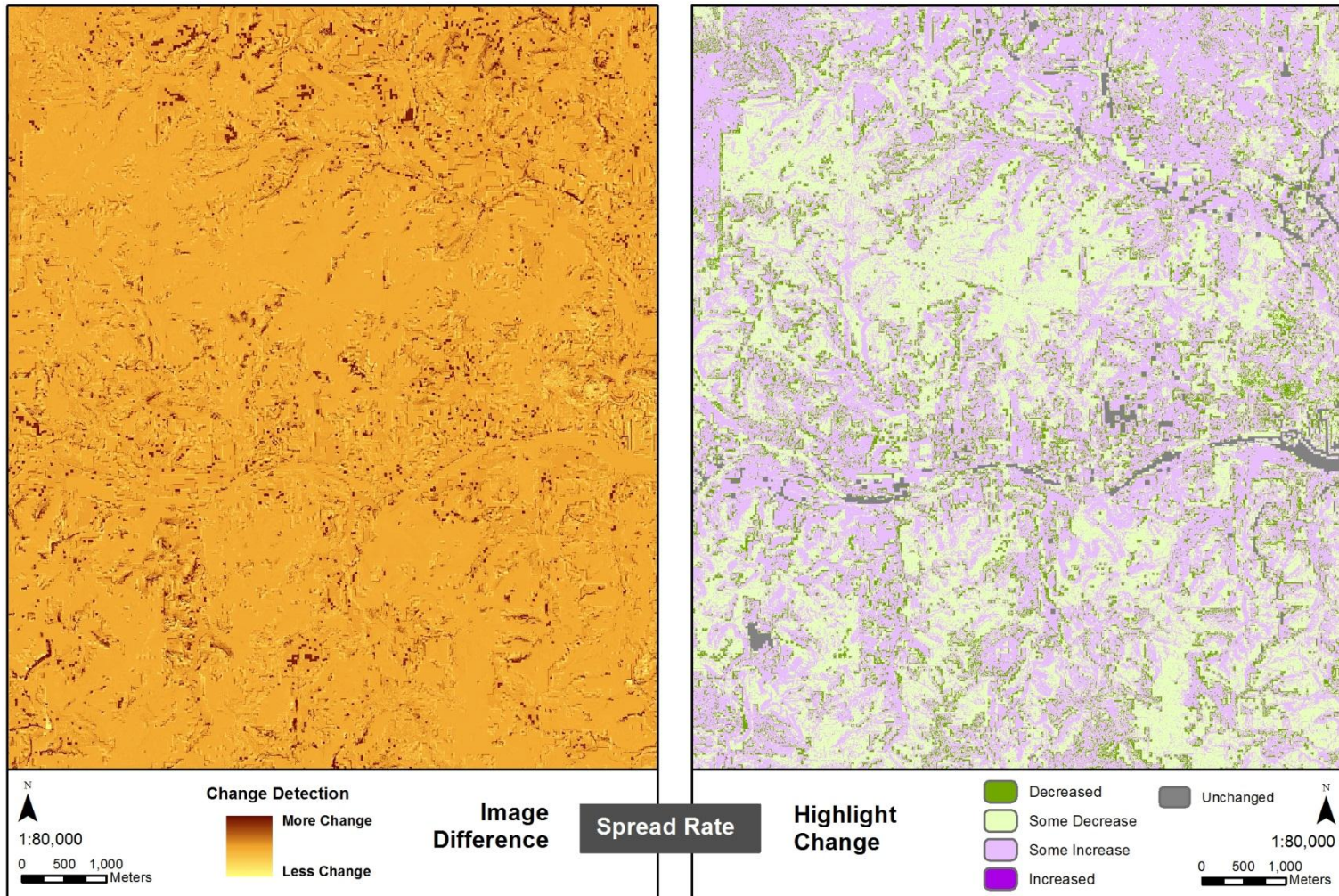


Figure 54. LANDFIRE Spread Rate Output.



**Figure 55.** Spread Rate Change Detection.

#### 4.2 Research Question II

The second research question focuses on the role of foliar moisture content (FMC) in wildfire modeling. Wildfire models such as Farsite and FlamMap incorporate homogeneously distributed moisture content for dead vegetation litter as well as homogeneous FMC of live vegetation. They do not allow for spatially variant moisture content (for live and dead vegetation) which is a more accurate scenario in a wildland urban interface, especially in drought conditions and/or in areas with anthropogenically induced watering schemes such as landscaped neighborhoods or farmland.

Moisture conditioning tables which include rainfall, wind and other weather data can simulate the absorption of water by forest litter but the amount of moisture present in the live vegetation is assumed by the model to remain constant. To exhibit the heterogeneous landscape of vegetation moisture, FMC was calculated for the Kerr study area and the Possum Kingdom study area using the normalized difference infrared index (NDII) from Landsat 5 TM satellite imagery for the purposes of comparison with the Moisture Conditioning technique and to draw a parallel between FMC and wildfire spread.

There are two components to Research Question II. The first uses the same Kerr study area from Research Question I and compares FlamMap outputs that have been pre-conditioned with moisture content for dead vegetation against maps of the same area with no moisture conditioning. Then these results are compared against an NDII map showing FMC of all vegetation, whether live or dead. The second component is set at Possum Kingdom Lake in Palo Pinto County and seeks to investigate whether FMC has an effect on where fire spreads under drought conditions in a wildland urban interface in Texas.

#### *4.2.1 Moisture Conditioning*

LANDFIRE data was used to create model outputs from FlamMap with and without moisture conditioning to compare the effect on model output maps. These output maps include the same information chosen for Research Question I: fireline intensity, crown fire activity, flame length, and spread rate. Since LANDFIRE data were used in Research Question I as an input to FlamMap and there was no moisture conditioning, the output maps were re-purposed for Research Question II to act as a control for comparison with the pre-conditioned results. These results are also evaluated with the added context of the Landsat 5 TM image in Figure 5.

The results for fireline intensity show a widespread decrease in values for nearly all of the study area when comparing the map with no moisture conditioning against the map including moisture conditioning (Figure 56). Locations that decreased the most are concentrated in patches of agriculture and grasslands, while the majority of forested areas experienced some decrease. The change detection maps (Figure 57) include the same techniques used for the first research question: image differencing and highlight change. The image difference map shows minor change for roughly half of the study area with the rest showing more change. In the highlight change map, urban and bare-earth terrain did not experience increase or decrease and are displayed as unchanged. Interestingly, a few isolated patches increased in fireline intensity when moisture conditioning was applied. The cause for this increase is not obviously apparent since there appears to be no distinguishing terrain features unique to the areas of increase. Many of these spots are in locations of transition between forest and grassland, so could be influenced by mixed pixels which could more easily fall into one category or another. However, many other

areas fit such a description yet showed results that were consistent with more homogeneously forested areas.

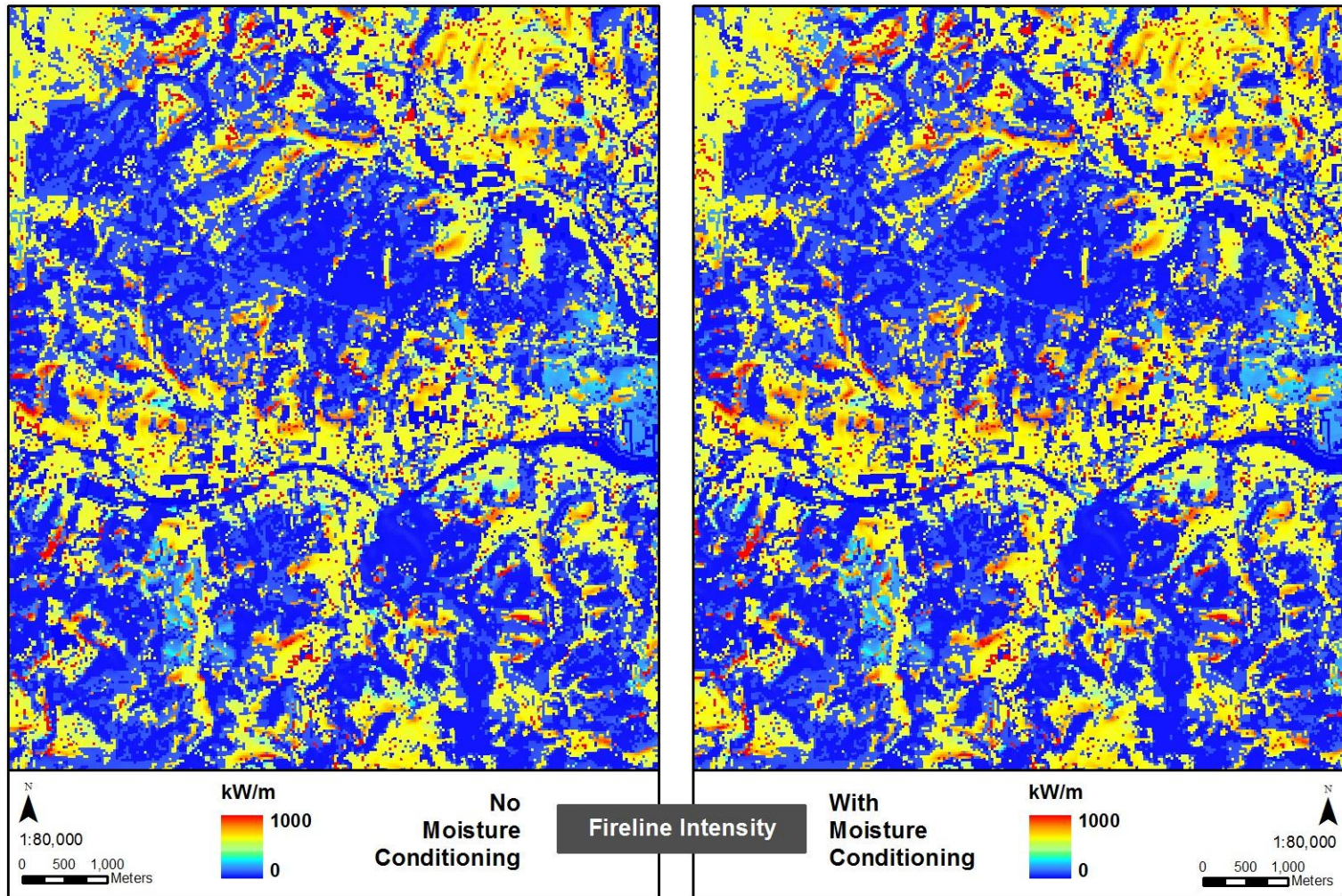
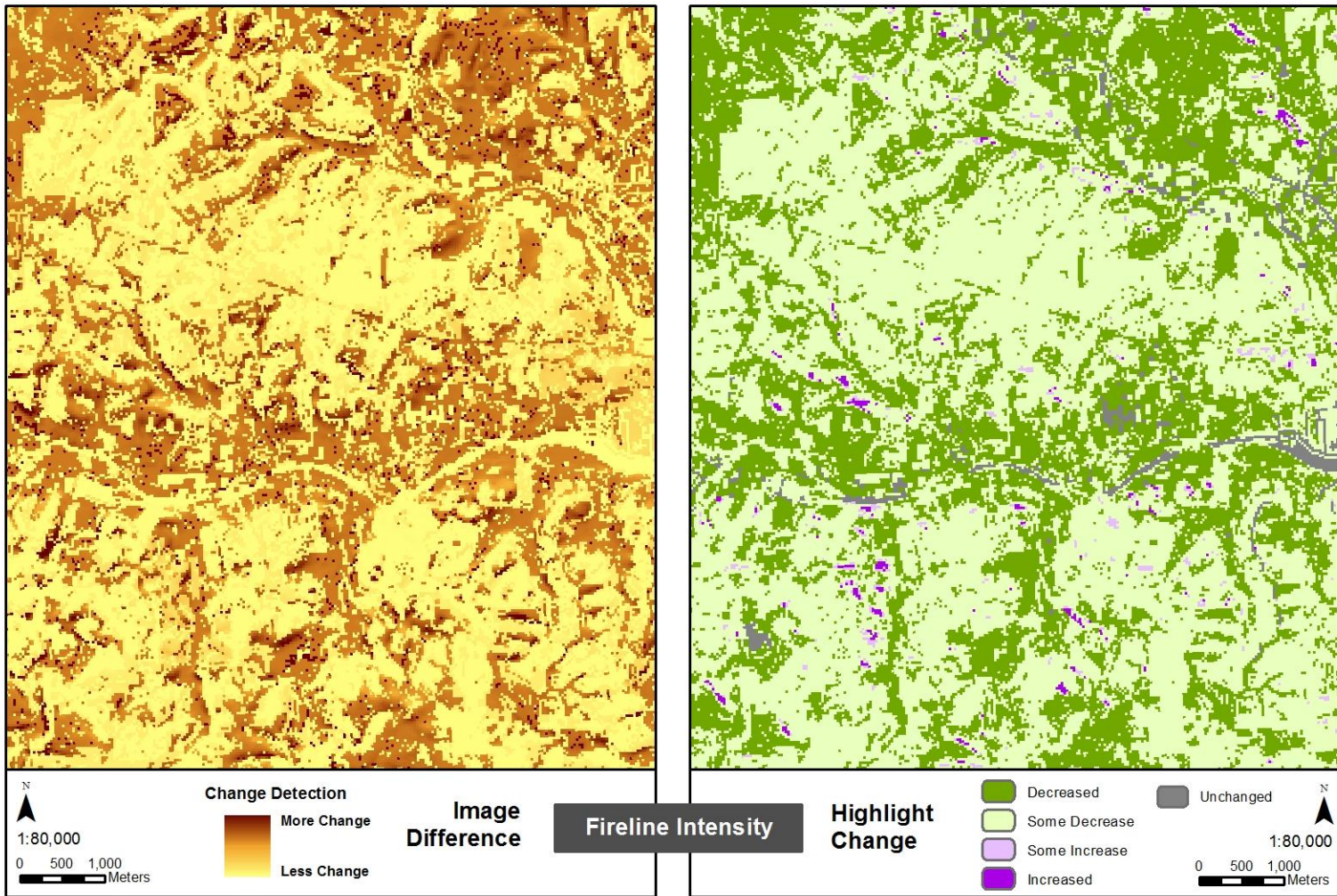


Figure 56. Fireline Intensity Output Comparison.



**Figure 57.** Fireline Intensity Change Detection for Moisture Conditioning.

The crown fire activity map with moisture conditioning appears to be identical when compared to the control map: all areas that are not urban or bare earth show the potential for surface fire (Figure 58). The change detection maps (Figure 59) support this observation by displaying no change for the entire study area.

At a glance, the comparison maps for flame length also appear to be identical (Figure 60). The values across the study area are all very low, hovering near one meter. However, the change detection maps tell a dramatically different story (Figure 61). The image difference map shows a wide range in degrees of change and the highlight change map indicates that nearly all of this change is decreased values. As in the fireline intensity maps, there are a few locations in Figure 61 showing increased values and the locations appear to be coincident with those from fireline intensity.

The final map output is spread rate and yet again the results from moisture conditioning appear to match the control map with no moisture conditioning (Figure 62). The spread rate is slow in heavily forested areas but increases to about seven minutes in terrain uninterrupted by vegetation. Also similar to fireline intensity and crown fire activity, the change detection maps uncover a slightly negative shift in values for much of the study area (Figure 63). The spatial patterns are also consistent with the others and include the very same locations of increased values present in this map.

The similar spatial patterns found in the change detection maps for fireline intensity, flame length and spread rate show the degree to which advance moisture conditioning can have an effect on wildfire maps produced from FlamMap. Almost

100% of the area in each of the three categories showed some change; predictably, they are mostly decreasing values after the injection of moisture into the simulation.

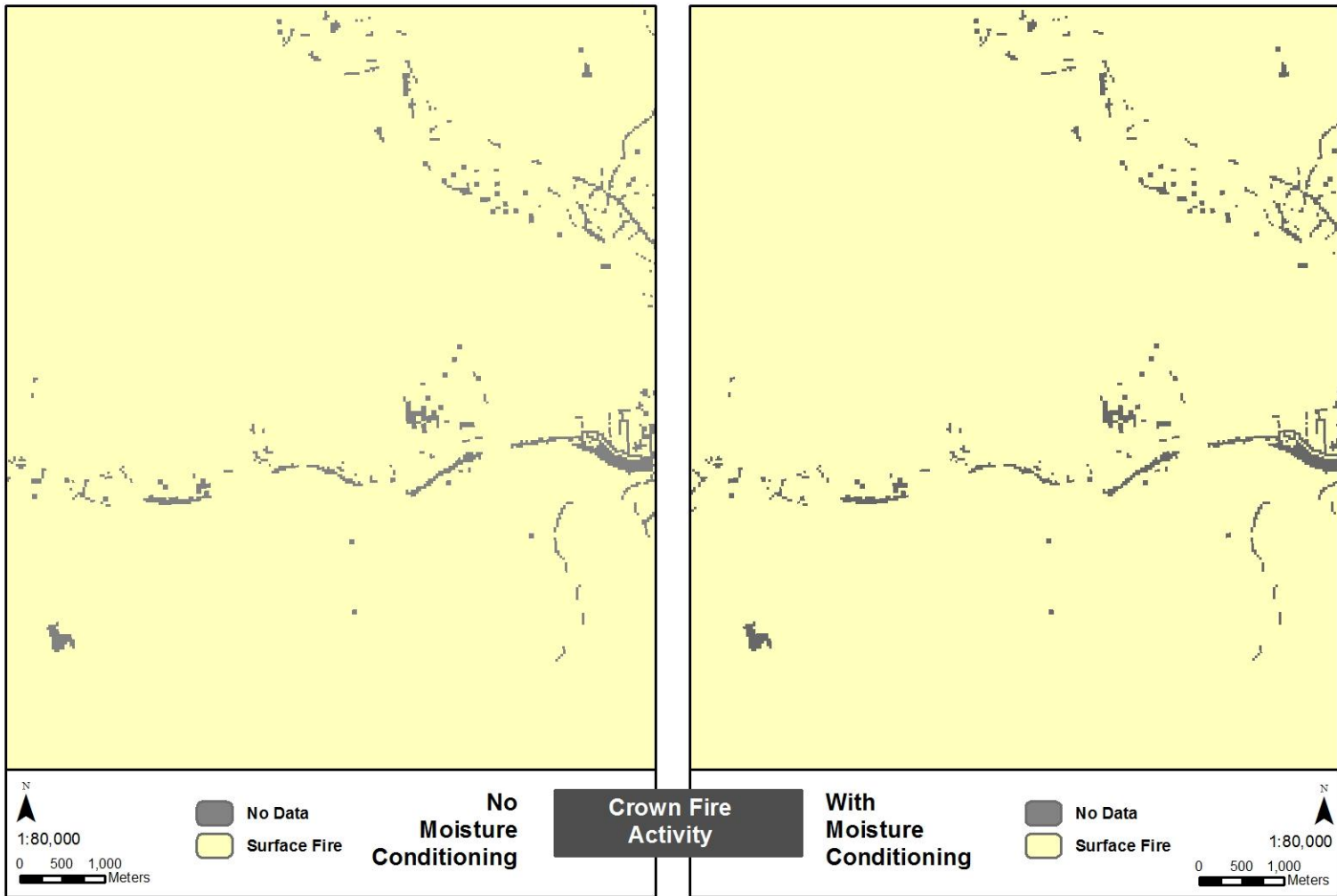


**Figure 58.** Crown Fire Activity Output Comparison.

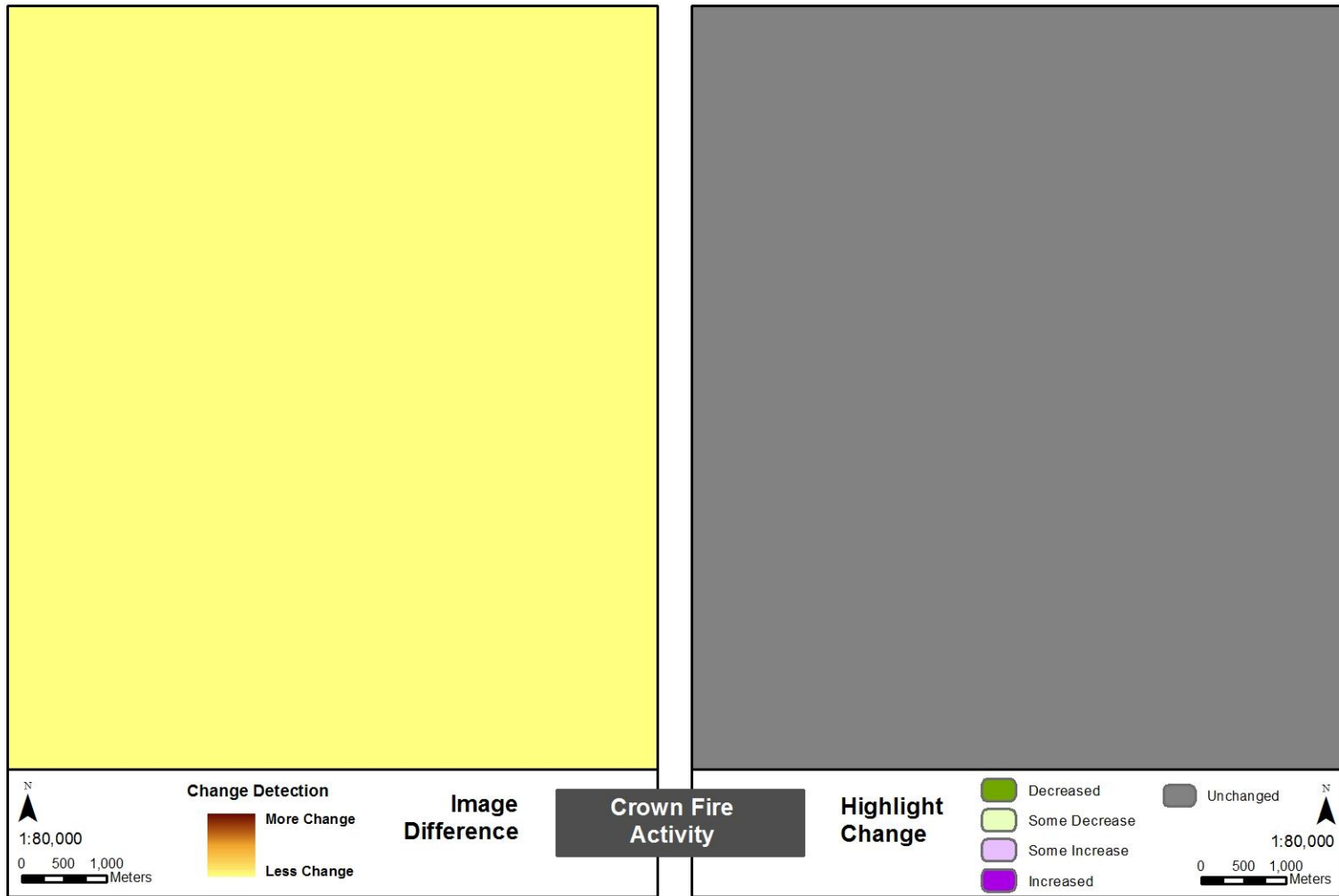


**Figure 59.** Crown Fire Activity Change Detection for Moisture Conditioning.

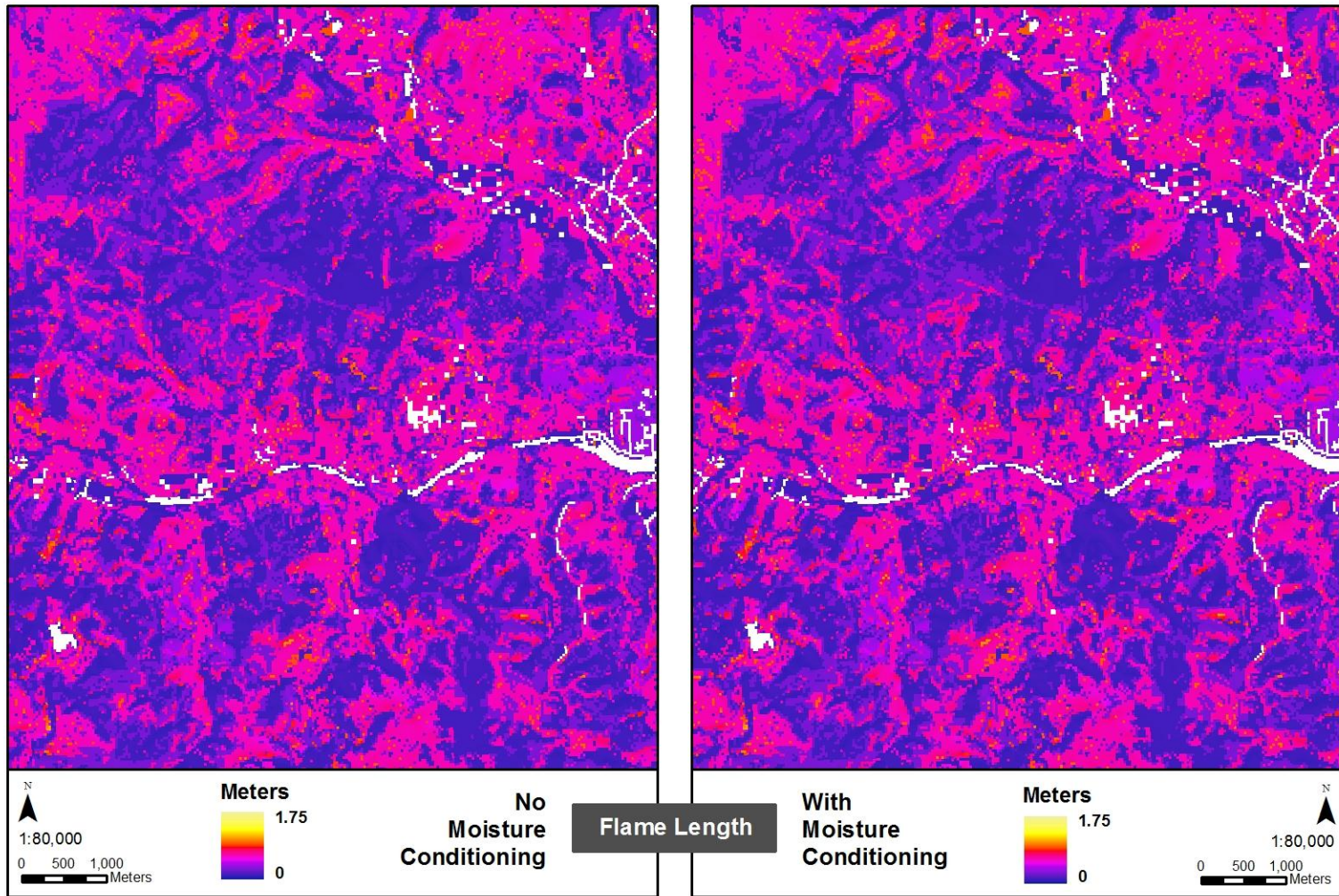


**Figure 60.** Flame Length Output Comparison.

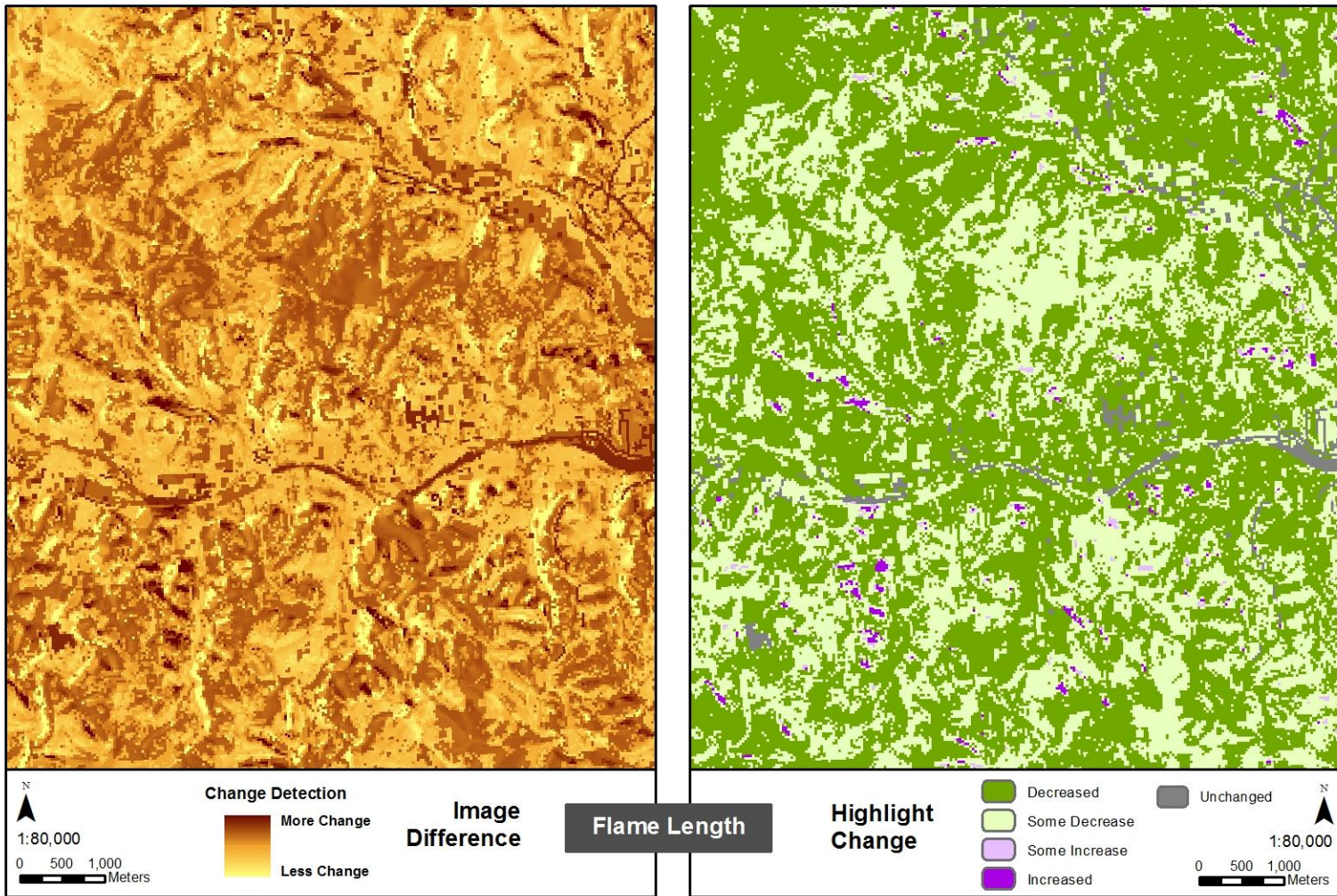


**Figure 61.** Flame Length Change Detection for Moisture Conditioning.

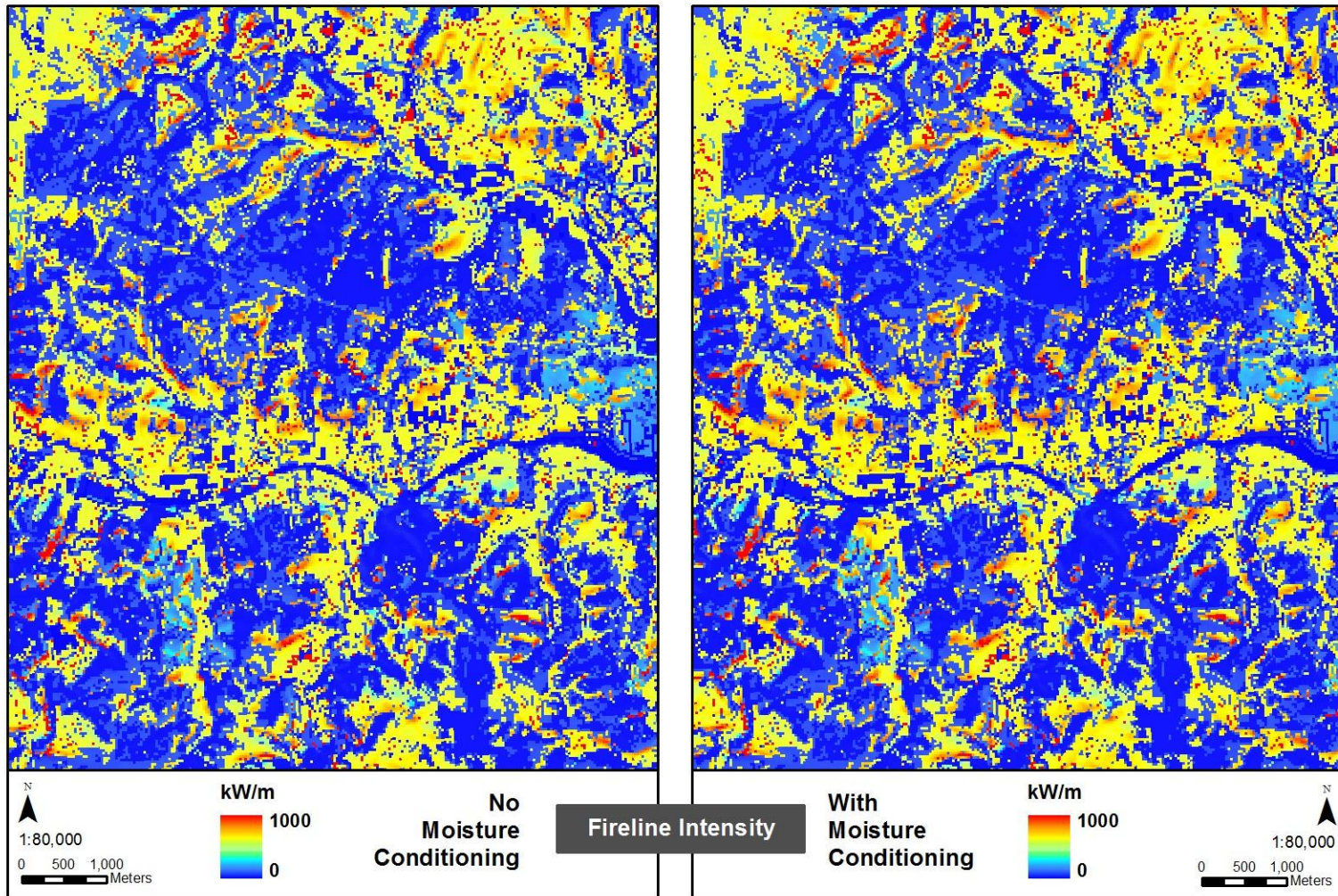


**Figure 62.** Fireline Intensity Output Comparison.

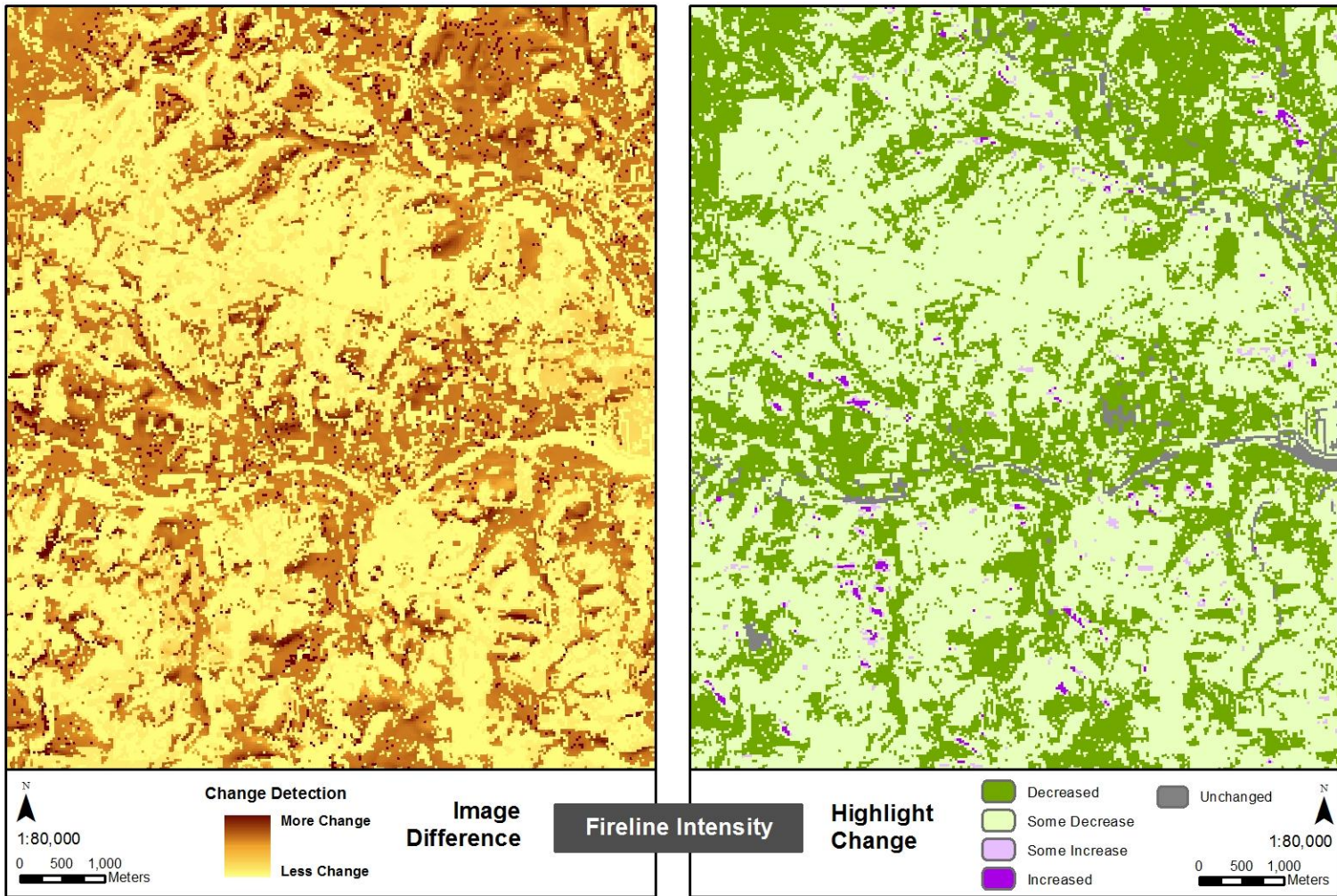


**Figure 63.** Fireline Intensity Change Detection for Moisture Conditioning.

Crown fire activity showed absolutely no change, but this type of information is categorical and the surface fire designation was still relevant to the terrain regardless of the additional moisture introduced. Therefore these seemingly divergent results bear no effect on the observation that the addition of moisture conditioning to the modeling process does indeed have an effect on map outputs. Another goal of the first part of Research Question II is to compare these spatial patterns with those produced from the measurement of foliar moisture content through the normalized difference infrared index. If the patterns are quite different, then this indicates that the presence of live vegetation moisture content has contributed to the total vegetation moisture content, or rather FMC.

The NDII values were calculated for the Kerr study area (Figure 64) and the results range from -0.40 to 0.38 out of a possible gamut of -2 (low moisture) to 2 (high moisture). Comparison with the satellite imagery (Figure 65) and land cover map (Figure 4) reveals that higher moisture values occur in grass/shrubland while the low moisture values are found in forested tracts. Most of the values near zero occur in transition areas with few trees or in the small urban section in the eastern side of the study area.

Comparing the patterns from the change detection analysis above with the NDII distribution reveals that while some patterns are identifiable in each (human influences such as the ROW cut, land parceling as well as the natural waterbodies), the NDII map uncovers subtle gradations of water content present (or missing, as the case may be) in the forested areas. These patterns are not immediately apparent in the change detection maps where the forested areas appear as large tracts of land that did not respond much (<10%) to moisture conditioning. The grassland adjacent to the Guadalupe River and Johnson Creek show the highest moisture values (relative to the scene) yet the same areas

in the change detection analysis yield mixed results with various levels of change along the banks.

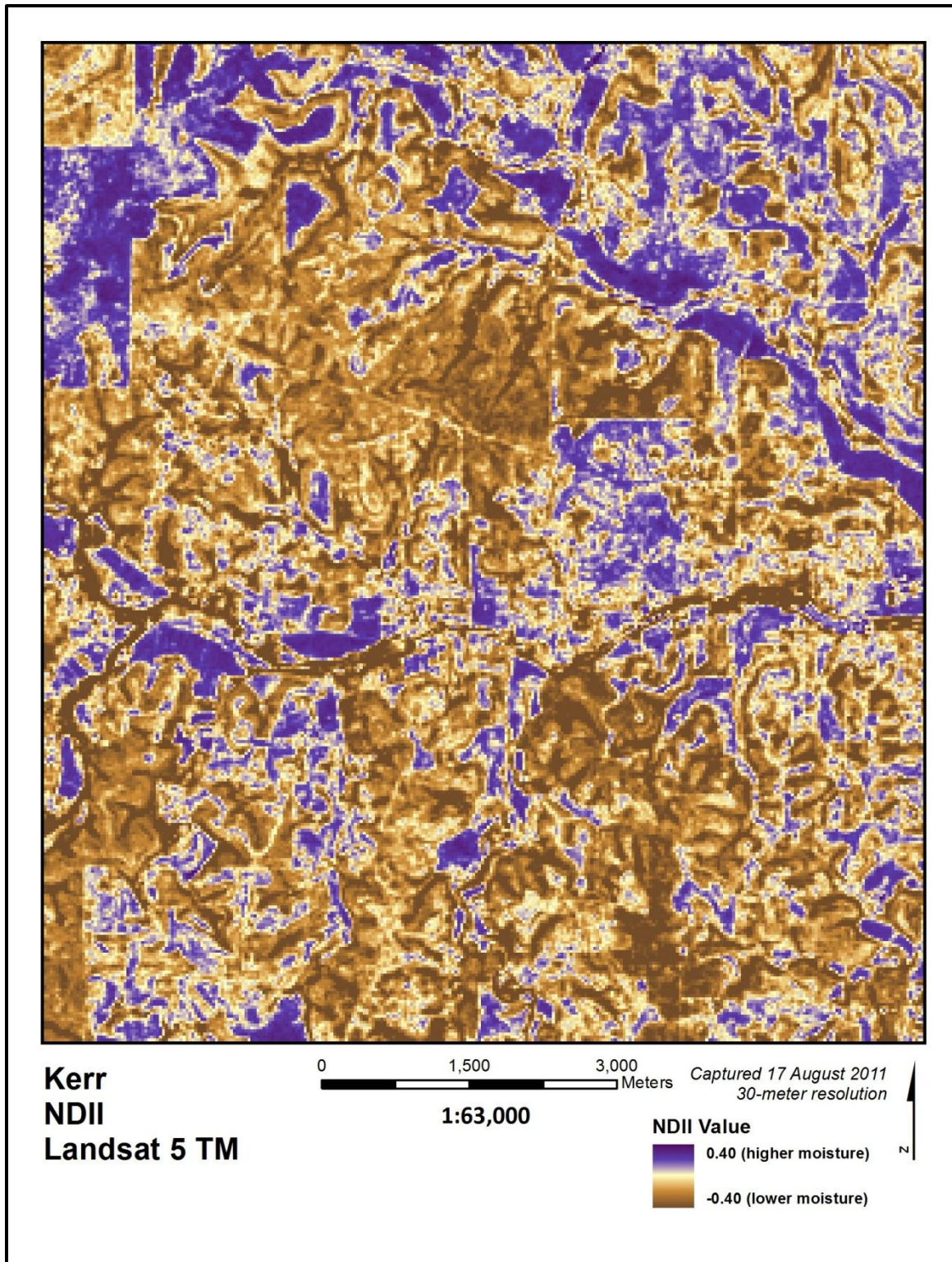


**Figure 64.** NDII of Kerr Study Area. Map generated by author from image captured 11 April 2011 and obtained from U.S. Geological Survey (2011).

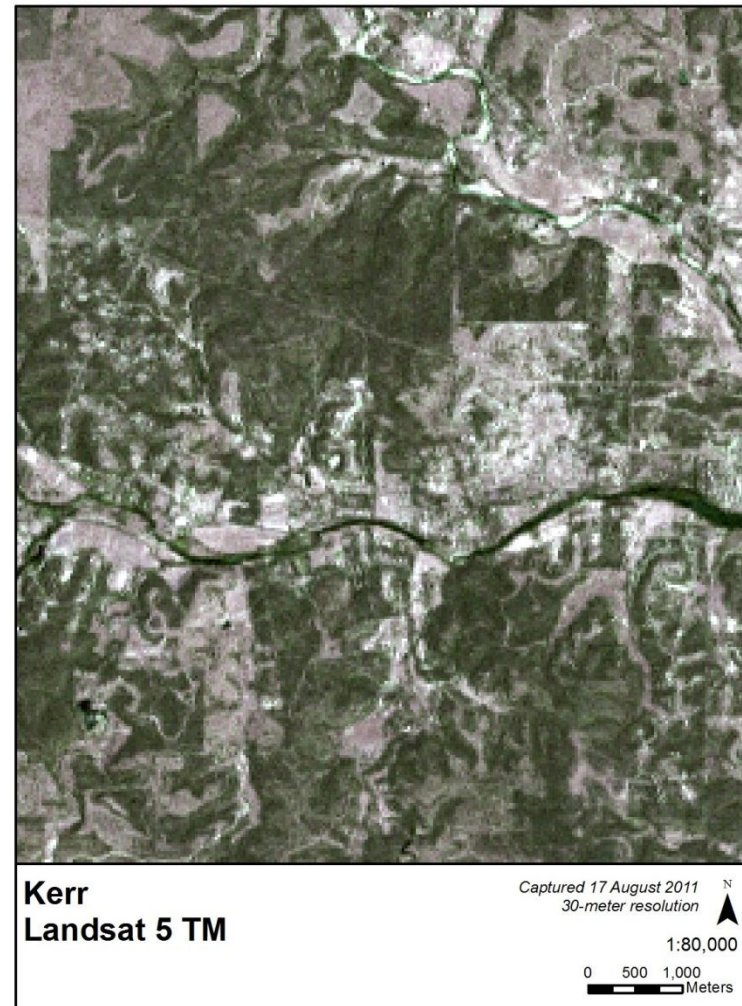
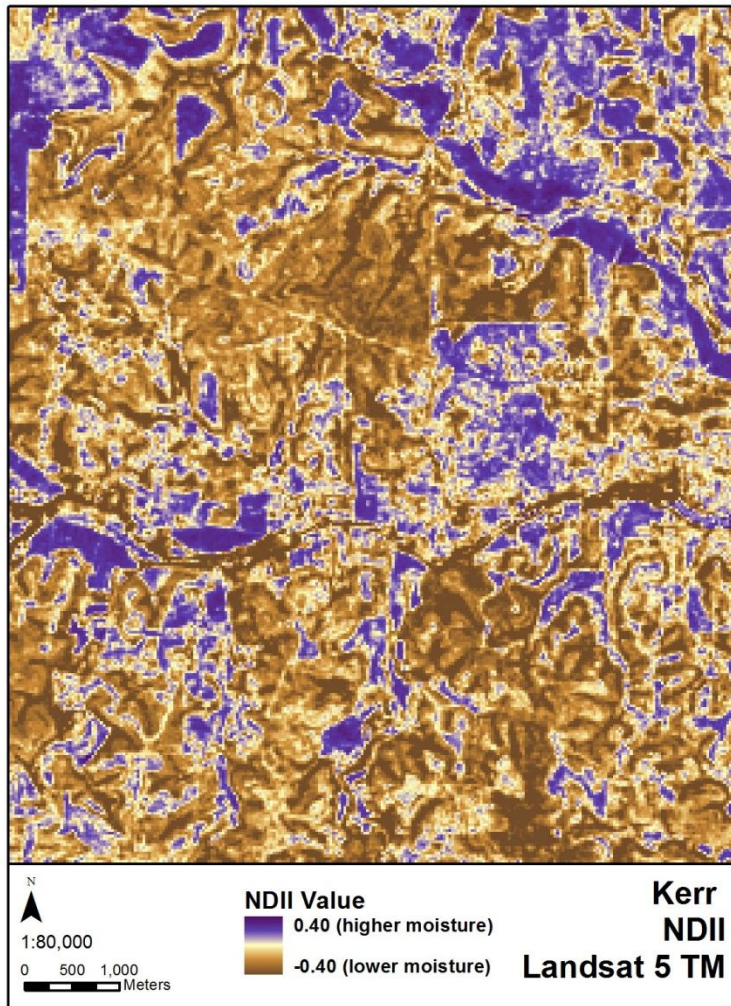


**Figure 65.** *Left*, NDII Map of Kerr Study Area. NDII generated from image at right. *Right*, Natural Color Image of Kerr Study Area. Landsat 5 TM image captured 11 April 2011 and obtained from U.S. Geological Survey (2011).

#### *4.2.2 Effect of Foliar Moisture Content on Fire Spread*

The first portion of Research Question II altered the moisture content found in dead vegetation to observe the impact on the FlamMap outputs, and then these results were compared with an NDII map of the study area showing moisture content of all vegetation, live and dead. The second portion of Research Question II takes this analysis a step further to investigate if NDII values (as a measure of foliar moisture content) might determine where a wildfire is going to spread.

To test this proposition, Possum Kingdom Lake was selected as a study area since a large portion of the land surrounding the lake was burned in a May 2011 wildfire and the local geography fits the WUI characteristic, making this fire a significant threat to humans and settlement. Additionally, the wildfire occurred during a drought so there was a strong possibility that the moisture content for the live vegetation would have high spatial variability.

The analysis produced two image classifications demonstrating areas that had been burned by the wildfire and those that had not (Figure 27). Each of the two areas was intersected with the corresponding NDII values calculated from before the fire to produce a table listing burned NDII values and unburned NDII values (Figure 66). The null hypothesis states that there is no difference in FMC values for the pixels in the burned areas compared to those in the unburned areas, while the research hypothesis asserts that there is a difference. The data were tested at a 5% significance level.

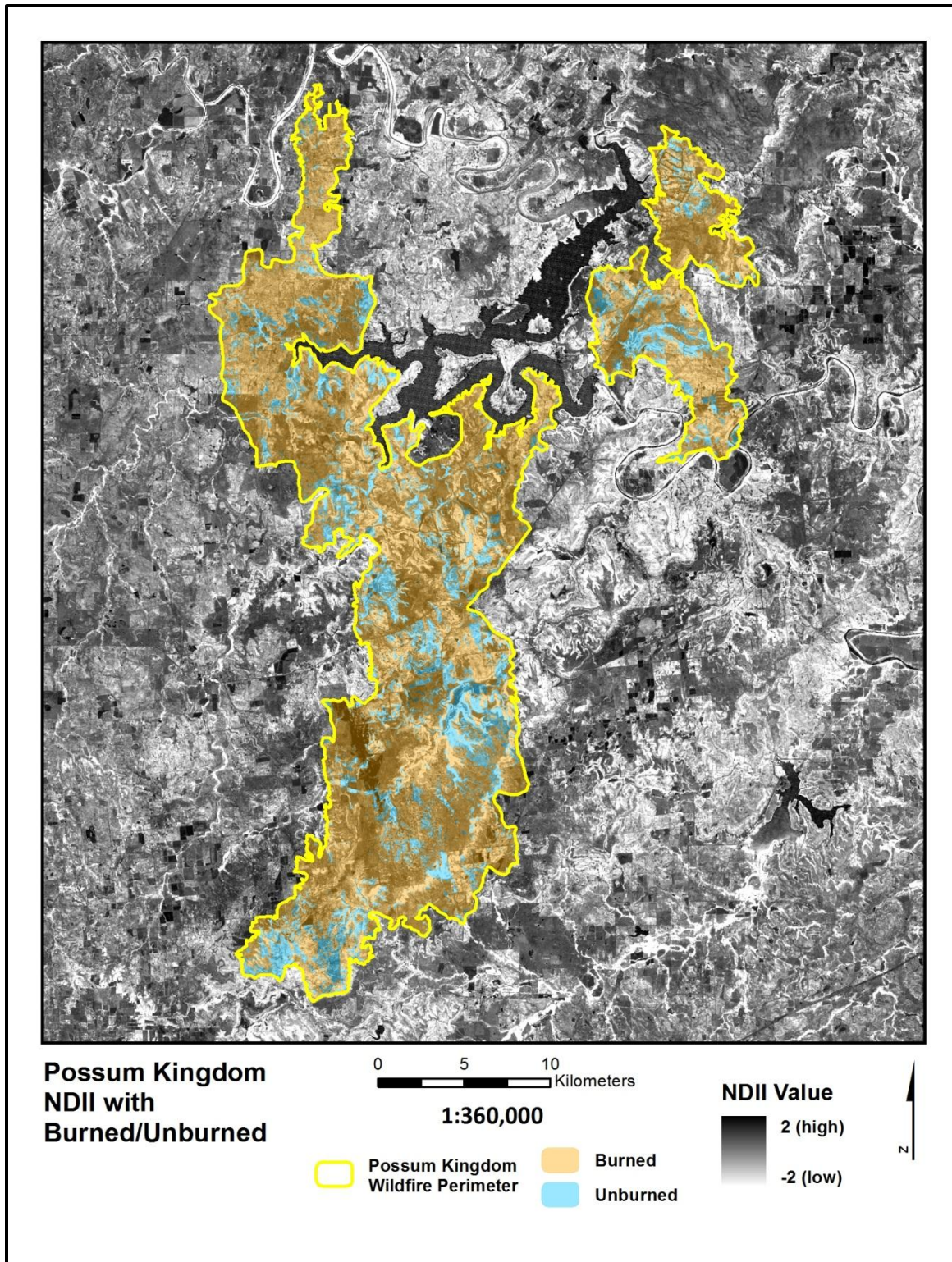


**Figure 66.** NDII and Burn Scar in Possum Kingdom Study Area. NDII generated by author from image captured 11 April 2011 and obtained from U.S. Geological Survey (2011).

A Kolmogorov-Smirnov test for normality was conducted in SPSS and neither the burned nor remnant NDII values are normally distributed (Table 4, Figures 68 and 69).

**Table 4.** Result of Kolmogorov-Smirnov Test for Normality.

Tests of Normality				
Type		Kolmogorov-Smirnov <sup>a</sup>		
		Statistic	df	Sig.
Burned	NDII	.048	450551	.000
Remnant	NDII	.008	118458	.000

a. Lilliefors Significance Correction

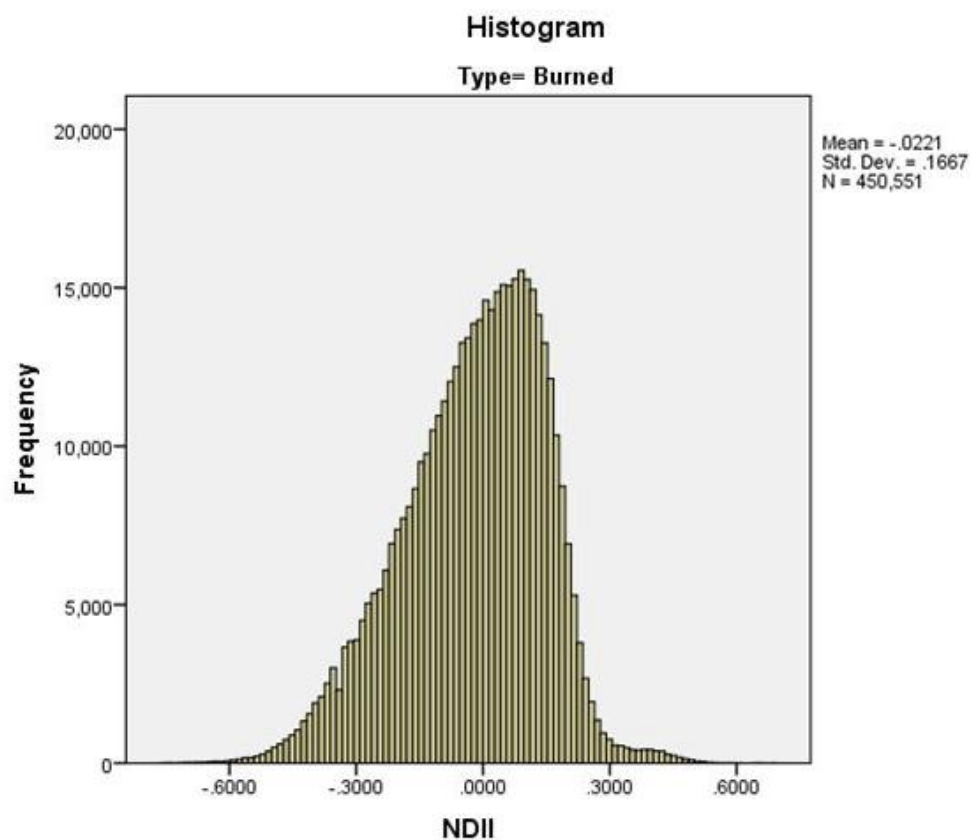


**Figure 67.** Histogram of Burned NDII Values.

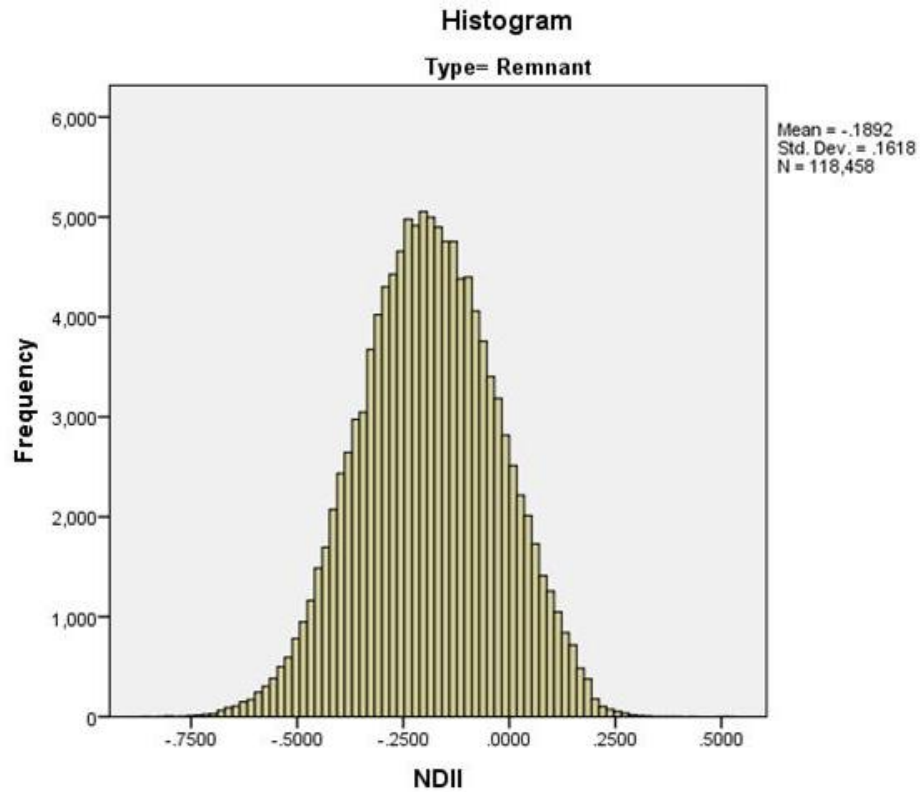


**Figure 68.** Histogram of Remnant NDII Values.

Since the data are not normal, the non-parametric Mann-Whitney U test for independent samples was conducted to compare the distribution of the burned areas with the distribution of the remnant areas. The result was significant at least at the .001 level allowing the research hypothesis to be accepted.

## CHAPTER V

### DISCUSSION

#### 5.1 Research Question I

In terms of practicality, the ease of use for obtaining and utilizing LANDFIRE data was exponentially superior to the lidar. LANDFIRE data download is available via two methods: direct download from an interactive map or through one of several access tools available as ArcGIS toolbars. On the main LANDFIRE website ([www.LANDFIRE.gov](http://www.LANDFIRE.gov)) data product categories include topographic data, fuel, vegetation, fire regimes and disturbance with a handy reference list of historical data versions and coverage. A bounty of information and metadata are listed under each data product such as links to detailed product descriptions, application and common usage, along with references to studies utilizing that particular data product.

Extensive documentation can be found from the LANDFIRE website on the program's founding, history, maintenance, organization, product updates, and more. Metadata included with data download includes meticulously outlined mapping procedures as well as accuracy and/or quality assessments. Proper data usage is defined along with limitations or possible discrepancies. Another advantage of LANDFIRE data is that when possible, standards and classifications are imported from external authoritative sources to maintain interoperability. For example, instead of commissioning a new set of vegetation fuel classes, the established Andersen Northern

Forest Fire Laboratory (NFFL) was used for this research. In another application not utilized in this study, vegetation products reference NatureServe's Ecological Systems classification (NatureServe 2012), "meeting the requirement that map units be identifiable, scalable, and model-able" (U.S. Department of Agriculture 2011b).

Conversely, there is not a data clearinghouse for nationwide lidar-derived vegetation products, much less fuels or other datasets tailored to wildfire modeling. Extracting meaningful information from the lidar was time-consuming, monotonous, complicated, and possibly error-prone. The CFE tool was able to produce two of the required inputs to FlamMap (CBD, CBH), but the remaining datasets had to be derived from a custom methodology (CH, CC) or manipulated from external sources (DEM, slope, aspect, NFFL). Then the bounding coordinates had to be exactly aligned, down to the pixel.

While the CFE tool was useful for extracting some vegetation information from the point cloud, several limitations of the software resulted in a frustrating user experience. To list a few: DOS-based restrictions on filepaths/filenames, processing on only one processor core, RAM-limited file sizes and abbreviated help documents. Additionally, the tool cannot interpret any existing ASPRS point classifications but instead separates the ground points from all remaining points which are assumed to be vegetation. Since many other structures and objects are bound to be included in the non-ground points, it is necessary to first extract the ASPRS classes for ground and vegetation prior to processing in the CFE tool (if they exist).

The scope of this study did not allow for conducting an accuracy assessment of the lidar-derived data and this severely weakens the authority of the model inputs themselves, and by default the output information as well. Additionally, two of the lidar-based metrics were derived from the Canopy Fuel Estimator tool intended for use in a vastly different land cover (Pacific Northwest) than that in the Kerr study area. Perhaps a future study using the CFE tool could make the same comparison of lidar against LANDFIRE data in its intended environment. An alternative could be to develop custom lidar tools to calculate canopy bulk density and canopy base height for the cedar (ashe juniper) and live oak trees in the Texas hill country. One study could test the accuracy and another could conduct the lidar and LANDFIRE method comparison.

The results of the comparison between the lidar method and the LANDFIRE method indeed shows an added level of detail detectable in the lidar-based outputs. With the exception of crown fire activity, for which there was no difference, the output maps exhibited similar variety, scope and pattern of change from one method to the other. Much of the difference highlighted in the change detection maps occurs at the fringes of clusters or larger tracts of homogeneous land cover types as a result of the 5-meter data identifying discrete clumps of vegetation which were previously unidentifiable or else amalgamated when grouped within a 30-meter pixel.

While these differences are notable, they are not exceptional. One point of investigation for this study was to determine if using lidar for wildfire modeling in a wildland urban interface would provide an additional level of detail which could have an effect on wildfire response or land management in a WUI. The change detection maps show primarily subtle change (less than ten percent increase or decrease), with a few of

the fringe areas described above as exhibiting greater than ten percent decrease. The maps showing the input vegetation datasets are dramatically different when comparing lidar to LANDFIRE, which led to an expectation of equally polarizing results. However, the output maps appear remarkably similar, considering the sources.

Considering this unexpected outcome and due to the LANDFIRE program's distinction as an easily accessible, standards-based source of well-tested remote sensing data with a spectrum of data products covering the entire country, it becomes clear that the LANDFIRE method is a more practical and equally or possibly more accurate option than lidar for wildfire modeling in a WUI environment. Lidar data are still inherently more precise of a measurement than the LANDFIRE technique, but the dearth of modern lidar tools means that vegetation and fuel data extraction is left to the researcher to find their own procedure, an arduous and daunting task for those lacking programming skills and/or an extensive background in GIS.

### 5.2 Research Question II

The results show that homogeneous moisture conditioning does have a profound effect on the resulting FlamMap outputs demonstrated in most areas as a greater than ten percent decline in wildfire risk variables (in terms of fireline intensity, flame length and spread rate). In fact, modifying the initial homogeneous moisture content proved to have a greater effect on the output maps than using two dissimilar data inputs (lidar and LANDFIRE).

FlamMap accepts data inputs for duff loading and coarse woody fuel which are defined by stem diameter and can be saturated to varying degrees during simulated

weather events. One limitation of this study is that timely data for this variable were not available and so the dataset was left out of the simulation. Instead, FlamMap uses information from the remaining vegetation variables such as NFFL and canopy cover to estimate the amount of moisture retained from a simulated rainfall event. It is through this mechanism that a variable distribution of risk parameters results instead of a consistent output where every cell is lowered uniformly to some degree. This method means the tool recognizes that the same blanket moisture parameter will affect a stand of vegetation differently than an adjacent patch of bare earth rock; it is not the same as a heterogeneous moisture parameter which will produce variable results *within* the same stand.

Since it is clear that moisture content is a robust variable in FlamMap, it is even more crucial that vegetation moisture content be represented accurately across the landscape. Comparison of the projected moisture outputs from a consistent moisture input with the heterogeneous, NDII-measured vegetation moisture map reveals a great deal of variability that cannot be accounted for in the FlamMap model. Furthermore, evidence is presented that supports FlamMap's predilection toward moisture content as an influential variable since it was clearly shown that the wildfire spread where the FMC values were lowest.

## CHAPTER VI

### CONCLUSION

Mutlu et al. (2008, 284) stated, “A future study will analyze the influence of a more accurate fuel map on modeling fire behavior and assessing fire risk. Resulting remote sensing methods and mapping products have the potential for driving changes in forest resources management practices related to mitigating fire hazard that threatens the public, human lives, and environmental health in Texas and nationwide.” This research was conducted with the view that utilizing lidar data as an input to a wildfire behavior model would result in wildfire maps with increased detail and resolution compared with those produced from 30-meter Landsat imagery, which in turn could contribute to our understanding of wildfire risk assessment. This research focused on a site covering the wildland urban interface because an area of diverse spatial heterogeneity was predicted to experience greater benefit from higher resolution inputs and outputs than a large, homogeneous expanse of wildland forest. It is the latter scenario for which FlamMap and the nationwide LANDFIRE landscape datasets were created. As the U.S. Department of Agriculture (2011b) warns, “the most effective use of the products is at the landscape scale. Thus, applying LANDFIRE data at an individual pixel level or in small groups of pixels is not recommended. Use of LANDFIRE products to support analysis in smaller

areas can result in outcomes that will vary in quality by product, location, and specific use.”

However, based on the results of this study the lidar outcomes were very similar to those from the LANDFIRE data. Although the LANDFIRE data were not meant for local-scale projects (as stated above by the U.S. Department of Agriculture), the lidar method used in this project was unable to improve significantly on the LANDFIRE technique despite the resolution differential.

One of the original rationales for this research was to examine whether there would be a need for expansion of lidar coverage (particularly in WUI areas) to improve the quality of wildfire risk mapping. Instead of a need for more lidar, there appears to be a need for more lidar *software*. Specifically, software that is interoperable across an array of operating systems and file formats, provides accurate tools for extracting specific data metrics from a point cloud, and can maximize the available processing power to produce results quickly. Then foresters and land managers could utilize the strengths inherent to lidar data but without sacrificing the time necessary to prepare it for a wildfire model only to have the advantage in precision nullified by the error threshold of a model constructed for a coarser data input.

The assessment of the effect of fuel moisture on wildfire spread from Research Question II does provide a reason for wildfire modeling analysts to consider live vegetation water content at a finer spatial scale than currently allowed when using the Scott and Burgan (2005) fuel model. Since the commonly used NFFL wildfire model only accounts for dead fuel moisture content, it will be the analyst’s choice to conduct

additional remote sensing analyses with a complementary tool as proposed in this study, or accept the limitations of fuel moisture as calculated through a fuel model.

Overall, two alternate applications of wildfire behavior modeling techniques were tested in this research to assess whether improvements in wildfire risk assessment in the wildland urban interface conducted from maps produced by wildfire behavior modeling software were possible. Results of the study have indicated that enhanced precision in vegetation measurement (lidar) does not produce wildfire model outputs that differ substantially from those produced by less precise but readily available Landsat-derived LANDFIRE data. This study has also demonstrated the value of including live foliar moisture content in the wildfire modeling process (particularly during a drought) due to the strong relationship found between FMC and the spread of wildfire in a WUI environment. It is hoped that these results will encourage development of new and improved software to calculate vegetation metrics from lidar (or possibly even new wildfire models that utilize lidar as a direct input) as well as incorporate heterogeneous foliar moisture content.

## REFERENCES

- Albini, F.A. 1984. Wildland Fires. *American Scientist* 72: 590-597.
- American Society for Photogrammetry and Remote Sensing. LAS Specification Version 1.4. [http://www.asprs.org/a/society/committees/lidar/LAS\\_1-4\\_R6.pdf](http://www.asprs.org/a/society/committees/lidar/LAS_1-4_R6.pdf) (accessed April 7, 2012).
- Andersen, H.E., R.J. McGaughey, and S.E. Reutebuch. 2005. Estimating forest canopy fuel parameters using LIDAR data. *Remote Sensing of Environment* 94, no. 4: 441-449.
- Andrews, P.L. 2007. BehavePlus fire modeling system: past, present, and future. In: Proceedings of 7th Symposium on Fire and Forest Meteorological Society. 2007 October 23-25; Bar Harbor, ME. 13 p.
- Arroyo, Laura, Cristina Pascual, and Jose A. Manzanera. 2008. Fire models and methods to map fuel types: The role of remote sensing. *Forest Ecology and Management* 256, no. 6: 1239-1252.
- Avitabile, Valerio, Alessandro Baccini, Mark A. Friedl, and Christiane Schmillius. 2012. Capabilities and limitations of Landsat and land cover data for aboveground woody biomass estimation of Uganda. *Remote Sensing of Environment* 117: 366-380.
- Baldwin, Benjamin. 2003. Catastrophic wildfire hazard assessment in pinyon-juniper woodlands utilizing a managerial paradigm. PhD diss., Utah State University.
- Bar Massada, Avi, Volker C. Radeloff, Susan I. Stewart, and Todd J. Hawbaker. 2009. Wildfire risk in the wildland-urban interface: A simulation study in northwestern Wisconsin. *Forest Ecology and Management* 258, no. 9: 1990-1999.
- Bhandary, Uddhab. 2007. Vulnerability to natural hazards: A study of wildfire-burned subdivisions in the wildland-urban interface using IKONOS imagery and GIS data. PhD diss., University of Colorado at Denver.
- Caccamo, G., L. A. Chisholm, R. A. Bradstock, and M.L. Puotinen. 2011. Assessing the sensitivity of MODIS to monitor drought in high biomass ecosystems. *Remote Sensing of Environment* 115, no. 10: 2626-2639.

- Ceccato, Pietro, Stephane Flasse and Jean-Marie Gregoire. 2002. Designing a spectral index to estimate vegetation water content from remote sensing data: Part 2. Validation and applications. *Remote Sensing of Environment* 82, no. 2-3: 198-207.
- Chen, Qi, Gaia Vaglio Laurin, John J. Battles, and David Saah. 2012. Integration of airborne lidar and vegetation types derived from aerial photography for mapping aboveground live biomass. *Remote Sensing of Environment* 121: 108-117.
- Cheng, Yen-Ben, Pablo J. Zarco-Tejada, David Riano, Carlos A. Rueda, and Susan L. Ustin. 2006. Estimating vegetation water content with hyperspectral data for different canopy scenarios: Relationships between AVIRIS and MODIS indexes. *Remote Sensing of Environment* 32, no. 4: 317-326.
- Clevers, J.G.P.W., L. Kooistra, and M.E. Schaepman. 2010. Estimating canopy water content using hyperspectral remote sensing data. *International Journal of Applied Earth Observation and Geoinformation* 12, no. 2: 119-125.
- Danson, F.M., & P. Bowyer. 2004. Estimating live fuel moisture content from remotely sensed reflectance. *Remote Sensing of Environment* 92, no. 3: 309-321.
- Davidson, Andrew, Shusen Wang, and John Wilmshurst. 2006. Remote sensing of grassland-shrubland vegetation water content in the shortwave domain. *International Journal of Applied Earth Observation and Geoinformation* 8, no. 4: 225-236.
- Esri 2012. ArcGIS Desktop: Release 10. Redlands, CA: Environmental Systems Research Institute.
- Finney, M.A., and P.L. Andrews. 1999. FARSITE – A Program for Fire Growth Simulation. *Fire Management Notes* 59, no. 2: 13.
- Finney, Mark A. 2006. A computational method for optimizing fuel treatment locations. In: Andrews, Patricia L.; Butler, Bret W., comps. 2006. Fuels Management-How to Measure Success: Conference Proceedings. 28-30 March 2006; Portland, OR. Proceedings RMRS-P-41. Fort Collins, CO: U.S. Department of Agriculture, Forest Service, Rocky Mountain Research Station. p. 107-123.
- Flaxman, Michael. 2001. Multi-scale fire hazard assessment for wildland urban interface areas: An alternative futures approach. PhD diss., Harvard University.
- Fry, J., G. Xian, S. Jin, J. Dewitz, C. Homer, L. Yang, C. Barnes, N. Herold, and J. Wickham. 2011. Completion of the 2006 National Land Cover Database for the Conterminous United States. *PE&RS* 77, no. 9: 858-864.

- Garcia, Mariano, David Riano, Emilio Chuvieco, Javier Salas, and F. Mark Danson. 2011. Multispectral and LiDAR data fusion for fuel type mapping using Support Vector Machine and decision rules. *Remote Sensing of Environment* 115, no. 6: 1369-1379.
- Gao, Bo-cai. 1996. NDWI – A normalized difference water index for remote sensing of vegetation liquid water from space. *Remote Sensing of Environment* 58, no. 3: 257-266.
- Gao, Zhigiang, Wei Gao, and Ni-Bin Chang. 2011. Integrating temperature vegetation dryness index (TVDI) and regional water stress index (RWSI) for drought assessment with the aid of LANDSAT TM/ETM+ images. *International Journal of Applied Earth Observation and Geoinformation* 13, no. 3: 495-503.
- Halligan, Kerry. 2007. Mapping forest canopy fuels in Yellowstone National Park using lidar and hyperspectral data. PhD diss., University of California, Santa Barbara.
- Hawbaker, Todd. 2009. Human-fire interactions: Patterns of fire and risk to housing in the U.S. PhD diss., The University of Wisconsin at Madison.
- Hunt, E. Raymond Jr., Barrett N. Rock, and Park S. Nobel. 1987. Measurement of leaf relative water content by infrared reflectance. *Remote Sensing of Environment* 22, no. 3: 429-435.
- Hunter, Bruce Allan. 2005. A geospatial tool for wildfire threat analysis in Central Texas. Master's thesis, University of North Texas.
- Jensen, Jennifer L.R., Karen S. Humes, Tamara Conner, Christopher J. Williams and John DeGroot. 2006. Estimation of biophysical characteristics for highly variable mixed-conifer stands using small-footprint lidar. *Canadian Journal of Forest Research* 36, no. 5: 1129-1138.
- Jensen, Jennifer L.R., Karen S. Humes, Lee A. Vierling, and Andrew T. Hudak. 2008. Discrete return lidar-based prediction of leaf area index in two conifer forests. *Remote Sensing of Environment* 112, no. 10: 3947-3957.
- Jensen, Jennifer L.R., Karen S. Humes, Andrew T. Hudak, Lee A. Vierling, and Eric Delmelle. 2011. Evaluation of the MODIS LAI product using independent lidar-derived LAI: A case study in mixed conifer forest. *Remote Sensing of Environment* 115, no. 12: 3625-3639.
- Jensen, John R. 2000. *Remote Sensing of the Environment: An Earth Resource Perspective*. Upper Saddle River, NJ: Prentice-Hall, Inc.
- Koch, Barbara. 2010. Status and future of laser scanning, synthetic aperture radar and hyperspectral remote sensing data for forest biomass assessment. *ISPRS Journal of Photogrammetry and Remote Sensing* 65, no. 6: 581-590.

- Lampin-Maillet, Corinne, Marielle Jappiot, Marlène Long, Christophe Bouillon, Denis Morge, and Jean-Paul Ferrier. 2010. Mapping wildland-urban interfaces at large scales integrating housing density and vegetation aggregation for fire prevention in the south of France. *Journal of Environmental Management* 91, no. 3: 732-741.
- Lefsky, M.A., W.B. Cohen, S.A. Acker, G.G. Parker, T.A. Spies, and D. Harding. 1999. Lidar remote sensing of the canopy structure and biophysical properties of Douglas-fir western hemlock forests. *Remote Sensing of Environment* 70, no. 3: 339-361.
- Lefsky, M.A., D.P. Turner, M. Guzy, and W.B. Cohen. 2005. Combining lidar estimates of aboveground biomass and Landsat estimates of stand age for spatially extensive validation of modeled forest productivity. *Remote Sensing of Environment* 95, no. 4: 549-558.
- Lein, James K. and Nicole I. Stump. 2009. Assessing wildfire potential within the wildland–urban interface: A southeastern Ohio example. *Applied Geography* 29, no. 1: 21-34.
- Long, A. Forest Encyclopedia Network. <http://www.forestencyclopedia.net/p/p467> (accessed September 12, 2012).
- Luo, Wei. 2004. A modeling approach to studying wildland urban interface fires. PhD diss., University of California, Berkeley.
- Maclean, G.A. and W.B. Krabill. 1986. Gross-merchantable timber volume estimation using an airborne LIDAR system. *Canadian Journal of Remote Sensing* 12, no. 1:7-18.
- Maune, D. F., ed. 2007. *Digital Elevation Model Technologies and Applications: The DEM Users Manual*. 2nd ed. Bethesda, MD: American Society for Photogrammetry and Remote Sensing.
- McVicar, Tim R. and David L. B. Jupp. 1998. The current and potential operational uses of remote sensing to aid decisions on drought exceptional circumstances in Australia: a review. *Agricultural Systems* 57, no. 3: 399-468.
- Mishra, Ashok K., and Vijay P. Singh. 2010. A review of drought concepts. *Journal of Hydrology* 391, no. 1-2: 202-216.
- Missoula Fire Sciences Laboratory. Fire Behavior and Fire Danger Software. <http://www.firemodels.org/index.php/national-systems> (accessed November 24, 2011).
- Mutlu, Muge, Sorin C. Popescu, Curt Stripling, and Tom Spencer. 2008. Mapping surface fuel models using lidar and multispectral data fusion for fire behavior. *Remote Sensing of Environment* 112, no. 1: 274-285.

- Naesset, Erik. 1997. Determination of mean tree height of forest stands using airborne laser scanner data. *ISPRS Journal of Photogrammetry & Remote Sensing* 52, no. 2: 49-56.
- The National Drought Mitigation Center. Current U.S. Drought Monitor. <http://drought.unl.edu/> (accessed September 25, 2011)
- Natural Resources Conservation Service. PLANTS Profile. <http://plants.usda.gov/java/profile?symbol=QUFU> (accessed September 12, 2012)
- NatureServe. Ecological Systems of the United States. <http://www.natureserve.org/publications/usEcologicalsystems.jsp> (accessed September 23, 2012)
- Nelson, R. M. 2000. Prediction of diurnal change in 10-h fuel stick moisture content. *Canadian Journal of Forest Research* 30: 1071-1087.
- National Oceanic and Atmospheric Administration (NOAA). U.S. Experiences Warmest Summer on Record. <http://txsdc.utsa.edu/> (accessed September 25, 2011).
- Popescu, Sorin C. and Kaiguang Zhao. 2008. A voxel-based lidar method for estimating crown base height for deciduous and pine trees. *Remote Sensing of Environment* 112, no. 3: 767-781.
- Popescu, Sorin C., Kaiguang Zhao, Amy Neuenschwander, and Chinsu Lin. 2011. Satellite lidar vs. small footprint airborne lidar: Comparing the accuracy of aboveground biomass estimates and forest structure metrics at footprint level. *Remote Sensing of Environment* 115, no. 11: 2786-2797.
- Radeloff, V.C., R.B. Hammer, S.I Stewart, J.S. Fried, S.S. Holcomb, and J.F. McKeefry. 2005. The Wildland Urban Interface in the United States. *Ecological Applications* 15: 799-805.
- Rhee, Jinyoung, Jungho Im, and Gregory J. Carbone. 2010. Monitoring agricultural drought for arid and humid regions using multi-sensor remote sensing data. *Remote Sensing of Environment* 114, no. 12: 2875-2887.
- Riano, D., E. Meier, B. Allgower, E. Chuvieco, and S.L. Ustin. 2003. Modeling airborne laser scanning data for the spatial generation of critical forest parameters in fire behavior modeling. *Remote Sensing of Environment* 86, no. 2: 177-186.
- Riano, D., E. Chuvieco, S. Condes, J. Gonzalez-Matesanz and S.L. Ustin. 2004. Generation of crown bulk density for *Pinus sylvestris* L. from lidar. *Remote Sensing of Environment* 92, no. 3: 345-352.

- Rothermel, R. C. 1972. A mathematical model for predicting fire spread in wildland fuels. General Technical Report INT-115. Ogden, UT: U.S. Department of Agriculture, Forest Service, Intermountain Forest and Range Experiment Station.  
[http://www.firemodels.org/index.php/behaveplus-introduction/behaveplus-publications#Rothermel\\_1972](http://www.firemodels.org/index.php/behaveplus-introduction/behaveplus-publications#Rothermel_1972)
- Rothermel, R. C. 1991. Predicting behavior and size of crown fires in the Northern Rocky Mountains. Research Paper INT-438. Ogden, UT: U.S. Department of Agriculture, Forest Service, Intermountain Research Station.  
[http://www.firemodels.org/index.php/behaveplus-introduction/behaveplus-publications#Rothermel\\_1991](http://www.firemodels.org/index.php/behaveplus-introduction/behaveplus-publications#Rothermel_1991)
- Rouse, J.W., R.H. Haas, D.W. Deering, J.A. Schell and J.C. Harlan. 1974. Monitoring Vegetation Systems in the Great Plains with ERTS. Proceedings, 3rd Earth Resource Technology Satellite (ERTS) Symposium. p. 48-62.
- Scott, Joe H., Robert E. Burgan. 2005. Standard fire behavior fuel models: a comprehensive set for use with Rothermel's surface fire spread model. Gen. Tech. Rep. RMRS-GTR-153. Fort Collins, CO: U.S. Department of Agriculture, Forest Service, Rocky Mountain Research Station.
- Shafran, Aric P. 2008. Risk externalities and the problem of wildfire risk. *Journal of Urban Economics* 64, no. 2: 488-495.
- Shan, J. and C. Toth, ed. 2008. *Topographic Laser Ranging and Scanning, Principles and Processing*. Boca Raton, FL: Taylor & Francis Group.
- Sims, Daniel A. and John A. Gamon. 2003. Estimation of vegetation water content and photosynthetic tissue area from spectral reflectance: a comparison of indices based on liquid water and chlorophyll absorption features. *Remote Sensing of Environment* 84, no. 4: 201-207.
- Su, Zhongbo, Abreham Yacob, Jun Wen, Gerbert Roerink, Yanbo He, Benhu Gao, Hendrik Boogaard, and Cees van Diepen. 2003. Assessing relative soil moisture with remote sensing data: Theory, experimental validation, and application to drought monitoring over the north China plain. *Physics and Chemistry of the Earth* 28, no. 1-3: 89-101.
- Texas Forest Service. TFS Newsroom.  
<http://txforests.tamu.edu/main/article.aspx?id=12888> (accessed September 25, 2011).
- Texas Natural Resources Information System. TNRIS Home Page. [www.tnr.is.org](http://www.tnr.is.org) (accessed December 10, 2011).
- Texas State Data Center. Texas State Data Center.

- <http://txsdc.utsa.edu/Index.aspx> (accessed December 10, 2011).
- Tian, Xin, Zhongbo Su, Erxue Chen, Zengyuan Li, Christiaan van der Tol, Jianping Guo, and Qisheng He. 2012. Estimation of forest above-ground biomass using multi-parameter remote sensing data over a cold and arid area. *International Journal of Applied Earth Observation and Geoinformation* 14, no. 1: 160-168.
- Theobald, David M. and William H. Romme. 2007. Expansion of the US wildland–urban interface. *Landscape and Urban Planning* 83, no. 4: 340-354.
- U.S. Department of Agriculture. 2011a. LIDAR & IFSAR Tools. [http://forsys.cfr.washington.edu/JFSP06/lidar\\_&\\_ifsar\\_tools.htm](http://forsys.cfr.washington.edu/JFSP06/lidar_&_ifsar_tools.htm) (accessed December 10, 2011).
- U.S. Department of Agriculture. 2011b. LANDFIRE. <http://www.landfire.gov> (accessed December 10, 2011).
- U.S. Forest Service. Wildland Fire Assessment System. <http://www.wfas.net/> (accessed December 10, 2011).
- U.S. Forest Service. Index of Species Information. <http://www.fs.fed.us/database/feis/plants/tree/junash/all.html> (accessed September 12, 2012).
- U.S. Geological Survey. Global Visualization Viewer. <http://glovis.usgs.gov/> (accessed December 10, 2011).
- U.S. Geological Survey. National Land Cover Institute. <http://landcover.usgs.gov/> (accessed February 19, 2012).
- Van Wagner. C. E. 1977. Conditions for the start and spread of crown fire. *Canadian Journal of Forest Research* 7 no. 1: 23-34.
- Verbesselt, J., B. Somers, J. van Aardt, I. Jonckheere, and P. Coppin. 2006. Monitoring herbaceous biomass and water content with SPOT VEGETATION time-series to improve fire risk assessment in savanna ecosystems. *Remote Sensing of Environment* 215, no. 1-3: 239-250.
- Verbesselt, J., B. Somers, J. van Aardt, I. Jonckheere, and P. Coppin. 2007. Monitoring herbaceous fuel moisture content with SPOT VEGETATION time-series for fire risk prediction in savanna ecosystems. *Remote Sensing of Environment* 108, no. 4: 357-368.
- Xu, Jianchun. 2006. An approach to spatial data gathering technology: Realizing large-scale fire modeling in the wildland urban interface. PhD diss., University of California, Berkeley.

- Yilmaz, M. Tugrul, E. Raymond Hunt Jr., and Thomas J. Jackson. 2008. Remote sensing of vegetation water content from equivalent water thickness using satellite imagery. *Remote Sensing of Environment* 112, no. 5: 2514-2522.
- Zarco-Tejada, P.J., C.A. Rueda, and S.L. Ustin. 2003. Water content estimation in vegetation with MODIS reflectance data and model inversion methods. *Remote Sensing of Environment* 85, no. 1: 109-124.
- Zhang, Yangjian, Hong S. He, and Jian Yang. 2008. The wildland–urban interface dynamics in the southeastern U.S. from 1990 to 2000. *Landscape and Urban Planning* 85, no. 3-4: 155-162.
- Zhao, Kaiguang, Sorin Popescu and Ross Nelson. 2009. Lidar remote sensing of forest biomass: A scale-invariant estimation approach using airborne lasers. *Remote Sensing of Environment* 113, no. 1: 182-196.
- Zheng, G., J. M. Chen, Q. J. Tian, W. M. Ju, and X. Q. Xia. 2007. Combining remote sensing imagery and forest age inventory for biomass mapping. *Journal of Environmental Management* 85, no. 3: 616-623.

## VITA

Shelby M. Coder was born in Dallas, Texas on September 16, 1984, and is the daughter of Craig E. Coder and L. Dianne Coder. After completing her work at Mineola High School in 2002, she entered Texas A&M University-College Station. Shelby graduated in 2006 with a Bachelor of Science in Environmental Geosciences and minors in Geoinformatics and Geology. During the following years she was employed as a GIS analyst for the City of Pflugerville and then a GIS consultant at Lockwood, Andrews and Newnam, Inc. Shelby has served as the GIS and lidar project manager at the Texas Natural Resources Information System since 2009. In the fall of 2010, she entered the Graduate College of Texas State University-San Marcos.

Permanent Address: shelbycoder@gmail.com

This thesis was typed by Shelby M. Coder.